Dissertation
submitted to the
Combined Faculties of the Natural Sciences and for Mathematics
of the Ruperto-Carola University of Heidelberg, Germany
for the degree of
Doctor of Natural Sciences

Put forward by
Dipl.-Phys. Marc Repp
Born in Freudenstadt
Oral examination: May 8th, 2013

Interspecies Feshbach Resonances in an Ultracold, Optically Trapped Bose-Fermi Mixture of Cesium and Lithium

Referees: **Prof. Dr. Matthias Weidemüller**
Prof. Dr. Markus Oberthaler

Abstract. This thesis reports on the tunability of interactions in ultracold Bose-Fermi mixtures of Cesium and Lithium. The first realization of an optically trapped ^{6}Li -^{133}Cs mixture enabled to perform trap loss spectroscopy measurements to identify magnetic Feshbach resonances. A total of 19 interspecies Feshbach resonances, all in the magnetic field range between 650 G and 950 G, were observed for the two energetically lowest spin states of each species. Two 5 G broad and especially two 60 G broad s-wave resonances give perspectives to produce a dipolar quantum gas of LiCs ground state molecules as well as to study the Efimov effect in highly mass imbalanced systems. In addition, a unique relative tunability of intra- and interspecies scattering lengths was found which makes the ^{6}Li -^{133}Cs system also well suited for the investigation of polarons. Evaporative cooling was performed on optically trapped samples which contained only one of the species. In this way, Bose-Einstein condensates of ^{6}Li molecules as well as ^{133}Cs samples at a phase-space density of $\rho = 4 \cdot 10^{-2}$ were prepared. All experiments were performed in a new apparatus, which has been designed and set up during this thesis.

Zusammenfassung. Die vorliegende Arbeit berichtet über die Einstellbarkeit von Wechselwirkungen in ultrakalten Bose-Fermi Mischungen aus Cäsium und Lithium. Die erstmalige Realisierung einer optisch gefangenen ^{6}Li - ^{133}Cs Mischung ermöglichte das Durchführen von Fallenverlustmessungen zur Identifizierung von heteronukleare magnetischen Feshbachresonanzen. Es konnten insgesamt 19 heteronuklearen Feshbachresonanzen zwischen den beiden Spezies in deren jeweils beiden niedrigsten Spinzuständen beobachtet werden, die alle im Magnetfeldbereich von 650 G bis 950 G auftreten. Zwei 5 G breite und besonderst zwei 60 G breite s-Wellenresonanzen sind für die Herstellung eines dipolaren Quantengases aus tiefgebunden LiCs Grundzustandsmolekülen sehr aussichtsreich. Zudem ermöglichen die gefundenen Resonanzen ein Untersuchen des Efimoveffektes eines Systems mit einem großen Massenungleichgewicht. Des Weiteren zeigte sich eine einzigartige Einstellbarkeit der relativen homonukleare und heteronuklearen Streulängen, die sehr geeignet sind, um mittels des ^{6}Li - ^{133}Cs Systems Polaronen zu untersuchen. Es wurden zudem Gase, die nur eine der beiden Spezies beinhalteten, evaporativ gekühlt. Es konnten damit Bose-Einsteinkondensate, die aus ^{6}Li Molekülen bestehen, hergestellt werden. Zusätzlich wurde eine Phasenraumdichte von $\rho = 4 \cdot 10^{-2}$ in ^{133}Cs Gasen erreicht. Sämtliche Experimente wurden in einem neuen Apparat durchgeführt, der im Rahmen dieser Arbeit entwickelt und aufgebaut wurde.

Parts of the work presented in this thesis is based on the following manuscripts and publications:

- *M. Repp, R. Pires, J. Ulmanis, R. Heck, E.D. Kuhnle, M. Weidemüller, E. Tiemann*
  Observation of interspecies ^{6}Li-^{133}Cs Feshbach resonances
  Physical Review A **87**, 010701 (2013)

- *M. Repp, R. Pires, J. Ulmanis, S. Schmidt, R. Müller, K. Meyer, R. Heck, E.D. Kuhnle, M. Weidemüller*
  A helical Zeeman slower for sequential loading of two elements with large mass difference into optical dipole traps
  Manuscript in preparation

In addition, the author has contributed to the following publications, which are summarized at the end of this thesis:

- *J. Ulmanis, J. Deiglmayr, M. Repp, R. Wester, M. Weidemüller*
  Ultracold Molecule Formed by Photoassociation: Heteronuclear Dimers, Inelastic Collisions, and Interactions with Ultrashort Laser Pulses
  Chemical Reviews **112**, 4890 (2012)

- *J. Deiglmayr, M. Repp, R. Wester, O. Dulieu, M. Weidemüller*
  Inelastic collisions of ultracold polar LiCs molecules with caesium atoms in an optical dipole trap
  Physical Chemistry Chemical Physics **13**, 19101 (2011)

- *J. Deiglmayr, M. Repp, O. Dulieu, R. Wester, M. Weidemüller*
  Population redistribution in optically trapped polar molecules
  European Physical Journal D **65**, 99 (2011)

- *J. Deiglmayr, A. Grochola, M. Repp, O. Dulieu, R. Wester, M. Weidemüller*
  Permanent dipole moment of LiCs in the ground state
  Physical Review A **82**, 335 (2010)

- *J. Deiglmayr, M. Repp, A. Grochola, K. Mörtlbauer, C. Glück, O. Dulieu, J. Lange, R. Wester, M. Weidemüller*
  Formation of ultracold dipolar molecules in the lowest vibrational levels by photoassociation
  Faraday Discussions **142**, 335 (2009)

- *J. Deiglmayr, P. Pellegrini, A. Grochola, M. Repp, R. R. Côté, O. Dulieu, R. Wester, M. Weidemüller*
  Influence of a Feshbach resonance on the photoassociation of LiCs
  New Journal of Physics **11**, 055034 (2009)
  Erratum: New Journal of Physics **12**, 079802 (2010)

- *A. Grochola, A. Pashov, J. Deiglmayr, M. Repp, E. Tiemann, R. Wester, M. Weidemüller*
  The $B^1\Pi$ state in LiCs studied by photoassociation spectroscopy
  Journal of Chemical Physics **131**, 054304 (2009)

- *J. Deiglmayr, A. Grochola, M. Repp, K. Mörtlbauer, C. Glück, J. Lange, O. Dulieu, R. Wester, M. Weidemüller*
  Formation of ultracold polar molecules in the rovibrational ground state
  Physical Review Letters **101**, 133004 (2008)

Contents

Chapter 1

Introduction

The invention of laser-cooling and trapping methods, which was awarded with the Nobel Prize in 1997 [Phillips, 1998; Chu, 1998; Cohen-Tannoudji, 1998], triggered a new epoch in physics three decades ago. The ability of preparing quantum gases at temperatures close to absolute zero enabled the first experimental realization of quantum degenerate gases at ultracold temperatures. Bose-Einstein condensation (BEC) was demonstrated for the first time in 1995 [Davis *et al.*, 1995; Bradley *et al.*, 1995; Anderson *et al.*, 1995], which was honored with the Nobel Prize in 2001 [Cornell and Wieman, 2002; Ketterle, 2002]. Only few years after the achievement of Bose-Einstein condensation, the first quantum degenerate Fermi gases were prepared from laser cold atoms [DeMarco and Jin, 1999; Schreck *et al.*, 2001; Truscott *et al.*, 2001; Hadzibabic *et al.*, 2002]. The developed preparation schemes are nowadays routinely applied in many laboratories around the world and an enormous progress has been made in the field of ultracold quantum gases. As an example, novel kinds of many-body effects [Bloch *et al.*, 2008] became accessible, such as the investigation of quantum phase transitions, like the one from a super-fluid to a Mott insulator phase [Greiner *et al.*, 2002] or quantum phase transition at lower dimension [Paredes *et al.*, 2004; Paredes *et al.*, 2004; Hadzibabic *et al.*, 2006]. However, the rapid growth of the field would not have been possible without magnetic Feshbach resonances [Chin *et al.*, 2010] with their outstanding feature to provide a unique tunability of quantum dynamic systems by precisely controlling inter-atomic interactions. Therefore the year 1998 marks an important milestone, when the tuning of interactions via magnetic Feshbach resonances was demonstrated for the first time [Inouye *et al.*, 1998; Courteille *et al.*, 1998].

A variety of phenomena are obtained by the precise control over quantum degenerate mixture experiments via Feshbach resonances. Such quantum degenerate

mixtures can either be Fermi gases out of two spin components or quantum degenerate gases, that consist of different species [Modugno *et al.*, 2001; Truscott *et al.*, 2001; Hadzibabic *et al.*, 2002; Goldwin *et al.*, 2004; Inouye *et al.*, 2004; Silber *et al.*, 2005; Papp *et al.*, 2008; Taglieber *et al.*, 2008; Catani *et al.*, 2008; Spiegelhalder *et al.*, 2010; Tey *et al.*, 2010; Lercher *et al.*, 2011; McCarron *et al.*, 2011; Park *et al.*, 2012]. Two component Fermi gases with tunable, weakly attractive interactions served as a model system for investigating the BCS theory, which was developed for describing low temperature super-conductance in solid state systems [Bardeen *et al.*, 1957]. A necessary requirement for the occurrence of super-conductance is pairing mechanism, which was investigated by making use of the broad Feshbach resonance in ^{6}Li [Chin *et al.*, 2004a; Schunck *et al.*, 2008]. Moreover, vortex formation and super-fluidity could be demonstrated in these gases [Zwierlein *et al.*, 2005; Zwierlein *et al.*, 2006]. A completely different behavior of a two component Fermi gas at low temperatures is obtained, if the interactions are tuned to be repulsive. In this case, weakly bound bosonic molecules are formed out of two fermions via three-body processes [Jochim *et al.*, 2003a; Chin and Grimm, 2004]. This requires the application of BEC theory for describing these systems. A benchmark was therefore the first demonstration of Bose-Einstein condensation of molecules within a Fermi gas [Jochim *et al.*, 2003b; Zwierlein *et al.*, 2003; Greiner *et al.*, 2003]. Furthermore, Feshbach resonances allowed to investigate the so-called "BEC-BCS cross-over" [Bartenstein *et al.*, 2004; Regal *et al.*, 2004; Bourdel *et al.*, 2004] that connects both regions at strong interactions. In contrast to quantum degenerate Fermi gases out of two spin components, where scattering between particles can only occur between atoms in different spin states, nonzero intra- as well as inner-species scattering lengths can be present in samples out of two different species. This can be used for instance for the investigation of pairing mechanism of a two component Fermi gas in the presence of a Bose-Einstein condensate [Bijlsma *et al.*, 2000]. The fermions can then also interact via the exchange of BEC-phonons, which leads to a modification of the fermionic scattering behavior.

Besides the study of pairing mechanism and supra-conductivity in two component Fermi gases, additional insight into solid states physics is provided by the possibility of preparing quantum gases out of an impurity species that interacts with surrounding atoms of a majority species. This is similar to the situation of a moving electron which interacts with the positively charged lattice atoms in a crystal. The Coulomb force leads to a local distortion of the surrounding lattice atoms whereas the back-action to the electron modifies its propagation dynamics. A powerful method for describing the movement of the electron is to treat it as a

quasi-particle, a so-called "Fröhlich polaron" [Fröhlich, 1954, for a review see Devreese and Alexandrov, 2009], that has a different mass and energy compared to the bare electron. Since the underlying Hamiltonian of an impurity in a BEC can be directly mapped to the Fröhlich Hamiltonian [Fröhlich, 1954; Cucchietti and Timmermans, 2006; Tempere *et al.*, 2009], such a system is a model system for investigating Fröhlich polarons. The Bogoliubov modes of the BEC serve as lattice phonons, whereas the intraspecies scattering length represents the phonon-electron coupling strength. The coupling constant α scales in this case with the ratio of the interspecies (intra-BEC) scattering length $\mathrm{a_{IB}}$ ($\mathrm{a_{BB}}$) as $\alpha \propto \mathrm{a_{IB}^2/a_{BB}^{4/5}}$ [Tempere *et al.*, 2009]. In order to reach the strong coupling limit, an advantageous system is therefore a mixture with broad interspecies Feshbach resonance and a nearly non interacting BEC, as it was found recently within the work of this thesis in mixture of ^{6}Li -^{133}Cs [Repp *et al.*, 2013; Tung *et al.*, 2013]. Pioneering experiments in the ultra-cold domain already studied polaronic behavior in spin imbalanced Fermi-Fermi mixtures [Nascimbène *et al.*, 2009; Schirotzek *et al.*, 2009; Koschorreck *et al.*, 2012; Kohstall *et al.*, 2012]. In these samples so-called "Fermi polarons" can be formed between the majority atoms and the minority component.

Another application of Feshbach resonances in ultracold gases is the study of the few-body Efimov effect [Braaten and Hammer, 2007]. Considering low energy collisions of nucleons, in the 1970s V. Efimov proposed an infinite series of three-body bound states with a universal scaling behavior for systems of diverging scattering lengths [Efimov, 1971; Efimov, 1979]. However, a clear evidence of the Efimov effect was not observed for 35 years. This could be realized within ultracold gases where an evidence of an Efimov feature was found for the first time by tuning a broad Feshbach resonance of ^{133}Cs [Kraemer *et al.*, 2006]. Since then, Efimov resonances were recorded in various homonuclear alkaline systems [Ottenstein *et al.*, 2008; Knoop *et al.*, 2009; Huckans *et al.*, 2009; Zaccanti *et al.*, 2009; Williams *et al.*, 2009; Gross *et al.*, 2009; Ferlaino *et al.*, 2009; Lompe *et al.*, 2010; Nakajima *et al.*, 2011; Berninger *et al.*, 2011; Gross *et al.*, 2011; Roy *et al.*, 2013] as well as K-Rb mixtures [Barontini *et al.*, 2009]. But a series of resonances was so far not reported. This might be realized by investigating mixtures of two species with a large mass imbalances of the constituents. In this case a decrease in the universal scaling factor [D'Incao and Esry, 2006; Helfrich *et al.*, 2010], which describes the spacing between the resonances, is expected. Therefore experiments dealing with ^{6}Li and ^{133}Cs are very promising. The extreme mass ratio of $m_{Cs}/m_{Li} \approx 22$ results in an advantageous scaling factor of $\exp(\pi/S_0) \approx 4.9$ for Cs-Cs-Li Efimov states. This is significantly smaller than $\exp(\pi/S_0) \approx 22.7$ as obtained for bosonic systems

of equal mass [D'Incao and Esry, 2006].

So far, only weakly bound molecules such as dimers at the BEC-side of a Feshbach resonance or Efimov trimers have been discussed, which have been formed in most of the considered cases via indirect recombination processes. An important feature of Feshbach resonances in ultracold samples is the ability of actively create weakly bound dimers out of the atomic sample by ramping a magnetic field over a Feshbach resonance ("magneto-association") [Herbig *et al.*, 2003; Regal *et al.*, 2003]. This gives access to deeply bound molecular levels, which can then be populated by a subsequent stimulated Raman adiabatic passage (STIRAP) process [Ni *et al.*, 2008; Danzl *et al.*, 2008; Lang *et al.*, 2008]. Performing high-resolution spectroscopy on the rich internal ro-vibrational as well as hyperfine structure of ultracold molecules gives access to study time variations of fundamental constants [Chin *et al.*, 2009] or to identify the possible permanent electronic moment of the electron [DeMille *et al.*, 2000]. Samples of polar molecules, like heteronuclear dimers, are of special interest. Besides the contact interaction, which has so far been considered, also dipolar interactions are present in these systems. Their long range and anisotropic character gives access to a variety of novel many-body phenomena (for reviews see e.g. [Carr *et al.*, 2009; Pupillo *et al.*, 2008b]), which will be discussed in detail in Sec. 5.1.1. Very promising for the investigation of dipolar effects are experiments with deeply bound LiCs molecules [Deiglmayr *et al.*, 2008b], since their permanent dipole moment of 5.5 D [Aymar and Dulieu, 2005; Deiglmayr *et al.*, 2010a] exceeds all other stable alkaline combinations. LiCs molecules have been already excessively studied in a series of photoassociation experiments [Jones *et al.*, 2006; Ulmanis *et al.*, 2012] at an early stage of this thesis [Deiglmayr *et al.*, 2008b; Deiglmayr *et al.*, 2009a; Deiglmayr *et al.*, 2009b; Grochola *et al.*, 2009; Deiglmayr *et al.*, 2010a; Deiglmayr *et al.*, 2010b; Deiglmayr *et al.*, 2011a; Deiglmayr *et al.*, 2011b], which is however beyond the focus of this work. The reader is therefore referred to Chapter A, where a summary of the results is provided.

In order to profit from the outstanding properties of Li-Cs systems, like the possibility of investigating the Efimov effect in a large mass imbalanced system or to prepare a dipolar gas out of LiCs molecules, besides the preparation of ultracold mixtures of the two species a control over the interspecies interactions via Feshbach resonances is required. A mixture of ^{7}Li -^{133}Cs was the first one, where trapping in a conservative potential at ultracold temperatures could be achieved [Mosk *et al.*, 2001]. Furthermore, sympathetic cooling of two different species was initially demonstrated with the ^{7}Li -^{133}Cs system [Mudrich *et al.*, 2002]. This thermalization measurements enabled to deduce elastic cross sections and scattering

lengths of ^{7}Li-^{133}Cs at zero magnetic field. Moreover, hyperfine changing collisions were investigated in this trapped Bose-Bose mixture [Mudrich *et al.*, 2004]. More recently, photoassociated ^{7}Li^{133}Cs molecules were trapped [Deiglmayr *et al.*, 2011a; Deiglmayr *et al.*, 2011b]. However, the ability of tuning the interactions of a Li-Cs mixtures was unknown until autumn 2012. Predictions of possible Feshbach resonances relied on calculations of the ground state potential curves. Initial *ab initio* calculations [Korek *et al.*, 2000; Aymar and Dulieu, 2005] could be improved by Fourier-transform spectroscopy in heat pipes [Staanum *et al.*, 2007], whereas photoassociation measurements lead to a more accurate value of the ground state dissociation energy [Grochola *et al.*, 2009].

Within the framework of this thesis, the tunability of interactions in the Li-Cs system by applying external magnetic fields was explored. The preparation of ultracold Bose-Fermi ^{6}Li -^{133}Cs mixtures for the first time allowed to perform trap loss spectroscopy. A total of 19 Feshbach resonances in the two lowest spin states of each species could be identified [Repp *et al.*, 2013]. Slightly later, the Chin group in Chicago reported of the observation of five Feshbach resonances at positions, which are consistent with our results [Tung *et al.*, 2013]. Four broad s-wave resonances were found which are well suited to study the Efimov effect in a large mass imbalanced system. This is advantageous for the observation of a whole series of resonances [D'Incao and Esry, 2006; Helfrich *et al.*, 2010]. Furthermore, studying dipolar physics [for a review see e.g. Carr *et al.*, 2009; Pupillo *et al.*, 2008b] with deeply bound LiCs molecules, created by magneto-association, followed by a subsequent STIRAP process, becomes now feasible. Moreover, two of the resonances are at magnetic fields where stable ^{133}Cs BECs exists that behaves nearly as an ideal gas. This gives excellent prospects for the investigation of Fröhlich polarons [Fröhlich, 1954; Cucchietti and Timmermans, 2006; Tempere *et al.*, 2009] with ultracold ^{6}Li -^{133}Cs mixtures.

This thesis is structured as follows: Chapter 2 gives a detailed overview over the experimental setup which is required for performing laser cooling of the two species. This includes a description of the vacuum as well as the laser system. High loading rates of magneto-optical traps are obtained from the implementation of a sequential loading scheme. The setup has been completely new designed in the framework of this thesis after moving the experimental apparatus from the University of Freiburg to Heidelberg. Chapter 3 describes the enhancement of the phase-space density via evaporative cooling of the two species in optical dipole traps. Molecular BECs of two component ^{6}Li Fermi gases as well as ^{133}Cs samples at phase-space densities close to quantum degeneracy were prepared. Furthermore, the first combined trapping of

a Bose-Fermi mixture of ^{6}Li -^{133}Cs is part of this chapter. Chapter 4 presents the observation of 19 interspecies Feshbach resonances by trap loss spectroscopy of the trapped mixture. Several of the found resonances give perspectives for investigating dipolar physics with deeply bound LiCs molecules, polaron physics as well as the study of the Efimov effect in a strongly mass imbalanced system. The main part of this work ends in Chapter 5 where the most important results of this thesis are concluded. A detailed discussion of these possible applications of the interspecies ^{6}Li -^{133}Cs Feshbach resonances is also given in this Chapter. In addition, a brief review of the investigation of LiCs molecules via photoassocation, which has been performed at the previous experimental apparatus at the beginning of this thesis, is provided in Chapter A.

Chapter 2

Experimental setup for preparing ultracold ^{6}Li and ^{133}Cs samples

Motivated by the results which were achieved at our previous experimental setup (see [Kraft, 2006; Lange, 2008; Deiglmayr, 2009]), like the formation of deeply bound ground state LiCs molecules [Deiglmayr *et al.*, 2008b], a move of the experiment from Freiburg to Heidelberg was used for a complete redesign of the about 15 years old experimental setup. The goal of the new design was to prepare ^{6}Li -^{133}Cs mixtures at much higher phase-space densities as compared to the previous machine, where experiments were mostly performed at temperatures of several tens of μK or higher. The first step is to prepare samples at high phase-space densities via laser cooling and trapping in an ultra-high vacuum chamber. A further increase of the phase-space density towards quantum degeneracy is obtained by further evaporatively cool the atoms within optical dipole traps, which is part of the next chapter.

The new vacuum system is described in the beginning of this chapter. Various coils are required during the measurements, which is the content of the following two sections. A set of helical coils is used for Zeeman decelerating an atomic beam that provides the flux for sequentially loading ^{6}Li - and ^{133}Cs magneto-optical traps (MOTs). In addition, several coils have been installed at the periphery of the experimental chamber. They generate the required gradient fields for operating the MOTs as well as homogeneous fields of different strengths as needed for the subsequent cooling methods. Besides good vacuum conditions and magnetic fields, laser beams of different frequencies are needed to laser cool the two species. Their frequency preparation as well as their beam paths in the main chamber periphery are part of the subsequent section. After mentioning the detection methods, which have been used for characterizing the atomic clouds within this thesis, the loading as well as

further compression of the MOTs is described in the subsequent section. In contrast to the old setup, a nearly spin polarized ^{133}Cs at temperatures of 1μK is prepared via degenerate Raman-Sideband Cooling (DRSC) as a last step of laser cooling.

2.1 Vacuum system

Experiments with atoms of temperatures of several hundred μK or less require ultra high vacuum systems. Otherwise, high collision rates with particles at room temperatures would lead to a fast heating and a rapid loss of atoms from the sample.

Our apparatus is illustrated in Fig. 2.1 and contains three sections. In the first one, an atomic beam of the two species is created by an effusive oven. Typical pressures at the operation temperatures are $p_{Cs} = 10^{-3}$ mbar and $p_{Li} = 10^{-5}$ mbar. This high pressure is in contrast to the required pressures in the experimental chamber, which is part of the third chamber. Therefore differential pumping is performed in the middle part of the chamber. These different parts are described in the following more in detail. In order to decelerate atoms out of the beam, a Zeeman slower based on helical coils is mounted on the middle part of the chamber. This is part of Section 2.2.

2.1.1 Atomic beam source

The task of the first section of the vacuum chamber is to generate an intensive atomic beam for loading the MOTs. This is done by an effusive double species oven with a similar design as described by Stan and Ketterle, 2005. This design enables selective control over the partial atomic fluxes regardless of the 10 (6) orders of magnitude lower vapor pressures of Li [Gehm, 2003] as compared to Cs [Steck, 2008] at temperatures $T = 375$ K ($T = 625$ K). A schematic drawing of the oven is depicted in Fig. 2.2 a). A ^{6}Li and a ^{133}Cs reservoir are connected by a 14 mm long capillary with a diameter of 1.5 mm [Kraft, 2006]. Furthermore, a conical hole with a diameter of 10 mm, which is mounted above the ^{6}Li reservoir, acts as nozzle for the atomic beam. Vacuum conductances of $C_{Cs}^{capillary} = 18 \cdot 10^{-3}$ l/s ($C_{Li}^{capillary} = 84 \cdot 10^{-3}$ l/s) for the capillary and $C_{Cs}^{nozzle} = 6.3$ l/s ($C_{Li}^{nozzle} = 29.7$ l/s) for the nozzle are expected for molecular flow [Wutz *et al.*, 1982]. The capillary enables a flux of ^{133}Cs atoms out of the vapor in the ^{133}Cs reservoir into the ^{6}Li reservoir. Since the vacuum conductivity of the nozzle is much higher than the one of the capillary, most of the ^{133}Cs atoms leave the ^{6}Li reservoir via the nozzle instead of flowing back into the ^{133}Cs reservoir. In dynamic equilibrium, the ^{133}Cs flux is determined by the vapor pressure of the

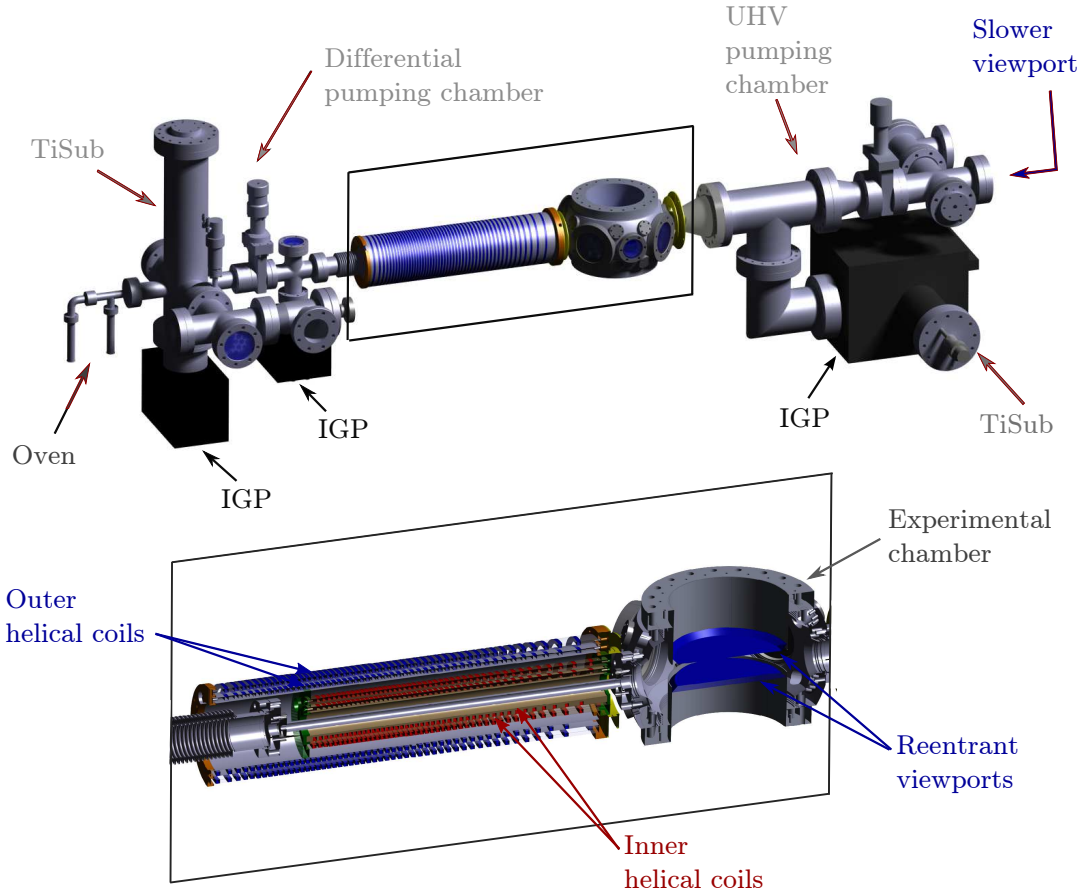

Figure 2.1: Vacuum chamber. Upper panel: Overview over the whole chamber. An atomic beam is created in an oven section, which is decelerated by a Zeeman slower made out of helical coils. Two differential pumping stages, three ion-getter pumps (IGP), two titanium sublimation pumps (TiSub) as well as a NEG coating in the main chamber, create the required vacuum conditions. Lower panel: Cut through the Zeeman Slower (for details see Sec. 2.2) and the experimental chamber. Additional coils are mounted in the periphery of the main chamber, which are depicted in Fig. 2.6 a).

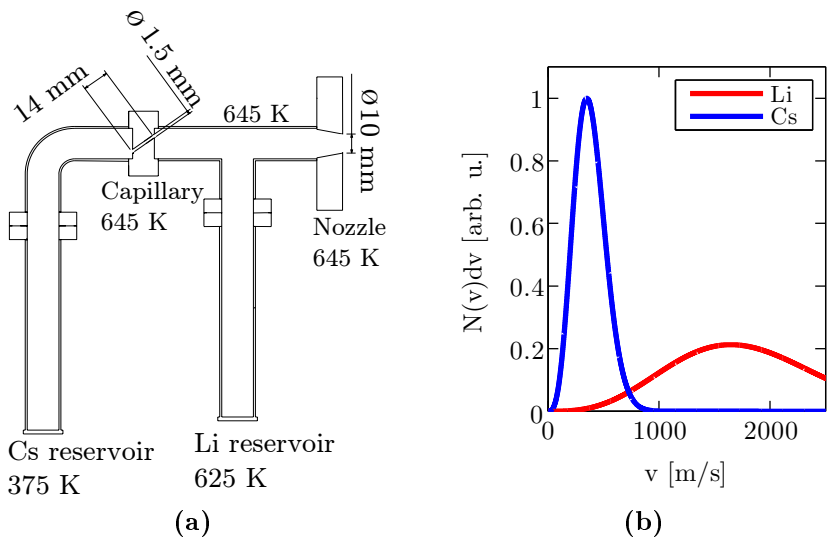

Figure 2.2: Double species effusive oven for ^{6}Li and ^{133}Cs . (a) Schematic drawing: The oven contains two reservoirs, typically operating at temperatures of 375 K (625 K) for ^{133}Cs (^{6}Li), which are connected by a 14 mm long capillary with a diameter of 1.5 mm. An atomic beam with fluxes of 10^{14} atoms/s for ^{133}Cs ($5 \cdot 10^{15}$ atoms/s for ^{6}Li) is created by the oven nozzle, with a diameter of 10 mm. The capillary, the oven nozzle and the upper part of the Li reservoir are typically heated to 645 K for avoiding depositing. (b) Calculated velocity distributions of the atomic beam at an oven temperature of 625 K.

^{133}Cs reservoir, which can be controlled via the temperature. Since the flux of ^{6}Li atoms out of the ^{6}Li reservoir is also determined by the vacuum conductivity of the nozzle, the ^{6}Li flux can be independently adjusted via the temperature of the ^{6}Li reservoir. At the typical operation temperatures, which are given in Fig. 2.2, partial atomic fluxes of $\Phi_{\mathrm{Cs}} = 10^{14}$ atoms/s and $\Phi_{\mathrm{Li}} = 5 \cdot 10^{15}$ atoms/s are expected.

The velocity distribution of the atomic beam is for both species determined by the temperature within the ^{6}Li reservoir. Due to the large mass, smaller velocities are much more likely for the heavy ^{133}Cs , as depicted in Fig. 2.2 b). In order to decelerate comparable fractions of both species in a Zeeman slower (see Sec. 2.2), much higher capture velocities are therefore required for ^{6}Li .

Temperature regulation in the oven is performed by five individual band heaters which are independently regulated by PI loops based on a micro controller [Deiglmayr, 2009]. To minimize possible leaks, which can be created at flanges by the aggressive hot Li [Stan and Ketterle, 2005], most of the parts are welded. Only two CF 16 flanges for connecting the reservoirs and one additional CF 40 flange for installing the oven at the nozzle to the other parts of the vacuum chamber are used. Since the commonly used copper gaskets are attacked by hot Li, a nickel gasket is

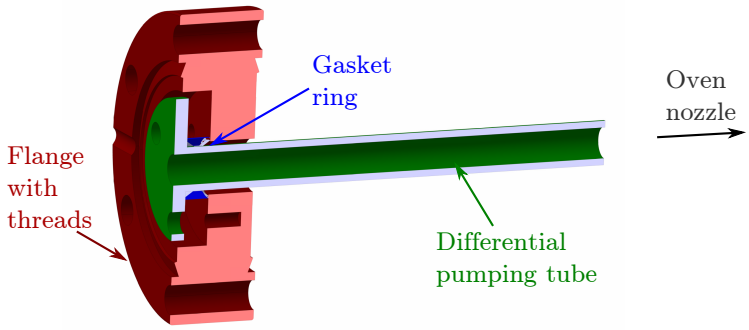

Figure 2.3: Differential pumping tube. An adjustable design allowed for a concentric alignment of the first differential pumping tube in respect to the oven nozzle in order to minimize the clipping of the atomic beam. See text for details.

used instead at the ^{6}Li reservoir [Stan and Ketterle, 2005].

2.1.2 Differential pumping and Zeeman slowing sections

In order to generate an atomic flux via an effusive oven, a certain vapor pressure is desired, as described in the previous section. This in contrast to the requirements of our experiments, where losses due to collisions of ultracold atoms with background atoms occur and therefore the background pressure should be minimized (see Sec. 4.3). In order to fulfill both requirements, two differential pumping stages have been set up in the middle part of our vacuum chamber. This is realized by two sections: In the first section, the oven is pumped by an ion getter[1] and a Titanium sublimation pump (TiSub)[2]. The first differential pumping stage is realized via connecting this section by a 103 mm long tube with an inner diameter of 7 mm, to the second section, which is pumped by another ion getter pump[3]. The construction of the tube is depicted in Fig.2.3. The second differential pumping stage is realized by connecting the middle part of the vacuum chamber with the experimental chamber by a 500 mm long tube with an inner diameter of 10 mm, while using the pumps of the main chamber. As depicted in Fig. 2.1 this tube is surrounded with the helical coils of the Zeeman slower (see Sec. 2.2). For ensuring maximum loading of the MOTs, the clipping of the atomic beam at the chamber walls needs to be minimized. Since the distance between the oven and the main chamber is about 1.5 m

[1]Starcell, Varian, pumping speed about 40-55 l/s.
[2]Delivered by Varian.
[3]20l/s Starcell, Varian.

and the tolerances during the welding of the flanges to the vacuum parts are about 1°, special care needs to be taken on the alignment of the thin components along the propagation axis of the atomic beam. This was done during the assembling of the chamber. Instead of the atomic beam, a laser beam, which was pointing from the middle of the oven nozzle towards the main chamber region was used instead. As the first step, the first differential pumping stage was aligned to be concentric in respect to the oven nozzle. The realization is depicted in Fig. 2.3. Therefore, the tilting angle was optimized via varying the stress of the screws, which are used for mounting the tube. A large available tilting angle was ensured by using a long gasket ring with a small contact surface, which was assembled between the mounting area of the tube and flange containing the threads for the screws. The slightly larger diameter of the clearance holes at the housing of the tube compared to the screw diameters allowed for a further lateral alignment. A flexible bellow, which was mounted between the two differential pumping stages, enabled an adjustment in a way that the beam propagates concentric through the second pumping stage and finally hits the center of the main chamber.

Two CF 63 viewports[4] in the first section, which are perpendicularly orientated to the atomic beam can be used for increasing the flux in the MOT region via performing transversal cooling [Hoogerland *et al.*, 1996] at a future extension of the experiment. A shutter[5], which is installed behind the oven nozzle, can mechanically block the atomic beam after the MOT loading is completed.

2.1.3 Experimental chamber

Experiments with ultracold atoms require good optical access for laser cooling and trapping. In our experiment this is ensured by the use of commercial octagon[6]. Optical access in the horizontal directions is provided by four CF 63 and two CF 40 viewports[7]. In addition, two custom made reentrant CF 150 viewports[8] with an outer separation of 42 mm are currently used for the vertical laser beams. The high numerical aperture allows for performing high resolution imaging or trapping of atoms in micro-traps [Serwane *et al.*, 2011] in a further stage of the experimental apparatus. Currently, the reentrant viewports are used for mounting the Feshbach and Curvature coils (see Sec. 2.3) close to the center of the experimental chamber. This

[4]VPZ63, Vacom, uncoated.
[5]DS450VPS, Lesker.
[6]MCF800-EO200080.16, Kimball physics Inc.
[7]Delivered by UKAEA Culham.
[8]Delivered by UKAEA Culham.

enables the creation of magnetic fields up to 1400 G, which are required for searching ^{6}Li -^{133}Cs Feshbach resonances (see Chapter 4). The relatively small distance limits the energy deposition within the coils since for a given magnetic field only a moderate current is needed. In combination with the non-magnetic glass surface of the viewports, the inductance is additional small what results in fast switching times of the colis.

Common viewports glass materials consist of a large fraction of OH, which a has an absorption band in the near infra red region. Since our optical dipole traps operate at 1064 nm (see Sec. 3.2.2), large thermal effects are expected at high laser intensities, which can lead to a modification of the trapping properties. In order to avoid this, all main chamber viewports are made out of poly-crystalline Suprasil 3001, which has an OH concentration below 1 ppm [Heraeus, 2013]. This is about 1000 times lower compared to other materials. High transmission efficiencies for the main chamber beams is further ensured by an anti-reflection coating of the surfaces[9]. The reflection coefficients per surface are below 0.5% for wavelengths of 670 nm and 850 nm and below 0.3% for 1064 nm for unpolarized light at an angle of incidence of 0°. Optical access for the bichromatic Zeeman slower beam is enabled by an additional viewport[10] with the same coating, which is mounted slightly behind the experimental chamber. This viewport needs to be heated to temperatures of about 120°C in order to prevent deposition of atoms out of the beam from the oven. For this reason high temperature resisting kodial was selected as glass material for this viewport. In addition, two small rf-antennas, where one is mounted within and second one outside the chamber, allow for a manipulation of ^{6}Li atoms via driving RF-transitions (see Sec. 3.5.4). The whole chamber is coated with a NEG material [Benvenuti *et al.*, 1999], which enables vacuum pumping directly in the main camber region. Further pumping is realized by connecting an ion getter pump and a TiSub pump[11] with a high vacuum conductivity to the main chamber.

Vacuum conditions

In order to reach good UHV vacuum conditions, the vacuum chamber was baked out. The NEG coating was activated by heating the main chamber part to temperatures of 170°C during the last stage. Homogeneous heating was ensured during the bakeout process by the use of three custom made insulating bakeout tents[12]. An ex-

[9] Performed by LaserComponents.
[10] VPZ63, Vacom.
[11] VacIon Plus 150 Starcell Kombipumpe, Varian.
[12] Deliverd by tectra.

tension of the 2 m long chamber of several cm is expected during the bakeout. For minimizing mechanical tension the different parts were mounted on teflon tracks, where a reversible displacement of several mm could be observed during bakeout. After the bakeout, a pressure of $p_{UHV} = 4 \cdot 10^{-11}$ mbar and $p_{oven} = 1 \cdot 10^{-11}$ mbar was measured in the main- and oven chamber region, respectively, by ion gauges[13], while still operating the oven. However, while performing experiments for the last two years, the vacuum conditions have degraded to $p_{UHV} \approx 10^{-10}$ mbar. This is probably caused by an imperfect performance of the two 15 years old ion pumps in the oven region.

2.2 Zeeman slower

The usual procedure for obtaining ultracold quantum gases is to first load a magneto-optical trap (MOT), followed by a subsequent cooling step, mostly by evaporating the samples in a magnetic or an optical dipole trap. A crucial point in this scheme is to generate an atomic beam with a high flux at low velocities for an effective loading of the MOT. Two approaches have turned out to be well suited, either creating a slow beam out of an additional two-dimensional MOT [Lu *et al.*, 1996] (2D MOT) loaded by a vapor gas, or to decelerate atoms emitted from an effusive source by a Zeeman slower [Phillips and Metcalf, 1982], like in our case.

2.2.1 Design of a double species Zeeman slower

In order to design a Zeeman slower for the efficient deceleration of two species without limiting the optical access for the experiment by using two individual Zeeman slowers, the mass dependence of the different parameters needs to be considered. The working principle of a Zeeman slower is the scattering of light, which results in a net force F_{Light}. This force is similar for all alkaline atoms when on resonance and at saturation intensity, and therefore almost independent of the mass. However, the deceleration $a = F_{Light}/m$ shows a strong dependence of the mass due to its inverse proportional scaling. Another important parameter for the design of a Zeeman slower is the capture velocity v_{cap}. Since usually effusive ovens serve as atomic sources, the capture velocity should be a significant fraction of mean velocity of a Maxwell-Boltzmann distribution v_{mean}^{MB}. The mass dependence of v_{mean}^{MB} provides an estimate of $v_{cap} \propto \sqrt{1/m}$. As a result, the length of a slower $L \propto a/v_{cap}^2$ does not show any mass scaling, which indicates that in this simple approximation, Zeeman

[13] UHV-24p Nude Bayard-Alpert Messröhre, Varian.

slowers for different species with the same length can be constructed. However, to obtain optimal light forces, the Doppler shift needs to be compensated via the Zeeman shift at each position z along the slower axis. As the velocity $v(z) \propto \sqrt{a \cdot z}$ scales with $\sqrt{1/m}$, the required magnetic fields $B(z) \propto \sqrt{1/m}$ show a mass dependence.

Consequently, the magnetic fields of a Zeeman-Slower for ^{6}Li and ^{133}Cs atoms differ by a factor of about five, making it impossible to efficiently decelerate both species simultaneously. To overcome this constraint, a Zeeman slower which generates optimized fields for either efficient deceleration of ^{133}Cs or of ^{6}Li was designed, using a sequential MOT loading scheme. One should note that another possibility for a double species slower is the division of the Zeeman slower into different segments which are optimized for decelerating one species, as demonstrated for Li and Rb [Marti *et al.*, 2010].

In order to design the magnetic coils for our setup, the required fields for the deceleration of ^{6}Li and ^{133}Cs atoms were calculated by a numerical simulation. A detailed description can be found in the Appendix (Sec. B.1) of this thesis and only a short summary is given here. For obtaining the optimal fields the deceleration process was inverted in the simulation by virtually accelerating the two species separately towards the oven with a starting velocity v_{start} at the MOT center. At each position, the optimal magnetic field was obtained by maximizing the photon scattering rate via the Zeeman shift. For typical magnetic field values, the Zeeman shift of ^{6}Li is larger than the hyperfine splitting and therefore closed optical transitions within the Paschen-Back regime were used in the calculation. To maximize the atomic flux, the field was selected in a way, that all three possible (the three lowest) m_I sublevels are decelerated. Effective capture into the MOT is ensured by using the radial field components of the MOT gradient (see Sec. 2.3 for the properties of the MOT coils) as the last part of the slower, which minimizes the transverse expansion of the atomic beam [Schünemann *et al.*, 1998].

In order to obtain the maximal velocity classes, which can be still captured, a second simulation was started, where the atoms were now ejected from the oven. For certain velocity classes, the deceleration as well as the transversal extension of the atomic beam [Joffe *et al.*, 1993] was investigated (for details see Sec. B.2). As depicted in Fig. 2.4, capture velocities of $v_{\text{capture}}^{\text{Slower}}$=150 m/s and $v_{\text{capture}}^{\text{Slower}}$=650 m/s are obtained for the ^{133}Cs atoms in the $m_F = 3$ and ^{6}Li atoms in the $m_j = -1$ state, respectively.

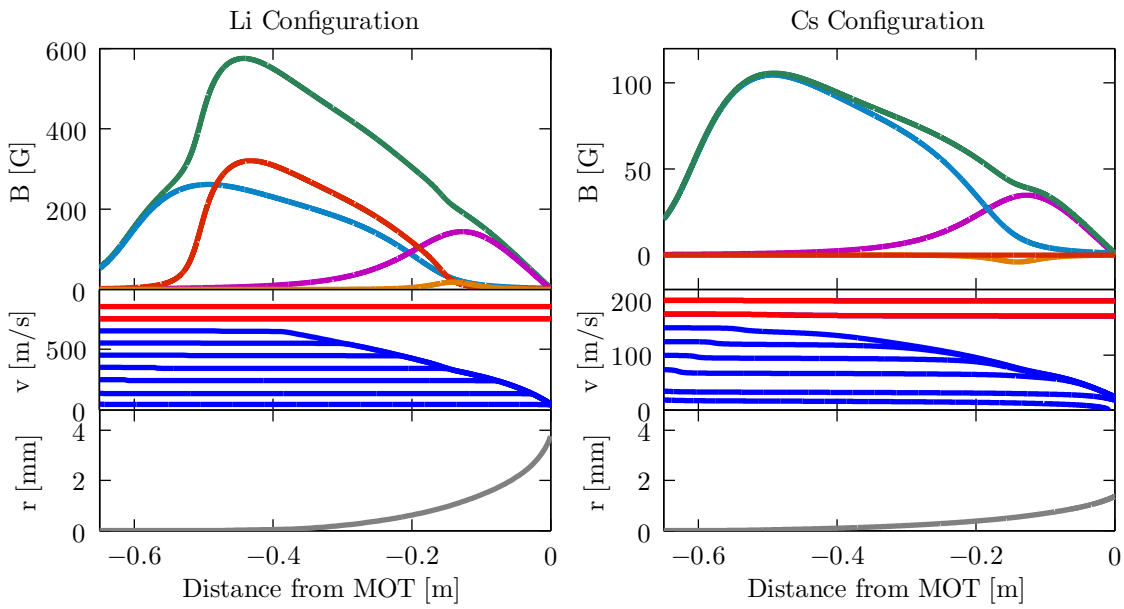

Figure 2.4: Field configurations and simulations of the deceleration process for ^{6}Li (left column) and ^{133}Cs (right column). Upper panels: The total fields (green) are sums of the fields from the inner helical coils (red), the outer helical coils (blue), the adaption coil (orange) and the radial fields from the MOT coil (violet) (See Tab. B.3 for used currents). Middle panel: The deceleration for different velocity classes (represented by the velocity at distance $d = -0.65$ m) at the oven has been investigated for the ^{133}Cs atoms in the $m_f = 3$ and ^{6}Li atoms in the $m_j = -1$ state. For velocity classes below a critical velocity (blue curves) almost no deceleration is obtained until the atoms of a certain velocity class match the position, where efficient photon scattering sets in, whereas velocity classes, with too large velocities do not feel large forces (red curves). Lower panel: The capture velocity $v_{\text{capture}}^{\text{Slower}}$ of the Zeeman slower was extracted from the maximum velocity class, where significant deceleration was observed. The radius of the atomic beam for ^{6}Li atoms in the $m_j = -1$ state (^{133}Cs atoms in the $m_f = 3$ state) due to transversal heating is plotted for atoms starting with $v_{\text{capture}}^{\text{Slower}}$=650 m/s ($v_{\text{capture}}^{\text{Slower}}$=150 m/s) at the oven chamber in the lower left panel. The radial extension of the ^{6}Li beam reaches almost the extension of the MOT laser beams, indicating the importance of ensuring efficient deceleration until the atoms reach the MOT center, especially for the light ^{6}Li .

2.2.2 Implementation and characterization

The standard procedure to generate the required magnetic fields for the slowing of one species is the use of various coils with different radii and winding numbers. However, the implementation of a design which allows two different field profiles would require a complicated arrangement of the various coils. To avoid this, we chose an approach similar to the one presented by Bell *et al.*, 2010, where the field profile is generated by a single layer with a variable pitch. In principle, the double species design can be realized by two individual coils, however, in order to reduce the electrical power consumption, our design is based on four interleaving layers. A schematic drawing is depicted in Fig. 2.1 and a detailed description of the parametrization is given in Sec. B.3. The two outer layers are optimized for the creation of the magnetic field for ^{133}Cs deceleration at a moderate current of 30 A. The design field for ^{6}Li is obtained by increasing the current of the two outer layers to 75 A and supplying the same current through the inner two coils. The small inductances due to the small number of windings allow for fast switching between ^{6}Li and ^{133}Cs loading. The profiles of the four helices have been directly milled into 7 mm thick aluminum tubes by CNC milling machines, where the shapes, which were parametrized exactly as in Bell *et al.*, 2010, could be directly used as an input. In order to avoid eddy currents during the coil switching, the mount of the coils is sliced.

The electrical insulation of the wire has to sustain temperatures of 250 °C, as the coils have to be mounted before the vacuum baking process. Therefore the aluminum tubes were sprayed with a commercial, electrical insulation car exhaust pipe spray. Additionally, the hollow core wires were first wrapped with a thin glass fiber wire and a high temperature resistance Teflon tape before winding it onto the aluminum tubes. In order to characterize the helical coils, the magnetic fields in axial direction were measured by a standard Hall probe. The obtained fields for the two configurations are plotted together with the expected fields in Fig. 2.5. Moreover, a photo of the slower is shown in Fig. B.1 within the appendix of this work.

Efficient cooling of the coils is performed by pumping water through the inner hole of the wires. A temperature increase ΔT of about 20 K is observed at maximal operational currents of our power supplies of 110 A, which is consistent with a simple heat transfer calculation assuming turbulent water flow in the tubes. Furthermore, an additional, thin adaption coil is mounted between the helical coils and the experimental chamber, which ensures a good matching of the fields from the helical coils

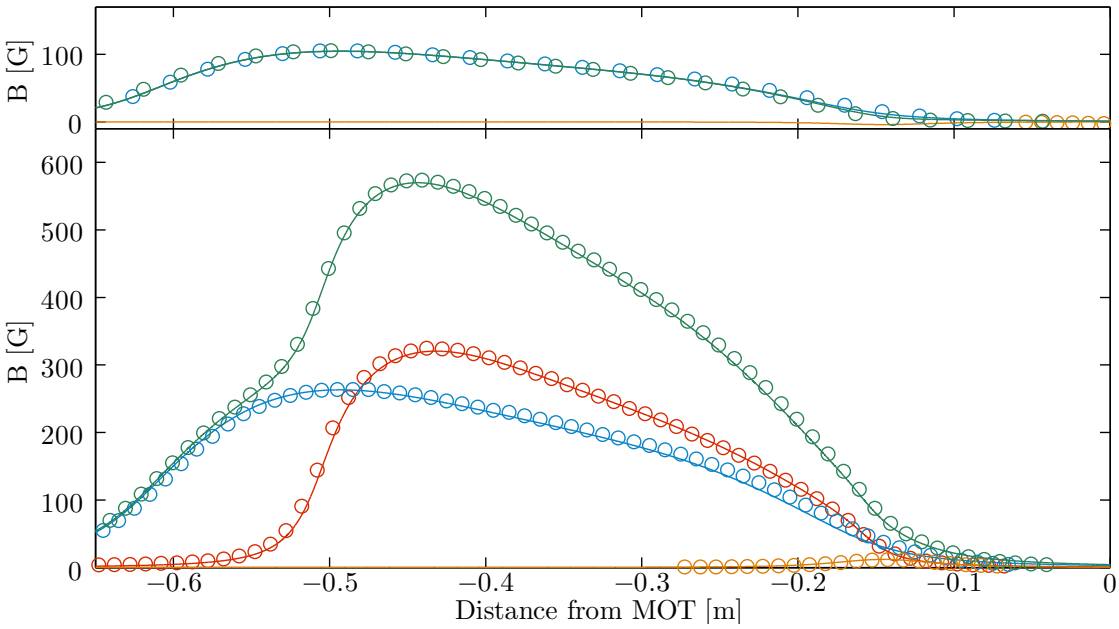

Figure 2.5: Magnetic fields of the helical coils and the compensation coil. The fields for deceleration of ^{133}Cs (upper panel) and of ^{6}Li (lower panel) at their design values are shown. The total field (green) is a sum of the fields from the inner helical coils (red), the outer helical coils (blue) and a small field from the adaption coil (orange). The dots are the measured values and the lines represent the results from the parametrization. The only free parameter is a global shift in the positions.

and the gradient fields. In order to mount the coils to our experimental chamber in a way as shown in Fig.2.1, a rotatable flange was cut into two pieces, which allowed the minimal inner diameter of the slower coil to be only slightly larger than the knife edge of a CF 16 flange.

2.3 Main chamber coils

As described in the last section, besides the helical coils, also the radial fields of the MOT coils are required for performing Zeeman slowing. The MOT coils are mounted together with several other coils, witch are needed for subsequent experimental sequences, at the periphery of the main chamber. Their individual properties are described in this section.

- **MOT coils.** The required gradient fields for loading the MOTs are created by two coils in anti-Helmholtz configuration. As described in Sec. 2.2, the radial fields are also used for Zeeman slowing. Each coil consists of 72 windings with a minimal radius $R_0 = 0.1$ m and a minimal distance from the chamber center of $A_0 = 0.102$ m, reflecting the geometry of the experimental chamber. The wires of each coil are arranged as $n = 6$ stacked layers with a distance of $\delta A = 0.0045$ m, where each layer has $m = 12$ windings with a distance of $\delta R = 0.0045$ m. The radial and axial field profiles have been calculated by making use of elliptic integrals [Bergeman *et al.*, 1987]. The design value for the current of the coils during the Zeeman slowing process is $I_{Cs} = 30$ A and $I_{Li} = 97.7$ A, respectively. This current creates magnetic gradients along the axial direction of $\partial B_{Cs}^{axial}/\partial z = 9.5$ G/cm and $\partial B_{Li}^{axial}/\partial z = 31.0$ G/cm. This enables the levitation of ^{133}Cs atoms [Weber *et al.*, 2003a], while loading a ^{6}Li MOT at the same time. The calculated radial field as well as the measured field are shown for the ^{6}Li configuration in Fig. 2.6 b). Each coil was made by first winding three layers out of 4 mm $\times$ 4 mm square copper hollow wires (inner diameter 2.5 mm) which had been shrouded in glass fiber before. Subsequently, the whole coil was first casted by low viscosity epoxy glue followed by an age hardening process for obtaining mechanical stability. The coils were installed at the vacuum chamber after the bakeout procedure. However, the relatively large inductance, caused by the amount of windings and the large coil volume as well as eddy current prevents switching off the coils faster than 10 ms.

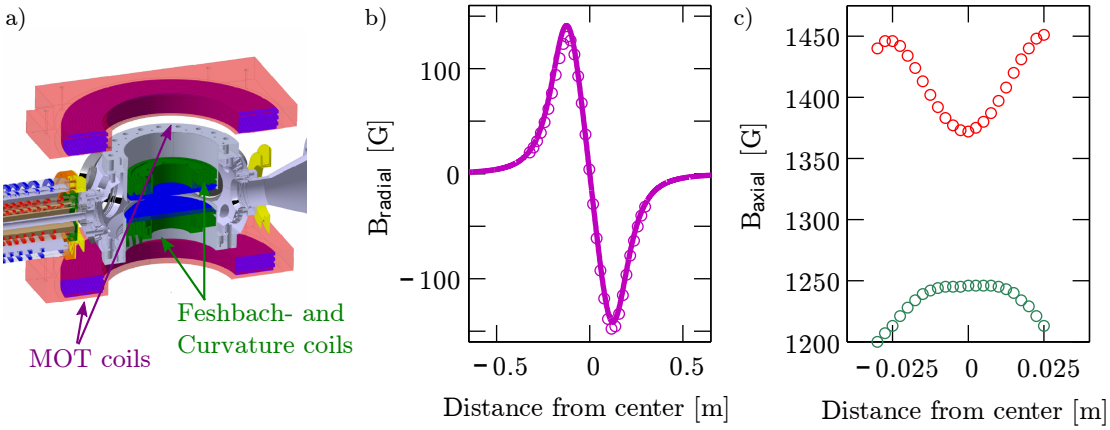

Figure 2.6: Coils at the main chamber. (a) Arrangement of the MOT (violet), Feshbach and Curvature coils (green) with respect to the experimental chamber. (b) Calculated (solid line) and measured radial field of the MOT coils at a current of 97.7 A. (c) Red (Green): Measured fields of the Feshbach coils at a current of 400 A without (with) compensating the field inhomogeneity via the Curvature coils.

- **Feshbach and Curvature coils**[14]. Homogeneous magnetic fields on the order of 1000 G are required to modify the scattering properties of ultracold samples, which is beneficial during an evaporative cooling phase (see Sec. 3.1.2) and necessary for measuring Feshbach resonances (see Sec. 4.4). This is enabled by a pair of two interleaving coils, which are directly mounted within the reentrant viewports of the main chamber (see Fig. 2.6 a)). The outer coils ("Feshbach coil") consists of 2×24 windings and generate a magnetic field of $B \approx 1400$ G at the maximum available current of $I = 400$ A. However, the geometry of the reentrant viewports prevents the realization of a perfect Helmholtz configuration. As seen in Fig. 2.6, this leads to a field inhomogeneity. At the center of the experimental camber, the field along the axial direction z can be approximated by $B_z = B + \alpha B z^2$, where $\alpha = 0.0145$ cm^{-2} reflects the inhomogeneity. In order to overcome this, an additional pair of coils ("Curvature coil") is mounted within the Feshbach coil. Since the coil volume as well as the amount of windings (2×4) of the Curvature coil differs from the Feshbach coil, a different field inhomogeneity is obtained. As depicted in Fig. 2.6 c), a homogeneous total field can be generated, by operating both coils in a Helmholtz configuration with currents in opposite directions. Furthermore, the low inductance of the Curvature coil leads to fast switching

[14] Designed by Rico Pires.

off times below 1 ms. In the experiments presented in this thesis, the MOT gradient after Zeeman slowing is generated by operating the Curvature coil in an anti-Helmholtz configuration, where subsequent sequences, like the Raman side-band cooling, benefit from this much smaller switching times.

- **Raman coil.** In order to perform degenerate Raman-Sideband Cooling (see Sec. 2.7), a precise control over fields on the order of few hundred mG is obligatory. This is enabled by a pair of coils which are directly wound around the flanges of the reentrant viewports. Each coil consists of 10 windings and a homogeneous field is generated by operating them in Helmholtz configuration. Commonly the Raman coil is also used for compensating the vertical magnetic stray fields as well as the earth magnetic field in this direction.

- **Compensation coils**[15]**.** The earth magnetic field as well stray magnetic fields in the laboratory on the order of two Gauss are compensated by a compensation cage. It has a dimension of 800 mm $\times$ 1380 mm $\times$ 660 mm and consists of 100 windings in x-direction, 150 in y-direction and 100 in z-direction. However, commonly only the fields in the horizontal direction have been created by the coils of the cage.

2.4 Laser system

After the move of the experimental setup from Freiburg to Heidelberg, besides the vacuum system, also the laser system has been completely re-designed. In contrast to the old setup (see [Kraft, 2006; Lange, 2008; Deiglmayr, 2009]), where the light was prepared by using several low power diode lasers which were locked to master lasers, the new design benefits from the ability of commercially available high power diode laser systems, which are nowadays available. This led to the implementation of a setup, where the different beams are generated out of few individual frequency stabilized lasers. In order to reach a high degree of passive stability as well as to ensure an easy realignment, various optical fibers are used. Furthermore, the lengths of the individual beam paths are minimized, especially for the MOT and Raman lattice beams, where intensity drifts where assumed to be critical for obtaining stable performance of the cooling schemes.

[15]Designed by Rico Pires.

Frequency preparation

A variety of laser beams of different frequencies and intensities are needed during an experimental run. This includes light for Zeeman-slowing, MOT cooling and trapping as well as imaging the two species. Furthermore, light for repumping the atoms in the cooling cycle after decay into unwanted states is required. In the case of ^{133}Cs , additional laser beams are needed for DRSC. An overview of the required frequencies as well as the locking scheme can be found in Fig. 2.7. The light at our experiment for laser cooling and absorption imaging at zero magnetic fields is provided by two commercial tapered amplifier lasers[16], which deliver output powers of 800 mW and 400 mW at the wavelengths of 852 nm and 671 nm, respectively ("Cs TA" and "Li TA"). In addition, one diode laser[17] with an output power of 130 mW at its operating wavelength of 852 nm is available ("Cs DL"). However, the coupling efficiency into optical fibers, which are mounted at each laser output[18], reduce the available power to about 60%. Besides the three commercial lasers a further home-build diode laser [Salzmann, 2007] with an output power of about 15 mW at a wavelength of 671 nm is installed at the current setup [Heck, 2012]. The frequency of this laser can be tuned over a large range and provides resonant light for ^{6}Li at high magnetic fields by compensating the Zeeman shift ("Li high-field laser"). The required beams for laser cooling and absorption imaging are prepared on optical setups, which are mounted on three breadboards. The setups using the commercial lasers are well described in the diploma thesis of Stefan Schmidt [Schmidt, 2011] for the ^{133}Cs system and for ^{6}Li in the one of Romain Müller [Müller, 2011], whereas the ^{6}Li high field laser system is part of Robert Heck's master thesis [Heck, 2012].

Fiber Clusters

While the light for ^{133}Cs Zeeman- slowing and repumping as well as for the Raman polarizer beam is directly sent to the experimental chamber via single mode optical fibers, all other beams are first sent to custom made Fiber Port Clusters[19] via optical fibers. These clusters allow for overlapping as well as splitting of different beam powers on a small length scale, which enables stable performance and easy alignment. In the case of the ^{133}Cs MOT beams, the light for the cooler as well as for the repumper is first combined, before six beams, which contain both components at the same polarization, are generated. Similarly, three MOT beams and one beam, which

[16] toptica TA pro 850 / TA pro 670.
[17] toptica DL pro 850.
[18] toptica FiberDock.
[19] Delivered from Schäfter & Kirchhoff.

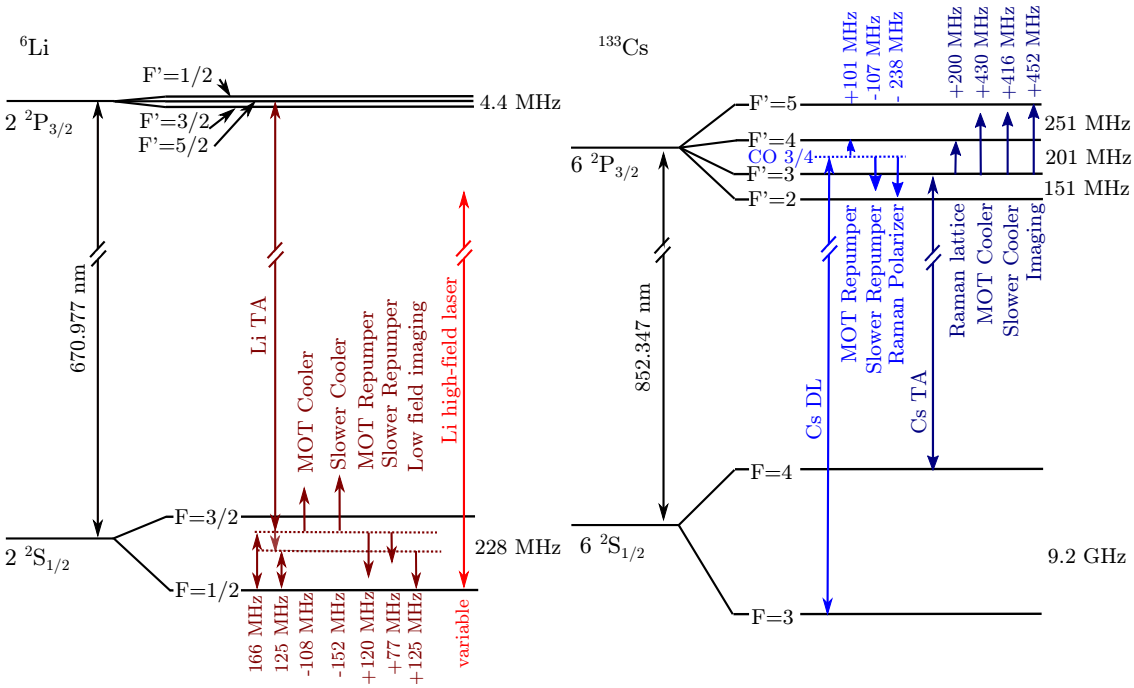

Figure 2.7: Locking scheme. For each species two lasers are available. The Li TA is detuned during the MOT loading (MOT compression and low field imaging) phase by +166 MHz (+120 MHz) from the transition $F = 1/2 \mapsto F'$, whereas the frequency of the Li high-field laser can be flexibly adjusted via an offset lock [Schünemann *et al.*, 1999] to the Li TA. The Cs TA is resonant with the transition $F = 4 \mapsto F' = 3$ and the Cs DL to the cross over peak in the spectroscopy signal between the $F = 3 \mapsto F' = 3$ and $F = 3 \mapsto F' = 4$ transitions (CO 3/4). All different frequency components are generated by AOMs, either in single- or in double pass configuration and typical values are shown. The settings of the Cs MOT Cooler and Cs MOT Repumper correspond to the frequencies during the MOT load. In a subsequent MOT compression phase, the value of the Cs MOT Cooler is changed to + 356 MHz and Cs MOT Repumper to +110 MHz. The values of the level schemes are taken form Gehm, 2003 (^{6}Li) and Steck, 2008 (^{133}Cs).

is used for Zeeman slowing, are generated in the ^{6}Li cube by first combining the two frequency components and afterwards dividing the light intensity. Furthermore, at two outputs at this two Fiber Port Clusters perpendicularly polarized light compared to the one of the MOT beams can be added. This allows to perform absorption imaging on the same optical axes, via using additional fiber based entrances. A further cluster is available, which splits the light for the Raman lattice into four beams. All outputs are connected with additional single mode fibers, which are used for sending the light to the main chamber.

Beam paths for laser cooling at the main chamber

One challenge during the design of an ultracold experiment, especially if two species are involved, is to minimize the amount of beam paths at the main chamber region. At our experimental setup, this is done by further combining several beams for the ^{6}Li and ^{133}Cs in front of the experimental chamber by using dichroic optics [Schmidt, 2011]. As depicted in Fig. 2.8, where the arrangement of the different laser beams is shown, only four optical axes are needed for Zeeman slowing, magneto-optical trapping as well as absorption imaging along two axes. This ensures enough space for the installation of additional beam paths, which are needed to perform degenerate Raman-Sideband cooling as well as for confining the atoms in optical dipole traps (see. Sec 3.2.2).

The ^{133}Cs MOT is set up out of six individual beams out of optical fibers, where fiber couplers[20] collimate each beam to a $1/e^2$ diameter of 20 mm. In contrast to ^{133}Cs , where the used cooling transition is nearly closed and therefore only a low intensity for ensuring repumping is necessary, the not resolved hyperfine manifold of the excited $2^2\mathrm{P}_{3/2}$ state of ^{6}Li requires comparable laser intensities for the $2^2\mathrm{S}_{1/2}, \mathrm{F} = 3/2 \rightarrow 2^2\mathrm{P}_{3/2}, \mathrm{F} = \mathrm{F}^*$ and $2^2\mathrm{S}_{1/2}, \mathrm{F} = 1/2 \rightarrow 2^2\mathrm{P}_{3/2}, \mathrm{F} = \mathrm{F}^*$ transitions. Furthermore, the available laser power for ^{6}Li is about half compared to the one for ^{133}Cs . To have sufficient laser intensity available for operating a ^{6}Li MOT, the beams are set up by three retro reflected laser beams. The beam diameters are expanded via fiber couplers[21] to $1/e^2$ diameter of 25 mm, which accounts for the transversal expansion of the atomic beam after Zeeman deceleration (see Sec.2.2). In order to prepare circularly polarized light out of the linearly polarized beams from the fibers, low order quarter waveplates[22], which operate for both wavelengths simultaneously, are mounted in front of the chamber.

[20] 60SMS-1- 4-A11-02, Schäfter & Kirchhoff.
[21] 60FC-T-4-M125-13, Schäfter & Kirchhoff.
[22] WPD0138-670;852, Döhrer Elektrooptik.

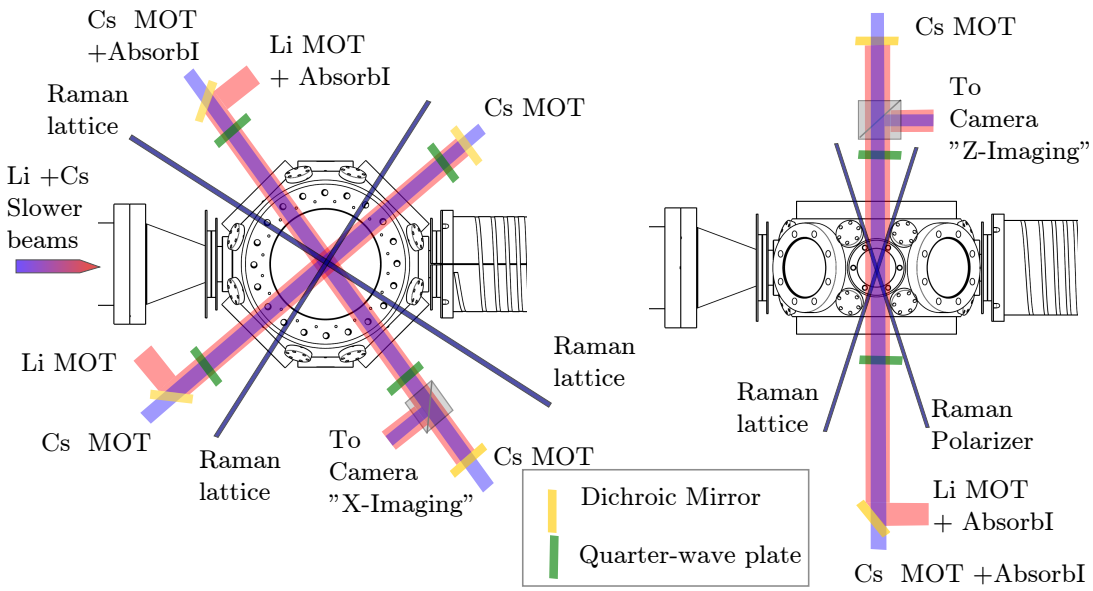

Figure 2.8: Top and side view on the experimental chamber illustrating the beams used for laser cooling. The ^{133}Cs MOT is set up out of three individual beams whereas for the ^{6}Li MOT a design out of three retro-reflected beams is implemented. Various beams are multiplexed in order to minimize the amount of optical axes.

The focused beams for Zeeman slowing match the MOT beam diameters at the center of the experimental chamber with a focal point slightly behind the oven chamber.

2.5 Detection methods

In order to perform experiments, a control over different laser powers and intensities as well as magnetic fields is required. This is reached via controlling the devices in our lab by using analog and digital in- and output channels of a FPGA based experimental control system, which has been developed in the institute's electronic workshop. The individual timings of the channels can be set via a LabView interface[23].

Absorption imaging

All relevant information of the properties of the atomic cloud are deduced by absorption imaging [Ketterle *et al.*, 1999] as the last step of each experimental cycle.

[23]Programmed by Juris Ulmanis and Hanna Schempp.

During this destructive method, three images are taken: (1) an absorption image via illuminating the atomic cloud with a resonant laser beam, (2) a division image with the same laser intensities but without atoms, as well as (3) a background image without laser beams. The intensity distributions of each camera pixel at the position (x, y) are $I_{abs}(x, y)$, $I_{div}(x, y)$ and $I_{back}(x, y)$, respectively.

The intensity $I(x, y)$ of a beam of initial intensity $I_0(x, y)$ after propagating in z-direction through an atomic cloud, characterized by a density $n(x, y, z)$, can be described by Beer's law:

$$I(x, y) = I_0(x, y)e^{-\sigma \int n(x,y,z)dz}. \tag{2.1}$$

Here, σ denotes the absorption cross section.

The column density $n(x, y) = \int n(x, y, z)dz$ of each pixel can be obtained by first calculating the transmission $T(x, y)$ of the laser beam via

$$T(x, y) = \frac{I(x, y)}{I_0(x, y)} = \frac{I_{abs}(x, y) - I_{back}(x, y)}{I_{div}(x, y) - I_{back}(x, y)} = e^{-\sigma \int n(x,y,z)dz}. \tag{2.2}$$

The column density is then given by

$$n(x, y) = -1/\sigma \; ln[T(x, y)]. \tag{2.3}$$

To extract atom numbers as well as cloud sizes, two dimensional density profiles are fitted to column density profiles. In the case of thermal clouds, which was the case for all the presented results besides the molecular ^{6}Li BEC (see Sec. 3.4.3), two dimensional Gaussian profiles have been used. For a cloud of N atoms, which is centered at a position (x_0, y_0) and tilted by an angle θ with respect to the camera axis, the column density $n(x, y)$ can be fitted as

$$n(x, y) = \frac{N\sigma}{\sqrt{2\pi\Delta_x}\sqrt{2\pi\Delta_y}} e^{-[\alpha(x-x_0)^2+2\beta(x-x0)(y-y_0)+\gamma(y-y_0)^2]} \tag{2.4}$$

with coefficients $\alpha = \frac{cos^2(\theta)}{2\Delta_x^2} + \frac{sin^2(\theta)}{2\Delta_y^2}$, $\beta = -\frac{sin(2\theta)}{4\Delta_x^2} + \frac{sin(2\theta)}{4\Delta_y^2}$ and $\gamma = \frac{cos^2(\theta)}{2\Delta_y^2} + \frac{sin^2(\theta)}{2\Delta_x^2}$. Here Δ_x and Δ_y denote the $1/e^2$ radi of the cloud along their main axis. This fits were used to determine the atom number as well as cloud extensions after each experimental cycle.

Time-of-flight thermometry

The temperatures of the prepared atomic clouds are deduced in our experiment by investigating the ballistic expansion of the clouds. This is done by varying the delay time t before absorption imaging is performed. The expansion dynamics of a thermal cloud along the x or y direction is given by

$$\Delta_{x/y}(t) = \sqrt{\frac{Tk_B}{m}t^2 + \Delta_{x/y}(t=0)}. \tag{2.5}$$

Fits to this formula are used in the experiment to extract the temperature T for a species of mass m.

Density determination

The three dimensional atomic density distribution $n(x, y, z)$ of a thermal cloud, centered at a position (x_0, y_0, z_0), is given by

$$n(x, y, z) = \frac{N}{\sqrt{2\pi\Delta_x}\sqrt{2\pi\Delta_y}\sqrt{2\pi\Delta_z}} e^{-[\frac{(x-x_0)^2}{2\Delta_x^2} + \frac{(y-y_0)^2}{2\Delta_y^2} + \frac{(z-z_0)^2}{2\Delta_z^2}]}, \tag{2.6}$$

where the value $n_0 = n(x_0, y_0, z_0)$ denotes the peak density. In order to deduce the atomic density distribution, knowledge about the cloud size along the integration direction of the camera is required. This can be obtained via symmetry arguments due to the underlying confining potential $U_{ext}(x, y, z)$, by setting the unaccessible cloud extension Δ_z along the integration axis z in relation to the fit values for Δ_x and Δ_y.

In the case of a three-dimensional harmonic potential $U_{ext}(x, y, z)$, characterized by trapping frequencies ω_x, ω_y and ω_z, $U_{ext}(x, y, z)$ can be written as

$$U_{ext}(x, y, z) = \frac{1}{2}m(\omega_x^2 x^2 + \omega_y^2 y^2 + \omega_z^2 z^2). \tag{2.7}$$

The density distribution is then given by [Grimm *et al.*, 2000]

$$n(x, y, z) = n_0 e^{-\frac{U_{ext}(x,y,z)}{k_B T}}, \tag{2.8}$$

A comparison between eq. 2.6 and eq. 2.8 leads to $\Delta_{x/y/z} = \frac{\sqrt{k_B T/m}}{\omega_{x/y/z}}$. Therefore, atomic density distributions can be deduced by an independent measurements of the trapping frequencies, the temperature as well as the atom numbers. Since the optical dipole traps in our experiment are well described by such three-dimensional harmonic

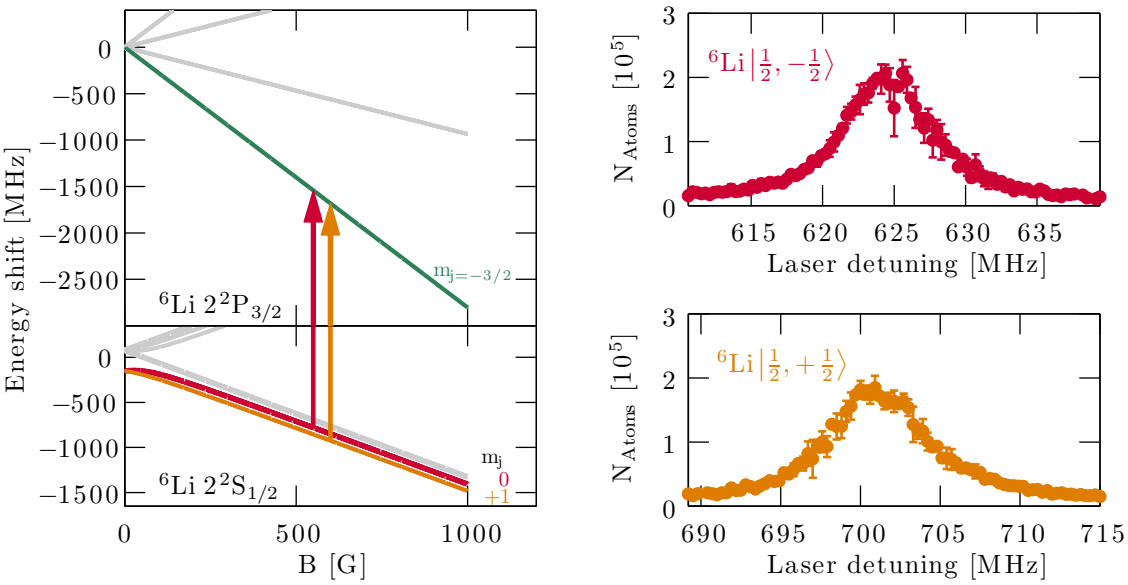

Figure 2.9: Spin selective detection of ^{6}Li at high magnetic fields Left side: Shift of levels in the ^{6}Li $2^2S_{1/2}$ and ^{6}Li $2^2P_{3/2}$ states. The red (orange) arrow mark the transition used for spin selectively removing and imaging atoms in the m_j =0 (m_j =1) state, corresponding to the $|F = 1/2, m_F = -1/2\rangle$ ($|1/2, +1/2\rangle$) state at zero magnetic field. Right side, upper (lower) panel: Frequency dependence of the absorption signal at a magnetic field B= 507.9 G, corresponding to atoms in $|F = 1/2, m_F = -1/2\rangle$ ($|1/2, +1/2\rangle$) state. The data points are taken from Heck, 2012.

trapping potentials (see Sec. 3.2.2), this method is used. Precise measurements of the trapping frequencies can be realized by two cameras where the positions and sizes along all three spatial directions can be deduced.

Cameras and cross sections

Two CCD cameras[24] are currently available in the experiment (see Fig.2.8 for their arrangement). One of them provides images from the top view for measuring horizontal trapping frequencies as well as to align the crossings of the dipole traps. The second one, which is commonly used for deducing atom numbers and temperatures, enables imaging on a horizontal plane. This camera was calibrated by using the center-of-mass dynamics of a freely falling ^{133}Cs atomic cloud in the presence of gravitational forces, where an effective pixel size of 7.84 μm $\times$ 18.4 μm was deduced.

Special care needs to be taken on the value of the absorption cross section σ.

[24]Both Guppy-38B, Allied Vision Technology.

The ^{133}Cs atoms are up to now[25] imaged at zero magnetic offset fields. Therefore the value of $\sigma_{\mathrm{Cs}} = 3.468 \cdot 10^{-9}$ cm^2 [Steck, 2008] for circular polarized light was used. In the case of ^{6}Li , the atoms are mostly imaged at magnetic fields within the Paschen-Back regime, where closed optical transitions are available. For imaging along the horizontal direction, the magnetic field is perpendicularly orientated with respect to the propagation direction of the circular polarized laser beam. Taking the resulting projections into account, this leads to a reduction of the cross section of properly polarized light of $\sigma_{\mathrm{Li}} = 5.374 \cdot 10^{-10}$ cm^2, which has been used for zero field imaging, by a factor of four to $\sigma_{\mathrm{Li}} = 1.3435 \cdot 10^{-10}$ cm^2 for high field imaging (see Heck, 2012 for details). The involved atomic states during high field imaging as well as scans, showing the frequency dependent absorption profiles, are depicted in Fig. 2.9. A detailed description of the high field laser system where lithium atoms can be imaged as well as removed up to magnetic fields of 1300 G, is given in the master thesis of R. Heck [Heck, 2012].

At the experimental apparatus, the imaged atomic clouds are commonly directly analyzed via a Matlab based graphical user interface, which is triggered by the experimental control. Furthermore, in order to improve the quality of the images, a fringe removal algorithm[26] [Ockeloen *et al.*, 2010] is often applied during post processing, especially in the case of small atom numbers.

2.6 Magneto-optical traps

A common method in ultracold experiments is to trap the atoms in magneto-optical traps (MOTs) [Raab *et al.*, 1987; Metcalf and van der Straten, 2003], where temperatures in the μK regime can be reached. In order to reach small cycle times, a high loading rate is usually desired. This holds especially for our sequential loading scheme. Since the first loaded species needs to be confined during the loading of the second one, large capture rates of the second species are advantageous to minimize the amount of losses. MOT loading rates can be extracted by recording the number of atoms in a MOT after different loading times. A typical loading curve for ^{133}Cs is depicted on the left part of Fig. 2.12, where a loading rate of $\mathrm{R}_{\mathrm{Cs}} = 2.1 \cdot 10^8$ atoms/s was deduced by a fit. The dynamics are an interplay of increasing the atom number via Zeeman decelerated atoms as well as density dependent loss mechanism from one-body collisions between MOT atoms and background gas atoms as well as two-body collisions from light assisted- and hyperfine changing collisions. In order

[25] A Cs high field imaging system is being currently set up.
[26] Provided by Shannon Whitlock.

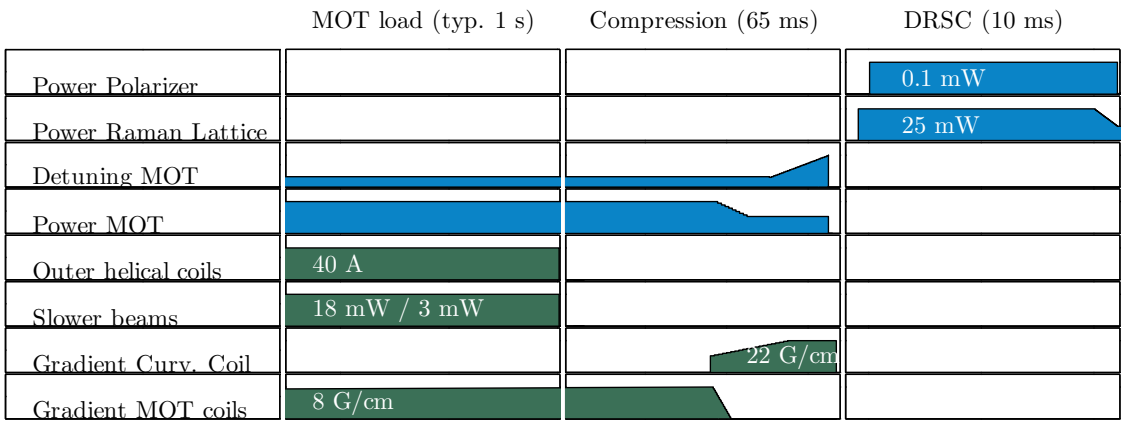

Figure 2.10: Typical sequence for the loading and the compression of a ^{133}Cs MOT as well as for DRSC. 35 ms after the coils as well as cooling and repumping laser beams for Zeeman decelerating are turned off, the MOT is compressed by increasing the gradient along the strong axis from 10 G/cm to 22 G/cm by decreasing the current in the MOT coils within 5 ms and increasing the current in the Curvature coils within 20 ms. At the same time the laser power of the cooler (repumper) laser beams is decreased (see text for values). 5 ms later the detuning of the cooler (repumper) laser beams is decreased (increased) within 25 ms from 430 MHz (100 MHz) to 354 MHz (110 MHz) with respect to the operating frequency of the lasers (see Fig. 2.7). The compression phase is completed 2 ms latter by switching off the laser beams followed by extinguishing the gradient fields 2 ms later. 2 ms after the gradient fields are turned off, the atoms are transfered into the Raman lattice. DRSC starts 1 ms later by turning on the polarizing beam, while the power of the lattice is decreased within the last 2 ms. Typical atom numbers are $N_{\mathrm{Cs}} = 2 \cdot 10^8$, $N_{\mathrm{Cs}} = 7 \cdot 10^7$ and $N_{\mathrm{Cs}} = 2 \cdot 10^7$ after the MOT load, the compression phase and the DRSC, respectively. The temperature is reduced from $T_{\mathrm{Cs}} \approx 300\ \mu$K after the loading of the MOT to $T_{\mathrm{Cs}} \approx 1\ \mu$K after the DRSC.

to account for this, a formula [Stuhler, 2001] using an effective volume for describing the density distribution was applied for the fit. To limit the systematic errors during the atom number detection, locally varying Zeeman shifts, which arise during the switch off of the magnetic gradient fields, need to be avoided. The slow expansion dynamics of the ^{133}Cs cloud allows for imaging the atoms after 30 ms, even for typical temperatures on the order of several hundred μK. Since this timescale is longer than the switching off time of our MOT coils (on the order of 10 ms) only negligible errors remain. However, the much faster expansion of the much lighter ^{6}Li atoms prevents an accurate atom number detection of MOT atoms, which have temperatures on the order of $\mathrm{T_{Li}} \approx 500\ \mu K$.

Colder temperatures and higher densities are advantageous for the following

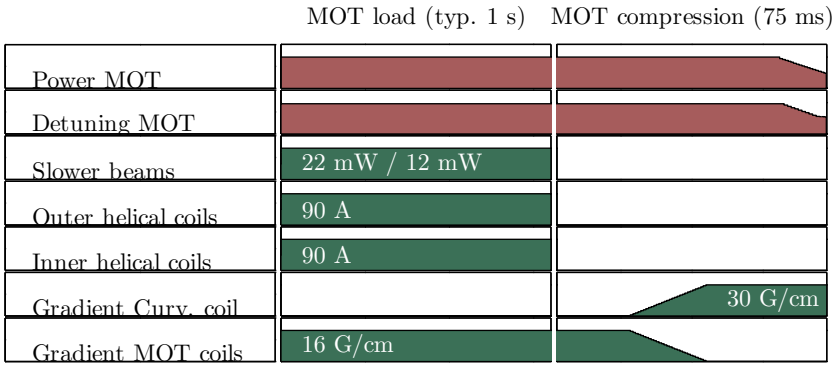

Figure 2.11: Typical sequence for the loading and the compression of a ^{6}Li MOT. Compression of the ^{6}Li MOT is performed by increasing the gradient along the strong axis within 20 ms to 36 G/cm by decreasing (increasing) the current in the MOT coil (Curvature Coil) 20 ms after the Slower beams and Coils are turned off. 20 ms later, the detuning of the MOT beams is decreased in a 10 ms long ramp by changing the lock point (see Fig. 2.7) of the laser. At the same time the power of the cooling and repumping beams is decreased within 15 ms (see text for values). At this stage 10^8 ^{6}Li atoms are trapped and the temperature is $T_{\mathrm{Li}} \approx 300\ \mu$K.

sequences like DRSC of ^{133}Cs as well as for transfer of ^{6}Li atoms into optical dipole traps. They can be reached in the subsequent compression phases. An overview over the sequences is depicted in Fig. 2.11 and Fig. 2.10. The densities for both species are increased after the MOT loading by lowering the beam intensities that minimizes repulsive forces arising from multiple scattering of photons and reduces light assisted collisions. A further compression of the clouds is reached by increasing the magnetic field gradient [DePue *et al.*, 2000]. In contrast to the Zeeman- slowing phase, the long range part of the radial gradient field is not any more important at this stage and the gradient is commonly provided by operating the Curvature coils in an anti-Helmholtz configuration. This is done by lowering the current of the MOT coils while simultaneous turning on the Curvature coils. The gradient fields can be then switched off on a time scale of 1 ms, which is especially important for performing DRSC on ^{133}Cs afterwards. Furthermore, the temperature decreases in this compression phase. For ^{133}Cs , temperatures on the order of some μK can be reached by performing sub-Doppler cooling via increasing the detuning of the laser beams [Drewsen *et al.*, 1994]. In the case of ^{6}Li the not resolved hyperfine structure of the excited $2^2\mathrm{P}_{3/2}$ state prevents to prepare atoms at sub-Doppler temperatures in a MOT[27]. Therefore, the detuning of the laser beams are decreased to a value

[27]Lasers for implementing more sophisticated cooling schemes are currently not available in the experiment. Recently, much lower temperatures were obtained, using gray molasses cooling at the

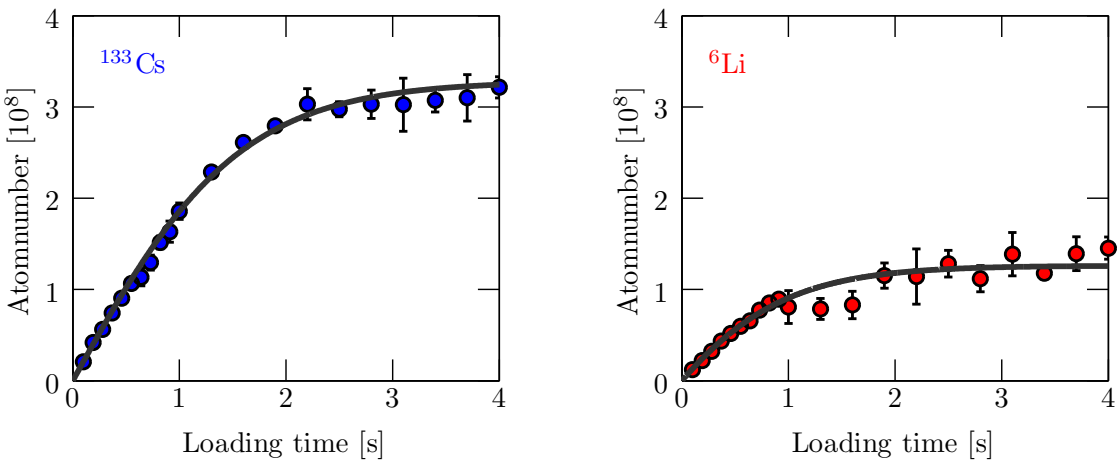

Figure 2.12: MOT loading curves. Time dependence of the number of ^{133}Cs atoms (left) in a MOT and ^{6}Li (right) after a subsequent compression phase. A loading rate of $R_{Cs} = 2.1 \cdot 10^8$ atoms/s for the ^{133}Cs MOT and a corresponding rate after the compression phase of $R_{Li} = 1.3 \cdot 10^8$ atoms/s for ^{6}Li where deduced by fits (gray), including one- and two body loss mechanisms. The compression as well as a reduced absorption during the imaging process (see text) leads to an underestimation of the ^{6}Li MOT loading rate. The Cs (Li) reservoir temperatures at the oven was $T_{Cs} = 120°C$ and $T_{Li} = 370°C$, respectively.

corresponding to half of the natural line width, where the lowest temperatures are expected. The reduced temperatures of $T_{Li} \approx 300\ \mu K$ in combination with the fast switching times enable to perform absorption imaging of ^{6}Li at this stage. As depicted in Fig.2.12 fluxes of $R_{Li} = 1.3 \cdot 10^8$ atoms/s can be deduced via recording the atom number. However, possible losses during this compression phase, lead to an underestimation of the loading rate of the ^{6}Li MOT without compression. A further systematic error remains from the value of the cross-section of the atom-light interaction at zero magnetic field. It is caused by the not resolved hyper fine structure, where atoms can be optically pumped into the upper hyperfine state. This is a dark state at the employed imaging scheme, where no repumper was present during the measurements, what leads to a further underestimation of the atom number.

Typical sequences for loading as well as compressing the MOTs are depicted in Fig. 2.10 and Fig. 2.11 for the case of ^{133}Cs and ^{6}Li , respectively. The different beam powers have been experimentally optimized and typical values are given here, whereas the frequencies are depicted in Fig. 2.7, where the looking scheme and the

D1 line [Fernandes *et al.*, 2012] or using additional narrow lines [Duarte *et al.*, 2011].

frequency preparation is shown. Common powers for the MOT loading per beam in front of the experimental chamber are $P^{Cs}_{MOTCool} = 7$ mW, $P^{Li}_{MOTCool} = 3$ mW, $P^{Cs}_{SlowerCool} = 18$ mW, $P^{Li}_{SlowerCool} = 22$ mW, $P^{Cs}_{MOTRep} \approx 0.5$ mW, $P^{Li}_{MOTRep} \approx 3$ mW, $P^{Cs}_{SlowerRep} = 3$ mW, $P^{Li}_{SlowerRep} = 12$ mW, $P^{Cs}_{AbsI} \approx 1$ and $P^{Li}_{AbsI} \approx 1$ mW. The values after the compression phases are $P^{Cs}_{MOTCool} = 4$ mW, $P^{Cs}_{MOTRep} \approx 0.05$ mW, $P^{Li}_{MOTCool} = 0.2$ mW and $P^{Li}_{MOTRep} \approx 0.05$ mW. Here, the power in the MOT beams are given for the beams along the weak magnetic gradient axes. The perpendicular MOT beams have about twice the power in the case of ^{133}Cs and two third in the case of ^{6}Li .

2.7 Degenerate Raman-Sideband Cooling

As the last step of laser cooling, the ^{133}Cs atoms are further cooled and spin polarized into their energetically lowest state $6^2S_{1/2}\,|F = 3, m_F = 3\rangle$ via three-dimensional degenerate Raman-Sideband cooling (DRSC) [Kerman *et al.*, 2000]. The working principle is depicted in Fig. 2.13 (a). Atoms are confined in an optical lattice ("Raman lattice"), which is characterized by an energy spacing $E_{vib} = \hbar\omega$ of the vibrational energy levels ν_i. In addition, a magnetic field $B = \hbar\omega/(g_F\mu_B)$ is applied, where g_F denotes the Landé factor and μ_B Bohr's magneton. This generates a Zeeman shift on the levels $|m_F|\nu_i\rangle$ and $|m_F \pm 1|\nu_i \pm 1\rangle$ such that their energy levels become degenerate. A circular polarized component of the optical lattice enables Raman transitions between such levels by scattering of lattice photons. Furthermore an additional laser beam which drives transitions into the $6^2P_{3/2}, F' = 2$ manifold is applied. A strong σ^+ component of the light polarization leads to a change of the magnetic sublevel by either $m_F = +1$ or $m_F = +2$ after a spontaneous decay back into $F = 3$ manifold during one pumping cycle, in the case that the atoms do not decay back into the original state. In the Lamb-Dicke regime, where the vibrational spacing extends recoil energy, the vibrational quantum number ν_i remains unchanged during the optical pumping cycle. Thus, the state of the atom is transfered from $|m_F|\nu_i\rangle$ to $|m_F + 1|\nu_i\rangle$ or $|m_F + 2|\nu_i\rangle$, which can be converted via subsequent Raman processes to $|m_F + 1 - k|\nu_i - k\rangle$ or $|m_F + 2 - k|\nu_i - k\rangle$, where k is a positive integer number. After several cycles this leads to optical pumping of population into the dark states $|m_F = 3|\nu_i = 0\rangle$,$|m_F = 3|\nu_i = 1\rangle$ and $|m_F = 2|\nu_i = 0\rangle$. A small linear polarized component of the optical pumping laser, leads to a further depletion of the $|m_F = 2|\nu_i = 0\rangle$ and, in combination with Raman transitions, of the $|m_F = 3|\nu_i = 1\rangle$ level. Consequently atoms in their internally lowest state remain

at the vibrational ground state of the optical lattice.

The implementation in our laboratory follows the realization of Treutlein *et al.*, 2001. The Raman lattice is created from four linear polarized beams and one optical pumping beam ("Polarizer"). The arrangement of the individual beams is depicted in Fig. 2.8 whereas the polarizations are similar to the one's given in Treutlein *et al.*, 2001. The power of each lattice beams (the Polarizer) is $P_{lat} = 25$ mW ($P_{Pol} = 0.1$ mW) in front of the experimental chamber. The frequency of the optical lattice is on resonance with the $F = 4 \mapsto F' = 4$ transitions and therefore red detuned by $\Delta = -9.2$ GHz for atoms in the $|F = 3, m_F = 3\rangle$ state. This ensures, that the lattice acts simultaneously as a repumper for atoms which are spontaneously decaying into the $F = 4$ manifold during the optical pumping cycle [Treutlein *et al.*, 2001]. In order to compensate for the light shift, the optical lattice generates on the $F = 3 \mapsto F' = 2$ transition, the polarizer is about $\Delta = -10$ MHz red detuned with respect to this transition. The beam diameter of $d_{Lat} = 2.2$ mm and $d_{Pol} = 2.5$ mm are generated in front of the experiment chamber via fiber couplers. High mechanical stability is obtained by mounting the fiber coupler together with polarization optics and high quality mirror mounts on massive aluminum blocks. The magnetic fields on the order of some hundred mG are generated by the Raman coil as well as from the coils of the offset cage (see Sec. 2.3 for a description of the coils).

In order to perform Raman-sideband cooling, ^{133}Cs atoms in the $F = 3$ manifold are first prepared in a MOT and further compressed and cooled to sub-Doppler temperatures as described in the previous section. After the laser beams are switched off, the atoms are transfered into the optical lattice by turning it on the maximum available power. Simultaneously, the required magnetic field is turned on. After 2 ms, when the magnetic field from the Curvature coils that generate the gradient field of the MOT, is nearly vanished, the polarizing beam is switched on. After performing DRSC for about 10 ms[28], the laser intensities and the polarizer detuning are decreased within 2 ms. This improves the performance of the DRSC. Atoms, which are not at the center of the Raman beams experience lower vibrational spacings due to the gaussian intensity distribution of the lattice beams. Since this does not match initially to the Zeeman shift, an efficient cooling of these atoms is ensured during this decrease of the lattice power. Typical sequences for loading as well as compressing of a ^{133}Cs MOT as well as for DRSC are depicted in Fig. 2.10. Loading a MOT of $2 \cdot 10^8$ atoms leads to a sample of $2 \cdot 10^7$ atoms at a temperature of $T \approx 1\ \mu K$. The degree of spin polarization can be measured by performing Stern-Gerlach separation,

[28]For preparing the ^{133}Cs atoms for combined trapping of a ^{6}Li -^{133}Cs mixture, which is described in Sec. 3.5, DRSC was performed for about 20 ms.

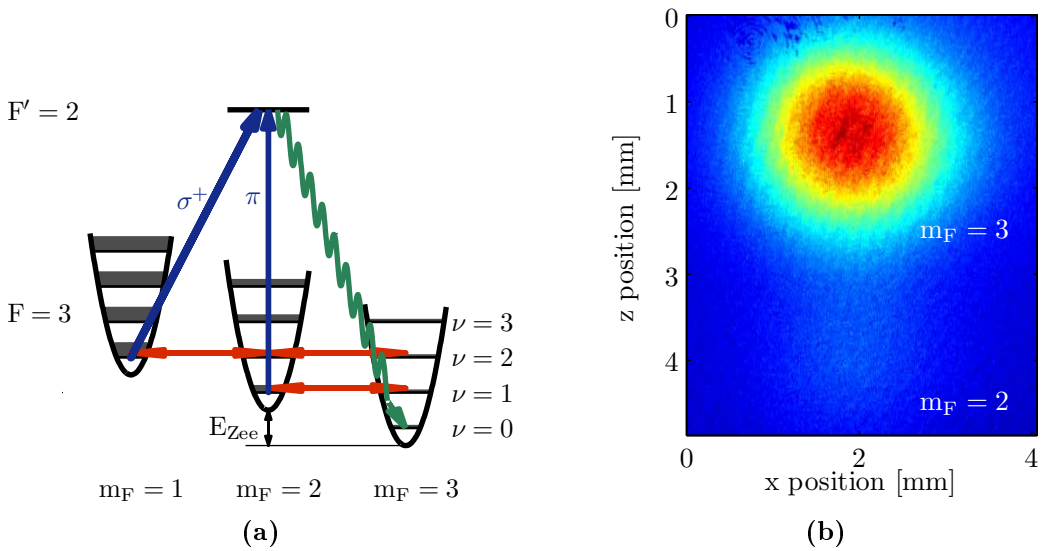

Figure 2.13: Degenerate Raman-Sideband Cooling. (a) Working principle: A Zeeman shift E_{Zee} between neighboring m_F sublevels levels equal to the energy spacing of atoms in an optical lattice enables Raman transitions (red), in which the m_F and the vibrational quantum number ν_i is reduced by one. Optical pumping with an almost circular polarized additional laser beam (blue) and spontaneous decay processes (green) pumps the atoms into their internal and external lowest state $|F = 3, m_F = 3, \nu = 0\rangle$. Adapted from Kerman *et al.*, 2000. (b) False color absorption image after Stern-Gerlach separation after degenerate Raman-Sideband Cooling. Most of the atoms ($\approx 85\%$) are prepared in the $|F = 3, m_F = 3\rangle$ state and the remaining fraction mainly populates the $|F = 3, m_F = 2\rangle$ state.

where the different m_F states are separated after an expansion phase in the presence of a magnetic gradient field. A typical absorption image after Stern-Gerlach separation is shown Fig. 2.13 (b). At our experimental apparatus, typically 85% of the atoms are after DRSC in the state $|F = 3, m_F = 3\rangle$ and about 15% populate the state $|F = 3, m_F = 2\rangle$. It might also be beneficial to perform DRSC with ^{6}Li atoms at a further stage of the experiment. Since not resolved hyperfine structure of the $2^2\mathrm{P}_{3/2}$ prevents efficient optical pumping, transitions into the $2^2\mathrm{P}_{1/2}$ state can be used instead [Vuletić *et al.*, 2001]. However, deep optical lattices are then needed for the light ^{6}Li atoms. This requires large laser intensities in order to fulfill the Lamb-Dicke criterion as well as for obtaining sufficient transfer efficiencies.

Chapter 3

Quantum degeneracy of ^{6}Li and realization of a ^{6}Li -^{133}Cs mixture in an optical dipole trap

During the last decade, enormous progress has been made on the preparation of alkaline mixtures between various different species, resulting in quantum degenerate mixtures of several alkaline combinations [Modugno *et al.*, 2001; Hadzibabic *et al.*, 2002; Goldwin *et al.*, 2004; Inouye *et al.*, 2004; Silber *et al.*, 2005; Taglieber *et al.*, 2008; Catani *et al.*, 2008; Spiegelhalder *et al.*, 2010; Lercher *et al.*, 2011; McCarron *et al.*, 2011; Park *et al.*, 2012]. Despite to the unique perspectives, like the study of the Efimov effect at a large mass imbalanced system [Braaten and Hammer, 2007; D'Incao and Esry, 2006] or the investigation of dipolar effects [Baranov, 2008; Carr *et al.*, 2009] within a sample of deeply bound, polar LiCs molecules [Deiglmayr *et al.*, 2010a], only limited effort was made in preparing ultracold Li-Cs mixtures. In pioneering experiments, Bose-Bose mixtures of ^{7}Li-^{133}Cs were prepared in the focus of a CO_2 laser beam [Mosk *et al.*, 2001], which made for the investigation of interspecies thermalization possible [Mudrich *et al.*, 2002]. In addition, trapped ^{7}Li^{133}Cs molecules were created in such a trap via photoassociation [Deiglmayr *et al.*, 2011a; Deiglmayr *et al.*, 2011b]. However, the Bose-Fermi mixture of ^{6}Li -^{133}Cs has remained unexplored.

This chapter describes important steps towards the realization of a quantum degenerate Bose-Fermi mixture of ^{6}Li -^{133}Cs . The different behaviors of trapped bosons and fermions are shortly reviewed at the beginning of this chapter. Since the employed preparation schemes are based on evaporative cooling of atoms or molecules, this method is also summarized. After briefly mentioning the working

principle of an optical dipole trap, an overview about the realization of such traps in the current experimental setup is given. The final conditions after laser cooling are quite different for the two species, which results in different optical trapping requirements during the preparation of quantum degenerate gases. Therefore two individual traps have been setup and their performance is described within this chapter. A ^{133}Cs sample containing $7 \cdot 10^4$ atoms at a phase-space density $\rho = 4 \cdot 10^{-2}$, which is below quantum degeneracy, was prepared at the ^{133}Cs setup. Quantum degeneracy, manifesting in a molecular Bose-Einstein condensate, was obtained via evaporative cooling a spin-mixture of fermionic ^{6}Li atoms. Furthermore, an all-optical preparation scheme is described, allowing to simultaneously trap an ultracold ^{6}Li - ^{133}Cs mixture by sequentially transferring ^{6}Li and ^{133}Cs atoms into an optical dipole trap with a magnetic field control up to 1300 G. This is the basis for investigating interspecies Feshbach resonances, which is part of the following chapter.

3.1 Bosons and Fermions in harmonic traps

A fundamental property of each particle is its spin, which can either have an integer or a half integer value. This leads to a classification of the particles: particles which possess a spin with an integer value are called *bosons*, whereas particles of half integer spin are labeled as *fermions*. One intention of our experiment is the investigation of both classes: ^{6}Li is a composite fermion, since the total spin, composed of the electronic spin $S_{Li} = 1/2$ and nuclear spin of $I_{Li} = 1$, leads to a half integer value of the total spin. In contrast, both, the nuclear spin $I_{Cs} = 7/2$ and the electronic spin $S_{Cs} = 1/2$ of ^{133}Cs have half integer values. Thus, ^{133}Cs is a composite boson.

The quantum nature leads to different behaviors of both classes. For identical bosons at positions $\vec{r}_1$ and $\vec{r}_2$, the spatial two particle wave function $\psi_{BB}(\vec{r}_1, \vec{r}_2)$ has to be symmetric against the exchange of particles and can be described as a product of the single particle wave functions $\psi_B(\vec{r}_i)$ leading to $\psi_{BB}(\vec{r}_1, \vec{r}_2) = \psi_B(\vec{r}_1) \cdot \psi_B(\vec{r}_2)$. The situation for identical fermions is different. For these, the spatial wavefunction $\psi_{F,F}$ needs to be antisymmetric against the exchange of particles, which results in $\psi_{F,F}(\vec{r}_1, \vec{r}_2) = [\psi_F(\vec{r}_1) \cdot \psi_F(\vec{r}_2) - \psi_F(\vec{r}_2) \cdot \psi_F(\vec{r}_1)]/\sqrt{2}$. This illustrates the *Pauli exclusion principle*: for $\vec{r}_1 = \vec{r}_2$ the spatial wave function $\psi_{F,F}(\vec{r}_1, \vec{r}_2)$ is zero. This prevents, that two identical fermions occupy the same state. For a many-body system, depending on, whether a particle is a boson or a fermion, the mean occupation number $\langle n^i \rangle$ of a level i with an energy ϵ_i needs therefore to be described with different distribution functions: $\langle n_F^i \rangle$ is described for fermions by the Fermi-Dirac

distribution, whereas for bosons $\langle n_B^i \rangle$ is given by the Bose-Einstein distribution:

$$\langle n_F^i \rangle = \frac{1}{e^{(\epsilon_i - \mu)/k_b T} + 1} \tag{3.1}$$

$$\langle n_B^i \rangle = \frac{1}{e^{(\epsilon_i - \mu)/k_b T} - 1}. \tag{3.2}$$

Here, μ denotes the chemical potential. The value of the latter is fixed by the fact, that the total particle number of an ensemble can be obtained for both cases by summing over all states: $N = \sum_i \langle n^i \rangle$.

3.1.1 Bose-Einstein condensates and degenerate Fermi gases

At high temperatures the two equations 3.1 and 3.2 are similar and systems of bosons and fermions are well described by the classical Boltzmann distribution. For $T \to 0$ the behavior differs and, depending on whether the particles are bosons or fermions, a Bose-Einstein condensation (BEC) or a degenerate Fermi gas is created. Quantum gases are often investigated in three-dimensional harmonic potentials. Therefore, the properties of BECs and Fermi gases are discussed for this kind of confinement. Usually, the trapping potential $U_{ext}(x, y, z)$ for a particle of mass m is expressed in terms of the trapping frequencies ω_x, ω_y and ω_z:

$$U_{ext}(x, y, z) = \frac{1}{2} m(\omega_x^2 x^2 + \omega_y^2 y^2 + \omega_z^2 z^2). \tag{3.3}$$

A useful parameter is the mean trapping frequency $\bar{\omega}$, which is given in this case by $\bar{\omega} = \sqrt[3]{\omega_x \omega_y \omega_z}$.

Bose-Einstein condensation

A Bose-Einstein condensate (BEC) is characterized by a macroscopic fraction of population that occupies the energetically lowest state. For a harmonically trapped ensemble, this is depicted on the left hand side of Fig. 3.1. Bose-Einstein condensation occurs below temperatures, where the thermal de Broglie wavelength $\lambda_{dB} = h/\sqrt{2\pi m k_B T}$ becomes comparable to the interparticle spacing n^{-3}, which is equivalent with a phase-space density $\rho = n\lambda_{dB}^3$ on the oder of unity. For a non-interacting, trapped gas, eq. 3.2 allows to deduce the critical temperature T_C at which Bose-Einstein condensation sets in:

$$T_C = 0.94 \frac{\hbar \bar{\omega}}{k_B} N^{1/3}. \tag{3.4}$$

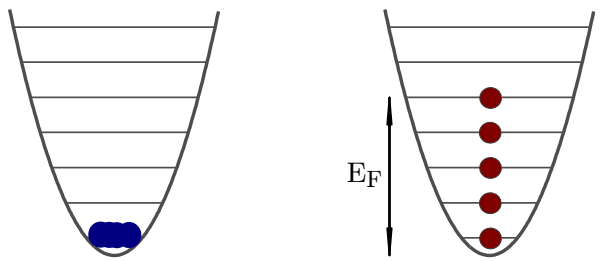

Figure 3.1: Trapped bosons (left) and fermions (right) at zero temperature. The bosons occupy the energetically lowest state, whereas fermions populate states up to the Fermi energy E_F with an occupation number of one.

The number of particles in the lowest state N_0 is for temperatures below the phase transition given by $N_0 = N(1-T/T_C)$, where the ratio N_0/N denotes the condensate fraction.

The properties of an interacting BEC at zero temperature can be extracted from the stationary solution $\Psi(x, y, z)$ of the Gross-Pitaevskii equation (GPe) [Ketterle *et al.*, 1999]

$$\mu\Psi(x, y, z) = \left(-\frac{\hbar^2}{2m}\nabla^2 + U_{ext}(x, y, z) + g|\Psi(x, y, z)|^2\right)\Psi(x, y, z). \tag{3.5}$$

Here, $\Psi(x, y, z)$ denotes the order parameter of the many-body ground state and the atomic density is given by $n(x, y, z) = |\Psi(x, y, z)|^2$. Binary, isotropic interactions of the particles are involved in the GPe via the interaction parameter $g = 4\pi\hbar^2 a/m$, where a represents the scattering length. For strongly interacting BECs, where the interactions dominate over the kinetic energy, the Thomas-Fermi approximation is justified, which neglects the kinetic energy term in the GPe. In this case, the density of a BEC can be written as

$$n(x, y, z) = \max\left(\frac{\mu - U_{ext}(x, y, z)}{g}, 0\right), \tag{3.6}$$

which corresponds to a parabolic density profile in a harmonic trap.

Degenerate Fermi gas

The occupation of a single quantum state by two or more identical fermion is forbidden by the Pauli exclusion principle. Instead, at sufficiently low temperatures, a degenerate Fermi gas is created, where the lowest energy levels are filled with exactly

one fermion per level. In the limit $T = 0$, this defines the so-called Fermi energy E_F, which is equal to the energy of the highest occupied state. The Fermi energy sets the energy scale of a degenerate Fermi gas. Furthermore, it allows to deduce temperature and momentum scales via introducing the Fermi temperature $T_F = E_F/k_B$ and the Fermi momentum $k_F = \sqrt{2mE_F/\hbar^2}$. For a harmonically trapped ensemble, this is depicted on the right hand side of Fig. 3.1. For a three dimensional fermionic system that is trapped in a harmonic potential, the Fermi energy can be expressed via the mean trapping frequency and atom number:

$$E_F = (6N)^{1/3}\hbar\bar{\omega}. \tag{3.7}$$

Molecular Bose-Einstein condensates

A weakly bound, universal dimer state, with a binding energy of $E_B = \hbar^2/(ma^2)$ [Chin *et al.*, 2010] is associated with large, positive scattering lengths in the vicinity of a Feshbach resonance. In the case of a strongly interacting, two component Fermi gas at low temperatures, this state can be populated via three-body recombination processes, where the dimer is created during a collision of three atoms. Since the recombination rate scales with the sixth power of the scattering length [Petrov, 2003], this process can lead to an effective creation of molecules at high densities.

A mixture of atoms and dimers in a two component Fermi gas at a finite temperature T is characterized by a dynamic equilibrium, where on the one hand molecules are formed by three-body processes, but on the other hand, molecules dissociate back into atoms [Jochim *et al.*, 2003a; Chin and Grimm, 2004]. This enables to express the molecular phase-space density ρ_{mol} via the atomic phase-space density ρ_{at} [Chin and Grimm, 2004]:

$$\rho_{mol} = \rho_{at}^2 e^{E_B/(k_B T)}. \tag{3.8}$$

A significant number of molecules is expected for $T \approx E_B/k_B$, which is typically reached at temperatures in the μK regime, whereas by lowering the temperature, a larger molecular fraction is present in the sample. Despite the fact that the dimers are formed out of two fermionic atoms, the total angular momentum of the molecule is an integer number, leading to a bosonic behavior. Therefore, Bose-Einstein condensation of molecules can be obtained when ρ_{mol} slightly exceeds one. This was demonstrated for the first time ten years ago for the two fermionic alkaline isotopes ^{6}Li [Jochim *et al.*, 2003b; Zwierlein *et al.*, 2003] and ^{40}K [Greiner *et al.*,

2003][1].

3.1.2 Evaporation towards quantum degenerate gases

In order to observe a quantum degenerate gas, the phase-space density ρ needs to be on the order of unity. This can not be reached via the application of common laser cooling techniques where the maximal achievable phase-space densities are several orders of magnitude lower. However, a large increase of the phase-space density can be obtained, by performing "forced" evaporative cooling [Ketterle and van Druten, 1996; Luiten *et al.*, 1996]. In such a process, the trap depth is lowered, leading to an ejection of "hot" atoms, whose energies extend the trapping potential, out of the trap. Elastic collisions between the remaining atoms lead to a redistribution of the kinetic energy and the resulting energy distribution can be described as a truncated Boltzmann distribution, with a decreased corresponding temperature. Efficient cooling schemes rely on a good ratio between high elastic scattering rates, which leads to a fast thermalization of the gas, and unwanted inelastic loss rates. A common method for realizing high scattering rates is to perform evaporation close to a Feshbach resonance, where high scattering lengths lead to large elastic collisional cross sections. Additionally, large scattering lengths are also advantageous for performing evaporation within atom-dimer mixtures in two component Fermi gases due to scaling behavior between "good" elastic and "bad" inelastic collision rates: The elastic scattering lengths α_{ad}^{el} (α_{dd}^{el}) for atom-dimer (dimer-dimer) collisions show a $\alpha_{ad}^{el} \propto 1.2\ a$ ($\alpha_{dd}^{el} \propto 0.6\ a$) dependence on the atom-atom scattering length a, while inelastic atom-dimer (dimer-dimer) loss rates β_{ad}^{inel} (β_{dd}^{inel}), arising from decay into more deeply bound molecular states, are strongly suppressed, since $\beta_{ad}^{inel} \propto a^{-3.3}$ ($\beta_{dd}^{inel} \propto a^{-2.55}$) [Petrov *et al.*, 2005]. Furthermore, a good choice of the truncation parameter $\eta = U/k_BT$, which describes the adjusted potential depth U at a given temperature T, needs to be found during performing forced evaporation.

3.2 Optical dipole traps

The production of atomic samples at quantum degeneracy or the capture of a cloud of atoms for a certain time, as needed to perform loss spectroscopy measurements in order to measure Feshbach resonances, requires the availability of a confining

[1] In contrast to the ^{6}Li experiments and the described procedure, ^{40}K Feshbach molecules were actively formed by ramping a magnetic field over a Feshbach resonance.

potential. This can be achieved by the use of optical dipole traps. Their properties and the implementation at the present experimental apparatus is part of this section.

3.2.1 Optical dipole potentials

A widely used method for creating confining potentials is optical dipole trapping [Grimm *et al.*, 2000]. The working principle is based on a fast oscillating electric field $E(t)$ of a laser beam that polarizes an atom. The induced atomic dipole moment $p(t)$ interacts with the electric field and, when averaged over time, a dipole potential $U_{\mathrm{dip}} = -1/2\langle E(t)p(t)\rangle_t$ is created. In the case of a laser field of frequency ω and an intensity $I(x, y, z)$, the dipole potential for an atom can be expressed by [Grimm *et al.*, 2000]

$$U_{\mathrm{dip}}(\vec{r}) = -\frac{3\pi c^2}{2\omega_0^3}\left(\frac{\Gamma}{\omega_0 - \omega} + \frac{\Gamma}{\omega_0 + \omega}\right) I(x, y, z). \tag{3.9}$$

Here, Γ denotes the natural linewidth of the atomic transition at a frequency ω_o. Furthermore a large detuning $|\omega_0 - \omega| >> \Gamma$ is assumed. Due to the selection of the trapping wavelengths, this approximation is valid for the optical dipole traps in our experiment.

A convenient realization of optical dipole traps employs the attractive forces that are created by focusing a red-detuned ($\omega < \omega_0$) gaussian beam. The intensity distribution $I(x, y, z)$ for a laser beam of power P, propagating along the z-direction is given by

$$I(x, y, z) = \frac{2P}{\pi w^2(z)} \exp\left(-2\frac{x^2 + y^2}{w^2(z)}\right), \tag{3.10}$$

where

$$w(z) = w_0\sqrt{1 + \left(\frac{z}{z_{\mathrm{R}}}\right)^2} \tag{3.11}$$

describes the $1/e^2$ beam radius. The minimal radius w_0 is called waist and $z_{\mathrm{R}} = \pi w_0^2/\lambda$ denotes the Rayleigh range for a laser, operating at a wavelength λ.

If the kinetic energy of a cloud is much smaller than the trap depth $U_0 = U_{\mathrm{dip}}(0, 0, 0)$, a harmonic approximation for the trapping potential can be made. The trapping frequencies ω_x, ω_y and ω_z along the radial directions and the propagation direction, respectively, can then be written as

$$\omega_x = \omega_y = \sqrt{\frac{4U_0}{mw_0^2}} \quad \text{and} \quad \omega_z = \sqrt{\frac{2U_0}{mz_{\mathrm{R}}^2}}. \tag{3.12}$$

The Rayleigh ranges are usually on the order of a cm or more, whereas the waists

have typically sizes below 1 mm. This leads to a large asymmetry of the confining potential with only weak trapping frequencies along the propagation direction of the beam. This can be overcome by crossing two laser beams under an angle. In this case, the trapping frequencies are usually determined by the waists of the individual beams. However, in a crossed dipole trap, the effective trap depth is most often equal to the one of the weaker potential.

3.2.2 Realization of trapping potentials

The design of an optical trapping potential requires a proper selection of the size of the trapping volume, the trap depth, as well as the trapping frequencies. In addition, heating effects should be minimized. This can be achieved via a appropriate selection of the laser power, the laser wavelength and the size of the focus.

- **Trapping volume:** At ultracold experiments, optical dipole traps are commonly loaded by transferring either a sample of laser cooled atoms or a further precooled sample, for instance out of a magnetic trap, into the optical dipole trap. In order to reach a good transfer efficiency the trapping volume should be at least on the same order as the extension of the atomic cloud before the transfer. Sufficient spatial overlap is obtained, if the beam waist is on the order of the cloud extension before the transfer.

- **Trap depth:** A further criterion for an efficient transfer is a sufficient trap depth U_0, which is proportional to the beam intensity. A good choice is $U_0 \approx 10k_BT$, where T denotes the temperature of the gas before the transfer. This ensures, that a large fraction of the atoms can be trapped, whereas heating effects, due to a conversion of potential energy into kinetic energy during the transfer, are still moderate.

- **Trapping frequencies:** Since the density of a trapped ensemble is determined by the trapping frequencies, a proper beam power as well as waists need to be found. During the preparation of an ultracold gas, large densities are advantageous because they lead to fast rethermalization times during an evaporation process. Furthermore, at a given atom number, high trapping frequencies are advantageous for the transition temperature of a BEC or result in high Fermi energies (see eq. 3.4 and eq. 3.7). However, possible two- and three-body loss rates depend on the density (see. Sec.4.3). For obtaining large trapping times, the trapping frequencies should be therefore still moderate.

- **Wavelength:** In addition, heating effects, arising from off resonant scattering of trap photons should be minimized. Since the photon scattering rate scales inversely quadratic with the detuning from optical transitions [Grimm *et al.*, 2000], heating can be minimized by the use of laser wavelengths, which are far detuned from all atomic transitions. In ultracold experiments, it is common to use fiber lasers, which are normally operating at wavelengths at 1070 nm and are sufficiently large detuned from the atomic resonances by several 100 nm. At the same time the absorption of laser light enables the use of the same viewport material as the laser beams used for laser cooling, since the absorption of the light at the vacuum viewports is still low.

Important criteria for designing an optical dipole potential are thus the properties of the atomic cloud before the transfer process. In the case of ^{6}Li and ^{133}Cs the conditions are quite different: While ^{133}Cs is routinely laser-cooled in our laboratory to temperatures of $T_{\mathrm{Cs}} \approx 1$ μK, the un-resolved hyperfine structure of the excited $2^2\mathrm{P}_{3/2}$ state in ^{6}Li prevents the application of simple sub-Doppler cooling schemes and ^{6}Li temperatures are on the order of $T_{\mathrm{Li}} \approx 300$ μK. Furthermore, for preparing a quantum degenerate gas of ^{6}Li , a high density of ^{6}Li atoms is advantageous for creating molecules via 3-body recombination (see Sec. 3.4.3). In contrast, too dense samples of ^{133}Cs should be avoided (typically n $> 10^{13}$ atoms/cm^3) because large 3-body coefficients [Weber *et al.*, 2003b] lead to high loss rates in a dense gas. In order to account for the different requirements of the two species, separate dipole traps have been set up: A large volume *levitated Cs trap* for ^{133}Cs and a *Li dipole trap* for ^{6}Li . A sketch of their arrangement is depicted in Fig. 3.2. The powers of each laser beam can be intensity stabilized via servo loops. The strategy of the separate trap design for ^{6}Li and ^{133}Cs is to first prepare individual samples at high phase-space densities at slightly different positions and combine them afterwards. However, in order to identify Feshbach resonances, only moderate phase-space densities are required. Therefore, a sequential loading scheme was applied for preparing a ^{6}Li - ^{133}Cs mixture in the Li dipole trap (see Sec. 3.5).

Li dipole trap

In order to provide an effective trap depth of $U_{\mathrm{Li}} \approx 1.6$ mK for Li during the transfer, a crossed optical dipole trap is formed by two intersecting foci (waists $\omega \approx 60$ μm) of a laser beam from a 200 W Yb doped fiber laser[2] (operating wavelength $\lambda = 1070$ nm). The two beams are crossed by an angle of 8.4° and have perpendicular linear

[2] IPG YLR-200-LP-WC.

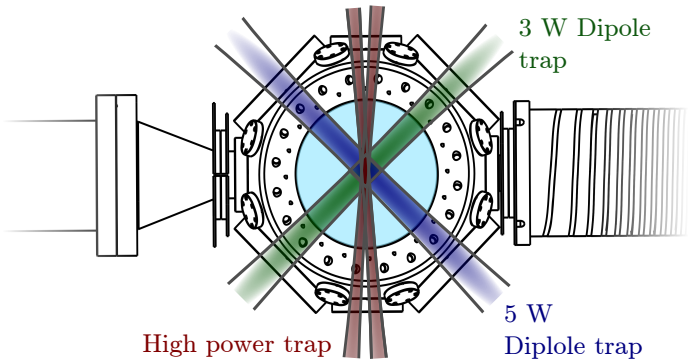

Figure 3.2: Top view of the experimental chamber for illustrating the arrangement of the optical dipole traps. A deep trap for Li can be created by two intersecting foci (waists $\omega \approx 60\ \mu m$) of a retro-reflected laser beam with a crossing angle of 8.4°, delivered by a 200 W laser (red). In addition, a crossed, shallow reservoir traps for ^{133}Cs can be formed out of a 3 W (green) and a 5 W (blue) laser beams with $\omega \approx$ 300 μm and a crossing angle of 90° degrees.

.

polarizations. The maximum achievable power of $P \approx 150$ W per beam in the experimental chamber generates trapping frequencies of $\omega \approx 10$ kHz, which ensures fast thermalization after the transfer process. In addition, one mirror is mounted on a piezo stack, which allows to shift the center position of the trap in subsequent experiments. The design follows an approach, developed within the Jochim group (see e.g. [Ottenstein *et al.*, 2008; Lompe, 2008]). A detailed description about the realization at our experiment is part of the master thesis of Robert Heck [Heck, 2012]. Furthermore, the trapping potential along the propagation direction of one laser beam as well as along the vertical direction is depicted in Fig. 3.3.

Levitated Cs trap

The intention of the implementation of the levitated Cs trap design is to follow the approach of Hung *et al.*, 2008, where the preparation of ^{133}Cs Bose-Einstein condensates on fast time scales is reported. This design consists of very weak optical trapping potentials, which account for the requirements for ^{133}Cs , to avoid too large densities. However, the optical potentials are so weak, that they can not confine the atoms against gravity. This can be compensated via additional magnetic potentials. The complex interplay of the different potentials will be discussed in the following.

The shallow optical trapping potential with an effective trap depth of $U_{\mathrm{Cs}} \approx 3\ \mu$K

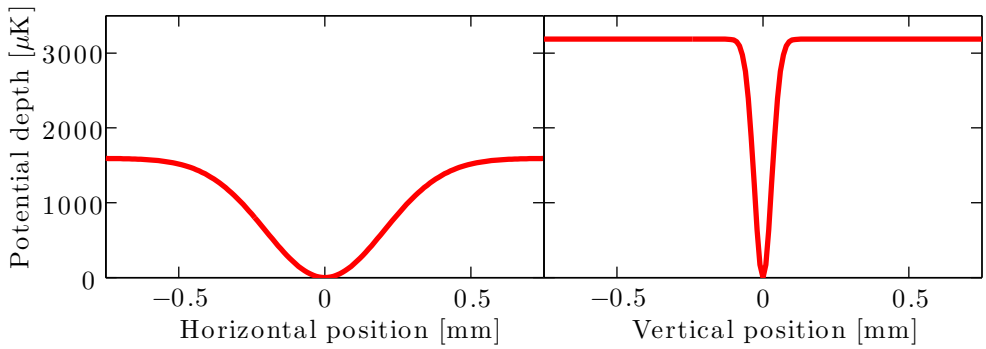

Figure 3.3: Trapping potential of the Li trap. The calculated trapping potential along the propagation direction of on beam (left) and along the vertical direction (right) is shown for Li a laser power of 150 W. The effective trap depth is given by the potential along the horizontal direction. The potential for ^{133}Cs is about four times larger.

.

for ^{133}Cs is realized by crossing two beams out of a 3 W[3] and a 5 W fiber laser[4] under an angle of 90°. Both fiber lasers operate at a wavelength of 1064 nm. The 3 W laser is focused to a waist $\omega \approx 310$ μm and delivers a laser power at the chamber of P=2.2 W, whereas the 5 W laser is focused to a waist of $\omega \approx 320$ μm and provides a power of P=3.6 W. The optical setup is well described within the diploma thesis of Kristina Meyer [Meyer, 2010] (3 W trap) and Romain Müller [Müller, 2011] (5 W trap)[5].

Besides forces arising from the optical potentials, gravitational forces act on the atoms. Therefore, a gravitational potential of $U_{grav} = mgz$ needs to be additionally taken into account. For the light ^{6}Li atoms, this potential is usually small compared to the optical one and can be most often neglected. However, for the heavy ^{133}Cs atoms, the gravitation can strongly influence the total potential. As depicted in Fig. 3.4, in the case of our weak ^{133}Cs traps, the gravitational potential even extends the optical potential, resulting in an acceleration of the atoms out of the trapping region. This can be avoided via applying a further magnetic gradient $\partial B_z/\partial z$ against the direction of gravity [Weber *et al.*, 2003a]. This generates an additional magnetic potential of $U_{mag} = -m_F g_f \mu_B |(\partial B_z/\partial z)| z$ for an atom in a state m_F, where g_f denotes the Landé factor. ^{133}Cs atoms in their energetically lowest state $|\mathrm{F} = 3, \mathrm{m_F} = 3\rangle$ are levitated, meaning that the magnetic gradient and gravitational potentials in z direction cancel each other when a gradient of $|\partial B_z/\partial z|$=31

[3]IPG YLD-3-1064-LP.
[4]IPG YLM-5-1064-LP.
[5]The beam sizes have been slightly modified.

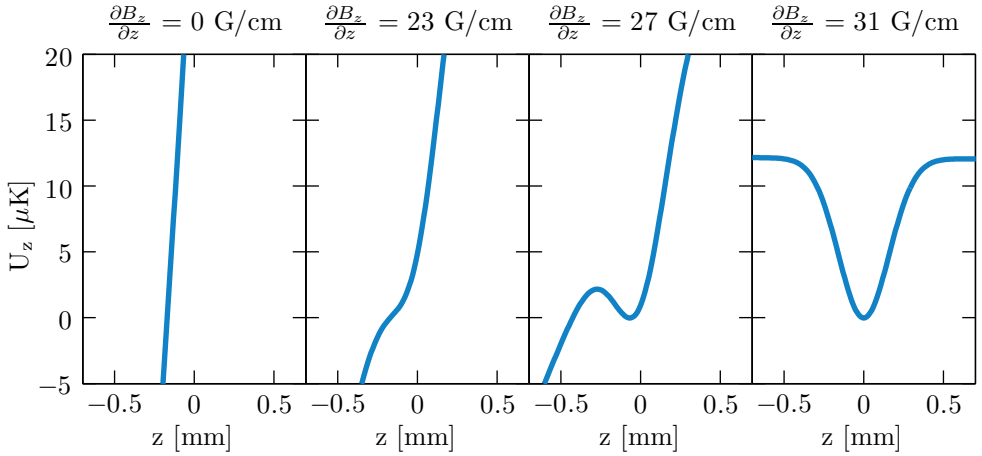

Figure 3.4: Calculated levitated Cs trap potential along the direction of gravity. Without applying a magnetic gradient ($\partial B_z/\partial z = 0$ G/cm) the gravitational potential extends the optical potential and no confinement along the gravitational axis is obtained. The influence of the gravity can be compensated via applying a gradient of $\partial B_z/\partial z = 31$ G/cm. This allows to perform an evaporative cooling scheme, where an increase or a decrease of the gradient reduces the trap depth along this direction [Hung *et al.*, 2008].

G/cm is applied.

However, according to Maxwell's law $\vec{\nabla}\vec{B} = 0$, a gradient in z direction $|\partial B_z/\partial z|$ is associated with a radial gradient[6] $|\partial B_r/\partial r| = 1/2|\partial B_z/\partial z|$. Applying a magnetic gradient leads therefore to a repulsive potential along the radial direction. This can be converted into an attractive configuration by applying an additional offset field via the Feshbach coils. As described in Sec. 2.3, the Feshbach coils deviate from a Helmholtz configuration, which leads to a parabolic shape of the field along the gravitational axis. This axial field inhomogeneity also modifies the directions of the magnetic field lines along the radial direction. For sufficiently large fields, the curvature of a magnetic field can influence the trapping potential so strong, that a two dimensional, magnetic reservoir trap can be created (for details see Hung, 2011). For our setup, the radial potential is depicted in Fig. 3.5 along the optical axis of the weakest confinement where at fields above $B_0 = 120$ G an attractive potential with trapping frequencies of few Hz is generated[7]. Inhomogeneities of the Feshbach coils have been taken into account.

The experimental challenge is to adjust the dipole trap to the center position of the magnetic trap. Furthermore, a small angle of few degrees, between the direction

[6]Here, cylindrical symmetry is assumed.

[7]The axial field from the Feshbach coils was calculated via $B_z(z) = B_0 + \alpha B_0 z^2$, whereas the inhomogeneity factor $\alpha = 0.0145\text{cm}^{-2}$ was deduced by a field measurement.

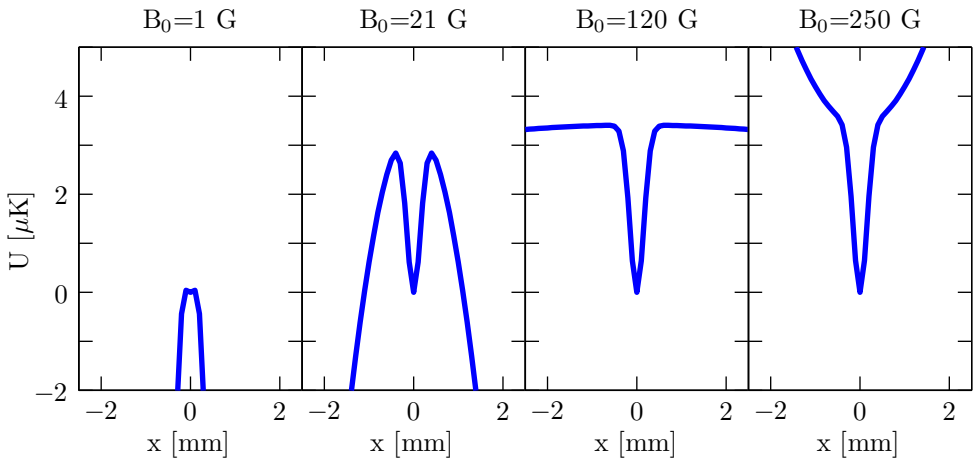

Figure 3.5: Calculated offset field dependency of the radial levitated Cs trapping potential. For four different offset fields B_0 the calculated total potential, consisting of optical and magnetic contributions, is shown for levitated ^{133}Cs atoms along the propagation direction x of the 5 W beam. The radial magnetic fields lead to an anti- trapping potential for offset fields below 120 G, whereas for higher offset fields a large reservoir is created. A field of $B_0 = 21$ G is shown, which is advantageous for creating ^{133}Cs BECs [Weber *et al.*, 2003a].

of strong gradient axis and offset field axis as well as residual fields from connection cables and slightly unsymmetrically winding and mounting the coils, strongly modify the magnetic potential. This is not satisfyingly solved yet at the current setup.

3.3 ^{133}Cs gas at high phase-space densities

This section describes the preparation of a ^{133}Cs gas in the levitated Cs trap. After the transfer of the atoms into the trap and a plain evaporation phase at a levitation gradient, forced evaporation via tilting the trap by changing the magnetic gradient was applied [Hung *et al.*, 2008]. A phase-space density of $\rho = 4 \cdot 10^{-2}$ could be reached, which is below the critical phase-space density for obtaining Bose-Einstein condensation. In order to reach higher phase-space densities, a change of the optical potentials might be beneficial, and a possible implementation is therefore given at the end.

3.3.1 Transfer into the levitated Cs trap

The transfer procedure of the levitated Cs trap starts with loading[8] $3 \cdot 10^8$ atoms in a MOT within 1 s. After a further sub-Doppler cooling and Raman-sideband cooling phase, in a procedure, similar to the one described in Sec. 2.7, $2 \cdot 10^7$ atoms in the energetically lowest state F=3, m_F=3 are prepared at a temperature of $T \approx 1\ \mu$K. The levitated trap design, requires a magnetic gradient field of $\partial B_z/\partial z = 31$ G/cm and benefits from an offset field of $B_0 = 250$ G where the curvature of the field of the Feshbach coil results in an attractive potential (see Sec. 3.2.2 and Fig. 3.4). In order to account for the switching times of the coils on the order of 10 ms, a confinement still is generated by the Raman lattice after DRSC, until the magnetic fields are sufficiently high for levitating the atoms and generating the two dimensional reservoir trap due to the curvature of the Feshbach coil. This is done by switching off the polarizing laser at end of the Raman-sideband cooling phase, while the atoms are still kept in the Raman lattice for about 10 ms. Transfer in the levitated Cs trap is performed afterwards by switching off the Raman lattice. The low power dipole trap beams are either directly switched on to their maximum power already during the MOT loading or within an up to 150 ms long ramp after the Raman lattice is turned off. This minimizes heating effects during a sudden increase of the potential energy and benefits from the ability of levitating the atoms and the radial magnetic confinement as well as the slow expansion time of the atomic cloud of the heavy and cold ^{133}Cs atoms. After a subsequent plain evaporation phase of 500 ms, $N_{\mathrm{Cs}} = 4 \cdot 10^6$ atoms remain at a temperature of $T_{\mathrm{Cs}} = 1.5\ \mu$K. A further measurement of the radial trapping frequencies of the 3 W laser beam (5 W laser beam) yields $\omega_{3\mathrm{W}} = 13$ Hz ($\omega_{5\mathrm{W}} = 16$ Hz). This allows one to deduce a peak density of $n_{\mathrm{Cs}} = 4 \cdot 10^{11}$ atoms/cm^3, which corresponds to a phase-space density of $\rho_{\mathrm{Cs}} = 7 \cdot 10^{-4}$ in this trap.

3.3.2 Evaporation to higher phase-space densities

In order to achieve higher phase-space densities, forced evaporation was applied. This was performed by following the approach of [Hung *et al.*, 2008], by either increasing or lowering the magnetic gradient along the gravitational axis. Because

[8] This atom number is slightly higher the one, obtained in Sec. 2.6 after loading a Cs MOT for 1 s. The fact, that no ^{6}Li atoms are needed during the measurements presented in this section allowed for lowering the temperature of the ^{6}Li reservoir (see Sec. 2.1.1), which leads to a modification of the velocity distribution of the atomic beam. In this case more atoms have velocities below the capture velocity of the Zeeman slower (see Sec. 2.2), what enhances the MOT loading rate by a factor of about two.

the total potential along this direction is the sum of the gravitational and the optical potential, an over- or an under-levitation leads to a tilt of the trap. For the under-levitated case, this is depicted in Fig. 3.4. The trapping frequencies remain in a wide range nearly unchanged. This scheme is advantageous for fast rethermalization, compared to common evaporation schemes, where a decrease of the optical power leads to a reduction of trapping frequencies. Furthermore, it allows to enter the runaway regime, where evaporation occurs with a constant or even increased elastic collision rate [Ketterle and van Druten, 1996].

Various ramps on timescales on the order of several seconds have been tested, mostly by decreasing the gradient to values, corresponding to a nearly vanishing confinement along the gravitational axis. For minimizing three- body losses [Weber *et al.*, 2003b], the magnetic offset field has been commonly lowered to $B_0 = 21$ G at a certain stage. However, the best schemes resulted in an atom number of $N = 7 \cdot 10^4$ at a temperature of $T = 100$ nK. This could be achieved by a 1 s long ramp of the magnetic field after a levitation phase of 1 s, followed by a 1 s long linear decrease of the gradient to $\partial B_z/\partial z = 27.7$ G/cm. The final conditions corresponds to a phase-space density of $\rho = 4 \cdot 10^{-2}$, while the atomic density is similar to the one after the plain evaporation phase. Further forced evaporation resulted in an atom number below the detection limit of our camera at these low densities. An onset of Bose-Einstein condensation was thus never recorded.

A useful parameter for describing the efficiency of an evaporation process is α, which can be calculated by $T(t)/T(0) = [N(t)/N(0)]^\alpha$. Here $N(0)$ ($T(0)$) denotes the atom number (temperature) before and $N(t)$ ($T(t)$) after an evaporation ramp of a duration t [Ketterle and van Druten, 1996]. Using the conditions after the plain evaporation phase and after forced evaporation leads to $\alpha = 0.7$ as total efficiency of our best evaporation schemes. This is below $\alpha = 1$, which is required for entering the runaway regime in a three dimensional trap for the best case, where no inelastic losses occur [Ketterle and van Druten, 1996]. However, such losses are crucial during an evaporation process, since they limit the duration of possible ramps. Taking one-body losses into account, leads to a criterion $R = \Gamma^{\mathrm{el}} \cdot \tau_{\mathrm{loss}} > R_{\mathrm{min}} \approx 300$ for parabolic three dimensional traps [Ketterle and van Druten, 1996]. Here Γ^{el} denotes the elastic scattering rate in the sample and τ_{loss} is the one-body lifetime of a sample, which is in our case given by the vacuum limited 1/e - lifetime of $\tau_{\mathrm{loss}} \approx 5$ s. Using the ^{133}Cs scattering length values of $a_{\mathrm{begin}} = 2131\ a_0$ and $a_{\mathrm{end}} = 217\ a_0$ for magnetic fields of $\mathrm{B}_{\mathrm{begin}} = 250$ G and $\mathrm{B}_{\mathrm{end}} = 21$ G [Julienne, 2012; Berninger *et al.*, 2012], which have been applied at the beginning and at the end of the forced evaporation process and taking furthermore the universal limit into account, leads to $\Gamma^{\mathrm{el}}_{\mathrm{begin}} = 39$

1/s and $\Gamma^{\mathrm{el}}_{\mathrm{end}} = 3$ 1/s which results in $R^{\mathrm{el}}_{\mathrm{begin}} = 195$ and $R^{\mathrm{el}}_{\mathrm{end}} = 15$. For both cases, this is much lower than required for performing evaporation in the runaway regime and demonstrates the fact, that evaporation is not efficient present setup. This is probably caused by the low trapping frequencies during the evaporation phase, which prevent rethermalization of the sample on sufficiently fast time scales. Since the given trapping frequencies in Hung *et al.*, 2008, where runaway evaporation is reported, are about twice as large, as one would expect for the given laser powers and beam diameters, leads to the assumption, that either higher laser powers or smaller beam diameters had been used. Furthermore, the high inelastic one body processes at our setup restricts the lengths of evaporation ramps to a few seconds. Besides improved vacuum conditions, it might be beneficial for subsequent experiments to modify the optical trapping potential in a way, that large volume reservoir trap with increased trapping frequencies is created out of two weaker focused beams at higher output powers, similar to designs, developed in the Grimm group (see e.g. Gustavsson, 2008]). This would create higher collision rates, leading to a faster rethermalization of the atomic samples. In this case, evaporation can be performed on much faster time scales. Moreover, higher transfer efficiencies are then expected.

Besides the presented scheme, which led to a realization of a ^{133}Cs BEC [Hung *et al.*, 2008] at one experimental setup, all other experiments, where the formation of a ^{133}Cs BEC was so far reported [Weber *et al.*, 2003a; Gustavsson *et al.*, 2008; Lercher *et al.*, 2011; McCarron *et al.*, 2011], are based on evaporation within an additional dimple trap [Pinkse *et al.*, 1997; Stamper-Kurn *et al.*, 1998]. By an adiabatic transfer of atoms in such a dimple trap the gain of several orders of magnitude in the phase-space density, leads to dramatically improved starting conditions for a subsequent evaporation phase. However, an initial implementation, based on free propagating laser beams, did not result in larger phase-space densities at the end of the evaporation phase. This was probably caused by bad transfer efficiencies during the loading phase, where collision rates within the reservoir trap were too low for ensuring a transfer on a fast timescale. This might be reached in a modified setup with larger reservoir trapping frequencies. Furthermore, the dimple might be produced by directly focusing down the beam out of optical fibers, leading to an improved beam quality and higher stability.

3.4 Evaporation and Molecular Bose-Einstein condensation of ^{6}Li

This section describes the transfer of ^{6}Li into the Li dipole trap. A subsequent evaporative cooling process enabled the preparation of a molecular Bose-Einstein condensate. The approach follows closely the procedure developed in the Jochim group (see e.g. [Ottenstein *et al.*, 2008; Lompe, 2008; Kohnen, 2008]), which is strongly influenced by pioneering experiments from the Thomas group, where a CO_2 trap [Granade *et al.*, 2002] was used, as well as from the Grimm group, where evaporation was performed in a standing wave trap in combination with a dimple trap [Jochim, 2004]. A detailed description of the realization in our experiment can be found in the master thesis of Robert Heck [Heck, 2012].

3.4.1 Transfer of ^{6}Li atoms into the traps

The transfer cycle starts with loading a ^{6}Li MOT for typical 1 s, where 10^8 atoms are trapped, by using the same laser powers, laser detunings and gradients as given in Sec. 2.6. The first steps improve the transfer efficiency into the optical dipole trap during the compression phase and are similar to the sequence, which has been already described in Sec. 2.6: In order to minimize the temperature and increase the density, the detuning as well as the intensities of the laser beams is decreased. In order to avoid disadvantages due to the relatively large switching times of the MOT coils (see Sec. 2.3), the coils, which deliver the gradient, are exchanged additionally to the much faster Curvature coils[9].

Transfer into the dipole trap starts with turning on the Li trap laser to its maximum output power 5 ms before the completion of the compression phase. This generates an effective trap depth of $U_{\mathrm{Li}} = 1.7$ mK for a laser power of 150 W per beam at the experimental chamber[10]. Furthermore, the repumping laser is switched off 200 μs before the cooling laser at the end of the compression phase. A two component spin mixture of atoms in the energetically lowest F=1/2 manifold is prepared, which is stable against inelastic two body collisions. The transfer process is completed by applying a homogeneous magnetic field close to the broad Feshbach resonance at 832 G. At the same time the gradient fields are switched off. An

[9]Furthermore, the zero position of the Curvature coil defines the center of our experimental chamber for subsequent cycles, such as ^{133}Cs transfer into the dipole trap.

[10]The conditions used for the preparation of Feshbach measurements (see Chapter 4) are given. The values slightly deviate from the one's reported in Heck, 2012 due to an imperfect alignment.

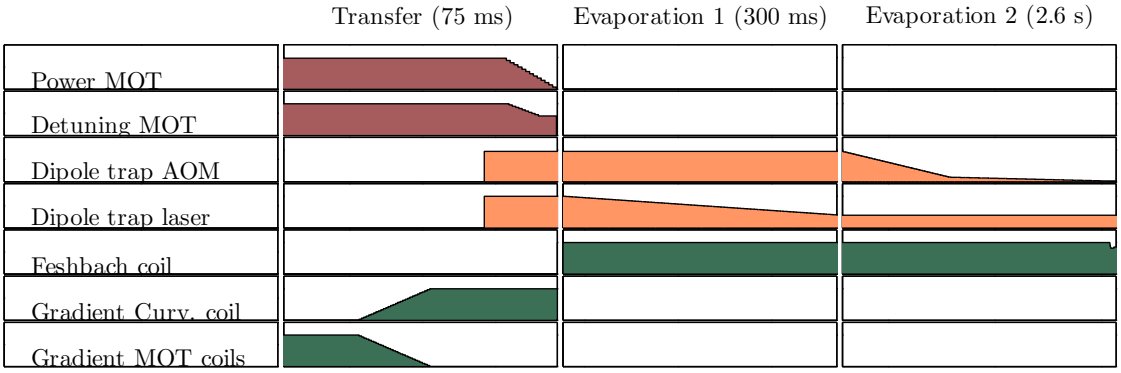

Figure 3.6: Scheme for transferring ^{6}Li atoms into the dipole trap as well as for evaporative cooling to obtain a molecular BEC. Transfer in dipole trap is performed during a MOT compression phase with the same settings as depicted Fig. 2.11 in Sec. 2.6. In addition, the optical dipole trap is turned on to its maximum power 20 ms before the compression phase is completed. The first evaporation is performed by decreasing the beam power from 150 W to 25 W at the chamber via controlling the output power of the laser. Four further intensity ramps are performed within the second stage of evaporation by decreasing the power at the experimental chamber via controlling the deflection efficiency of an AOM. In addition, a magnetic field which is generated by the Feshbach coils is applied during the evaporation. After loading a MOT for 1 s, typically 10^6 ^{6}Li atoms are transfered into the trap and the temperature is $T_{\mathrm{Li}} \approx$ 300 μK.

overview of the whole scheme, which allows for a transfer of 10^6 atoms into the dipole trap, is shown in Fig. 3.6.

3.4.2 Evaporation of ^{6}Li

For performing evaporation at spin mixtures of ^{6}Li , it is convenient to apply a magnetic offset field close to the Feshbach resonance at 832 G [Zürn *et al.*, 2012], where the large scattering length results in fast thermalization times due to high elastic collision rates [Granade *et al.*, 2002; Ottenstein *et al.*, 2008]. For relatively high temperatures, it does not matter on which side on the Feshbach resonance the evaporation is performed. However, if the temperatures are sufficiently low, the properties of the sample as well as the efficiency of the evaporation process depend on the sign of the scattering length. For attractive interactions (a<0, "BCS side"), the evaporation process becomes inefficient, if $T \approx T_F$. At these temperatures a significant fraction of states up to the Fermi energy are occupied and the number of final levels is then decreased for an elastic collision event. This can be overcome by performing evaporation at the side of the Feshbach resonance with repulsive interactions (a>0, "BEC side"). As described in Sec.3.1.1, at these fields a universal

dimer state with a binding energy of $E_B = \hbar^2/(ma^2)$ exists, which can be efficiently populated via three-body recombination processes for temperatures $T \leqslant E_B/k_B$. For $T \ll E_B/k_B$ a nearly pure molecular sample is obtained. Since the dimers have a bosonic character, scattering processes do not rely on the Fermi statistic anymore, and efficient evaporation is still possible. In order to study cold Fermi gases on the BCS side, it is therefore convenient to first perform evaporation on the BEC side and ramp afterwards the magnetic field over the Feshbach resonance.

Commonly it is advantageous to begin the cooling process with a "plain" evaporation phase, where the potential depth remains at maximum power, until thermalization after the atom transfer is reached. However, at the present experimental setup, large thermal effects created by the enormous beam intensities of the Li dipole trap when operating at large powers, significantly modifies the trap properties on a time scale of several 10 ms [Heck, 2012]. Therefore, typically only 15 ms long plain evaporation phases are applied after loading the Li dipole trap at maximum available power. Forced evaporation is then performed by slowly decreasing the beam intensity, either by directly reducing the output power of the laser or via controlling the diffraction efficiency of two acusto-optical modulators. A detailed characterization of experimental sequences, where $T_{\mathrm{Li}} = 270$ nK cold samples, containing $N_{\mathrm{Li}} = 3 \cdot 10^4$ ^{6}Li atoms which corresponds to $T_{\mathrm{Li}} \approx T_F$, could be prepared, can be found in the master thesis of Robert Heck [Heck, 2012].

3.4.3 Observation of molecular Bose-Einstein condensation

The bosonic character of the dimers, created out of a two component Fermi gas with repulsive interactions, form a molecular Bose-Einstein condensate, if the molecular phase-space density is on the order of one (see Sec. 3.1.1). In order to prepare such a quantum degenerate gas of ^{6}Li , evaporative cooling was performed in the presence of a magnetic field of 690 G at the experimental apparatus after transferring atoms from a MOT that was loaded for 2.2 s. As depicted in Fig. 3.6 five experimentally optimized evaporative ramps with a total duration of 2.9 s have been applied whereas the final power of the last ramp was varied from P=14 mW to P=91 mW. Afterwards, the density distribution after a 10 ms long time of flight phase was recorded via performing absorption imaging at this magnetic field (see Sec. 3.5.3 and Heck, 2012 for details on the high field imaging system).

As depicted in Fig. 3.7, the transition from a thermal gas to a molecular Bose-Einstein condensate was observed by varying the trap depth at the end of the evaporation process. For higher final values of the laser beam powers, the atomic cloud

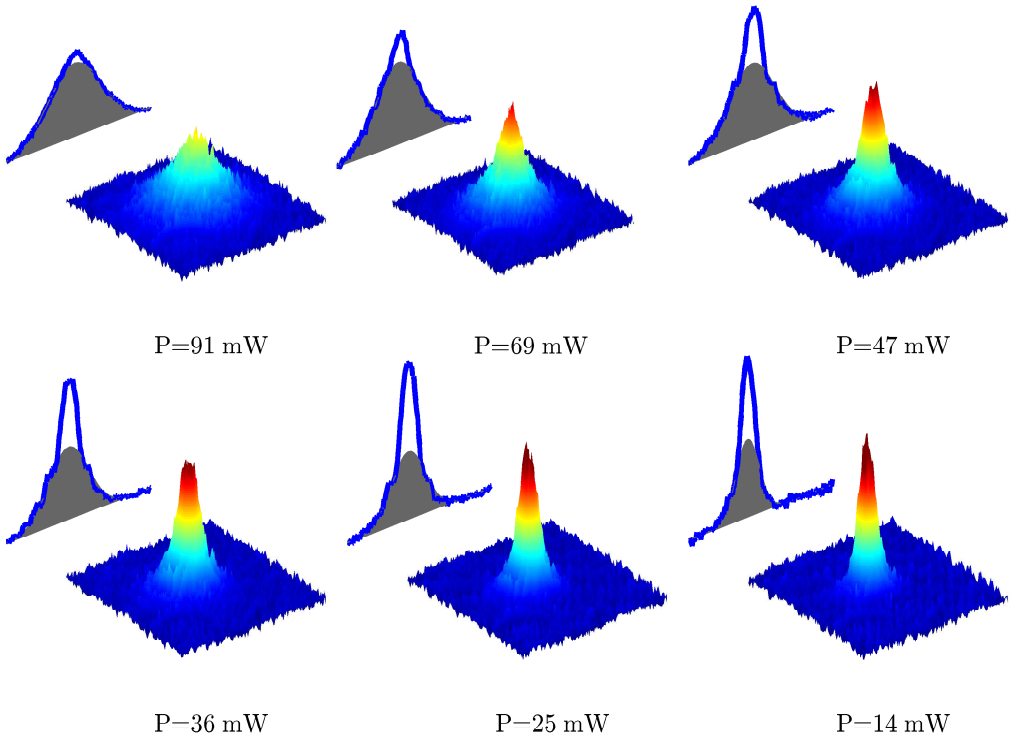

Figure 3.7: Onset of molecular Bose-Einstein condensation in a two component ^{6}Li gas. A signature of the transition from a thermal gas into a Bose-Einstein condensation is the change of the density distribution from a gaussian profile to a bimodal shape. This could be observed by varying the trap power P at the end of the last evaporation ramp. The two dimensional absorption images are averages over 40 experimental realizations and the one dimensional plots represent a normalized summation along one axis. For the lowest power of P=14 mW a condensation fraction of 30% was deduced by fitting bimodal distribution onto the integrated profile, whereas the gray areas mark the thermal fractions.

shows a gaussian density profile, which corespondents to a thermal gas. Lowering the final beam power modifies the shape of the cloud, and the profile is well described by a bimodal distribution. This is expected for a gas with a certain condensate fraction. In order to deduce the condensate fraction, the two dimensional absorption images have been integrated along one axis and bimodal distribution functions have been fitted to the obtained density profiles. This leads to a condensate fraction of 5% at final laser power of P=91 mW, whereas for the lowest power of 14 mW a condensate fraction of about 30% is reached.

3.5 Combined trapping of a ^{6}Li and ^{133}Cs mixture

This section describes the first preparation of a trapped ultracold Bose-Fermi mixture of ^{6}Li and ^{133}Cs [11], as required for identifying Feshbach resonances by performing trap loss spectroscopy. The experimental challenge was to find a good procedure to efficiently transfer laser cooled ^{6}Li and ^{133}Cs atoms into one trap, regardless of their different temperatures of $T_{\mathrm{Li}} \approx 300\ \mu$K and $T_{\mathrm{Cs}} \approx 1\ \mu$K, respectively. A subsequent loading scheme, by first transferring and evaporatively cooling ^{6}Li atoms to temperatures which are comparable with the temperatures of laser cooled ^{133}Cs atoms, before transferring ^{133}Cs atoms allowed to created sufficient conditions for the measurements of interspecies Feshbach resonances, which are described in the following chapter.

3.5.1 Loading procedure

The first step of the loading scheme is the preparation of an ultracold Li sample. For this, a similar as procedure described in Sec. 3.4 was applied[12]. In brief, a mixture of 10^6 ^{6}Li atoms in their two lowest spin states is transfered into the crossed dipole trap at a laser power of 150 W out of a MOT, containing 10^8 particles. Forced evaporative cooling is performed by ramping down the laser power to 0.9 W within 900 ms at the presence of a homogeneous magnetic field of 760 G. After a subsequent 200 ms long plain evaporation phase, which allows for thermalization of the atoms, 10^5 ^{6}Li atoms remain with a temperature of $T_{Li} = 2.5\ \mu$K. At this point the magnetic field is switched off. However, applying at these conditions the following experimental loading sequence for ^{133}Cs , leads to a loss of all ^{6}Li atoms. The fact that these losses occur, if all ^{133}Cs beams are blocked, indicates that the losses occur during switching the magnetic fields, as required for performing the ^{133}Cs loading sequence. In contrast, exposing the ^{6}Li sample with the ^{133}Cs MOT laser beams, while not switching the magnetic fields, did not influence the lifetime of the trapped ^{6}Li atoms. Since the losses arise thus through residual magnetic potentials during switching the magnetic field, the losses can be minimized by applying a higher optical potential. This is realized by increasing the optical dipole trap in an adiabatic ramp to 1.8 W within 100 ms.

[11] Shortly after our realization [Repp *et al.*, 2013], this was also achieved within the Chin group in Chicago [Tung *et al.*, 2013].

[12] In contrast to the sequence of Sec. 3.4, the final gradient provided by the curvature coil was $\partial B/\partial z = 28$ G/cm and the dipole trap was turned on at the same time, when the intensity of the MOT lasers was decreased.

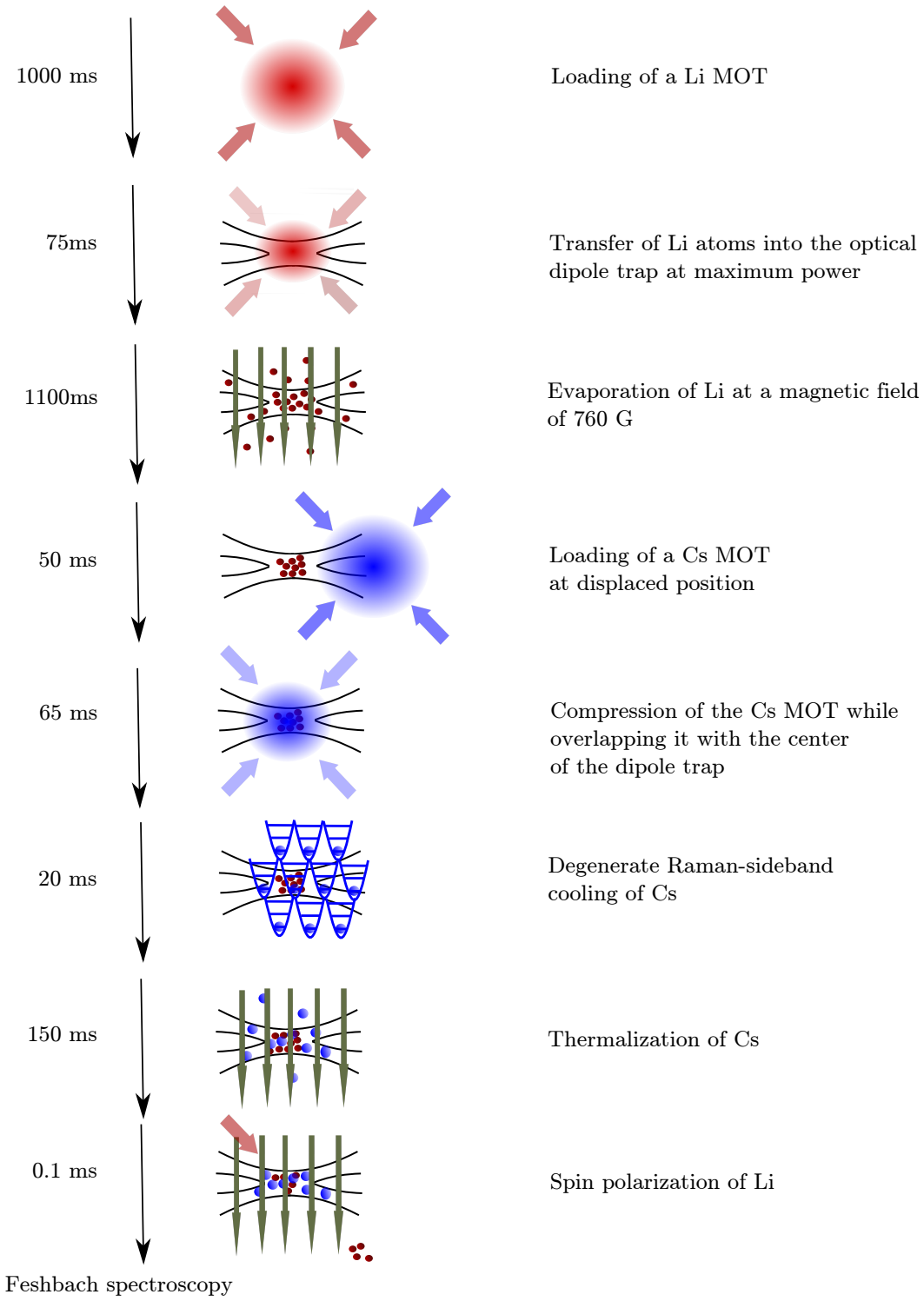

Figure 3.8: Schematic procedure for sequentially loading ^{6}Li and ^{133}Cs into the optical dipole trap. See text for details.

The ^{133}Cs preparation starts 20 ms later with loading of 10^7 Zeeman-cooled ^{133}Cs atoms in a MOT with a typical loading time of 50 ms. In order to avoid interspecies two-body losses of the ^{6}Li sample via inelastic collisions with ^{133}Cs atoms in an excited state [Schlöder *et al.*, 1999], the center of the ^{133}Cs MOT is displaced by roughly 1 mm with respect to the center of the optical dipole trap. This is achieved by adding a small homogeneous magnetic offset field to the gradient field. After switching off the Zeeman slower coils and laser beams a compression phase in the same way as described in Sec. 2.6 is applied, where the densities are increased by lowering the beam intensity and increasing the gradient. The temperature is furthermore decreased by increasing the detuning of the MOT beams. Moreover, the coils which deliver the gradient are exchanged from the MOT coils to Curvature coils, which have much faster switching off times (see Sec. 2.3). During this phase the ^{133}Cs cloud is superimposed with the center of the optical dipole trap by shifting the zero magnetic field position via the homogeneous magnetic offset field.

As a next step, the ^{133}Cs atoms are transfered into the Raman lattice, where further cooling to temperatures of $T_{Cs} \approx 1\ \mu K$ as well as spin polarizing is reached by performing three-dimensional degenerate Raman-sideband-cooling [Kerman *et al.*, 2000; Treutlein *et al.*, 2001], similar to the procedure described in Sec.2.7. Simultaneously the laser power of the optical dipole trap is ramped again down to a power of 0.9 W within 50 ms. After performing DRSC for 20 ms, the Raman polarizer beam is turned off. At this point a homogeneous magnetic field of 81 G, delivered from the Feshbach coils, is applied, which maintains the spin polarization. Transfer into the optical dipole trap is performed 5 ms later by releasing the atoms from the Raman lattice. However, since the extension of the ^{133}Cs cloud at this stage is significantly larger than the trapping volume of the optical dipole trap, the atoms are accelerated towards the trap center. Besides heating due to the conversion of potential into kinetic energy, this results in oscillations of the ^{133}Cs atoms cloud along the axis of weak confinement. They are damped out after 125 ms where the ^{133}Cs cloud is thermalized.

3.5.2 Trapping properties

The preparation scheme, which has been described in the previous section was applied for measuring the interspecies Feshbach resonances. They are described in detail in the next chapter. In order to characterize the conditions of the trapped mixture during these measurements, various diagnostic techniques have been applied.

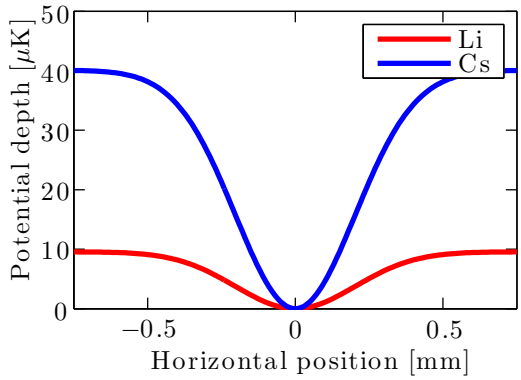

Figure 3.9: Effective optical potentials for Li (red) and Cs (blue) at a laser power of 0.9 W. The ^{133}Cs (^{6}Li)temperature during the Feshbach measurements was $T_{\mathrm{Cs}} = 8\mu$K ($T_{\mathrm{Li}} = 2\mu$K).

The number of particles was deduced via standard absorption imaging, resulting in $N_{\mathrm{Cs}} = 5 \cdot 10^4$ ^{133}Cs and $N_{\mathrm{Li}} = 2 \cdot 10^5$ ^{6}Li atoms. Furthermore, time of flight measurements of the atomic clouds after releasing the atoms out of the trap were performed, which resulted in temperatures $T_{\mathrm{Cs}} = 8$ μK and $T_{\mathrm{Li}} = 2$ μK of the two species. The different temperatures reflect the 4 times larger polarizabilities of ^{133}Cs compared to ^{6}Li for light at 1070 nm. As depicted in Fig. 3.9, this leads to effective trap depths of $U_{Cs} = 40$ μK and $U_{Li} = 10$ μK at a laser power of 0.9 W. Since plain evaporation processes result in temperatures of $T \approx U/10$, thus the observed difference in temperature is expected for the two species. Furthermore, as described more in detail in Sec. 4.3, this trap configuration leads mostly to a loss of the involved ^{6}Li atoms during interspecies collisions, which prevents an interspecies thermalization of the sample.

In order to deduce the trapping frequencies, ^{133}Cs and ^{6}Li samples were initially prepared in potentials created out of laser powers slightly below 0.9 W. A sudden jump of the laser power to 0.9 W excited dipolar oscillations of the atomic clouds. The oscillation frequencies correspond to twice the trapping frequency[13]. As depicted in Fig. 3.10 the hold time after increasing the trap depth was varied during these measurements and the widths of the clouds were recorded. Damped sine fits resulted in trapping frequencies of $\omega_{\mathrm{Cs}}/2\pi = (380, 380, 30)$ Hz and $\omega_{\mathrm{Li}}/2\pi = (900, 900, 65)$ Hz. From these measurements, atomic peak densities of $n_{\mathrm{Cs}} = 3 \times 10^{11}$ cm^{-3} and $n_{\mathrm{Li}} = 1 \times 10^{12}$ cm^{-3} were deduced, which are well suited for performing trap loss spectroscopy. To quantify the spin polarization of the Cs atoms, Stern-Gerlach measurements (see. Sec. 2.7), for which the optical dipole trap was switched off, showed,

[13]Harmonic potentials are assumed.

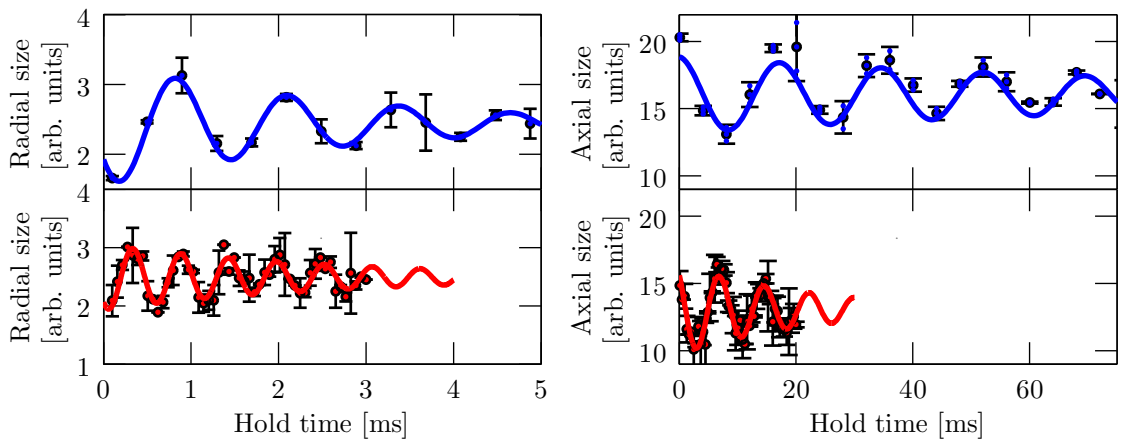

Figure 3.10: Measurement of the trapping frequencies. Left (right): Radial (axial) trap oscillations for Li (red) and Cs (blue) at a laser power of 0.9 W. The data points correspond to the measured sizes whereas the solid lines represent a damped sine fit in order to extract the axial (radial) trapping frequencies of $\omega_{\mathrm{Li}}^{\mathrm{ax}}/2\pi = 65$ Hz ($\omega_{\mathrm{Li}}^{\mathrm{rad}}/2\pi = 900$ Hz) for ^{6}Li and $\omega_{\mathrm{Cs}}^{\mathrm{ax}}/2\pi = 30$ Hz ($\omega_{\mathrm{Cs}}^{\mathrm{rad}}/2\pi = 380$ Hz) ^{133}Cs , respectively. Each data point is an average over two experimental realizations.

that 85% of the ^{133}Cs atoms are in the energetically lowest $|F = 3, M_F = 3\rangle$ state, while the remaining fraction populates the $|3, +2\rangle$ state.

3.5.3 Spin polarizing and spin selective imaging of ^{6}Li

After the ^{6}Li -^{133}Cs mixture has been loaded into the same optical dipole trap the ^{6}Li sample consists of a mixture of the states $2^2\mathrm{S}_{1/2}, |\mathrm{F} = 1/2, \mathrm{m_F} = +1/2\rangle$ and $2^2\mathrm{S}_{1/2}, |1/2, -1/2\rangle$. However, in order to investigate Feshbach resonances via trap loss spectroscopy, it is advantageous, to prepare a spin polarized sample. This results in defined collisional channels, which allows one to unambiguously analyze the measurements.

In order to spin polarize the ^{6}Li sample, the magnetic field is first ramped close to the zero crossing of the interspecies scattering length at about 530 G [Jochim *et al.*, 2002; O'Hara *et al.*, 2002], where scattering processes within the ^{6}Li cloud are minimized. Furthermore, individual optical transitions to sublevels of the $2^2\mathrm{P}_{3/2}$ state are well resolved at this field. After the field ramp and a relaxation period of 50 ms, the sample is illuminated for 800 μs by a laser pulse, which is on resonance with one of the transitions and what removes one spin component from the trap via light forces. A significant heating of the opposite spin state is not observed.

Furthermore, the ability to tune and stabilize the laser frequency on atomic

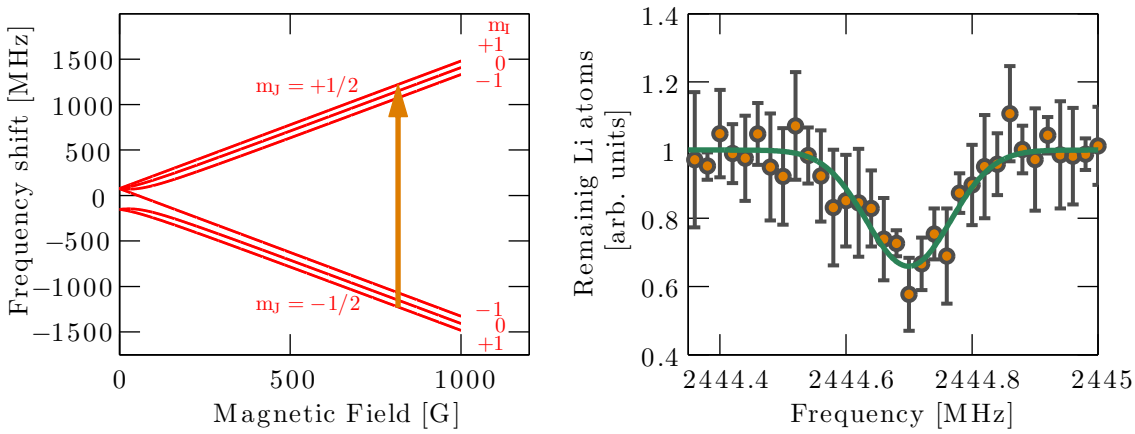

Figure 3.11: Calibration of the magnetic field Left side: Splitting of the lowest two Hyperfine manifolds in ^{6}Li (red lines). The microwave transition $|m_j = -1/2, m_I = +1\rangle \mapsto |m_j = +1/2, m_I = +1\rangle$ was used for calibrating the magnetic field (orange arrow). Right side: Typical loss spectra at a magnetic field of 816.24 G. A Gaussian fit(green solid line) was applied to the data points in order to deduce the FWHM of 156 kHz, corresponding to a field accuracy of 110 mG.

resonance at high magnetic fields enabled the spin selective detection of ^{6}Li atoms in the subsequently described measurements. It was verified that by first removing one spin component and afterwards imaging the same state, no population of that state could be observed. This corresponds to a spin polarized ^{6}Li sample. A detailed description of the high field laser system, allowing for removing and imaging lithium atoms at magnetic fields up to 1300 G, is given in the master thesis of R. Heck [Heck, 2012].

3.5.4 Calibration of the magnetic field

An important issue for an accurate determination of the position of a Feshbach resonance is a good calibration of the magnetic field. In addition, for identifying narrow resonances, a certain degree of field homogeneity is necessary, since the extension of the atomic clouds along the axial trap direction is on the order of 100 μm and possible resonances could be otherwise averaged out. Furthermore, a temporal field stability is required, since the trap loss spectra are based on holding the sample for a certain time, where the magnetic field should be stable.

The magnetic fields were calibrated for all 19 obtained interspecies Feshbach resonances (see Sec: 4.4) by driving a microwave transition of ^{6}Li into the $m_j = +1/2$ manifold for a certain holding time. If the applied microwave frequency coincides

with the transition frequency at a certain field, a loss of ^{6}Li atoms due to inelastic collisions occurs, since dipolar collisions are no longer suppressed if atoms in the $m_j = +1/2$ manifold are involved. The corresponding magnetic field value can be inferred from the Breit-Rabi formula. Fitting a Gaussian line profile to the microwave spectra yields FWHM of 200 kHz at the largest considered fields of about 950 G, indicating a magnetic field accuracy of 140 mG. The fact that all expect one obtained widths follow a linear behavior indicates, that inhomogeneity of the magnetic field along the atomic cloud is present in the current apparatus. However, in subsequent experiments, this can be avoided by minimizing the inhomogeneity of the Feshbach coil via the Compensation coil (see Sec. 2.3), which was not done within the measurements presented in this thesis. An overview of the transitions as well as a typical loss spectra are depicted in Fig. 3.11.

Chapter 4

Interspecies ^{6}Li -^{133}Cs Feshbach resonances

Parts of this chapter are based on the following publication:

M. Repp, R. Pires, J. Ulmanis, R. Heck, E.D. Kuhnle, M. Weidemüller, E. Tiemann
Observation of interspecies ^{6}Li-^{133}Cs Feshbach resonances
Physical Review A **87**, 010701 (2013)

The ability to control and manipulate atomic interactions via magnetically tunable Feshbach resonances presents a unique toolbox for the field of ultracold atoms (for a review see Chin *et al.*, 2010). A main application is the precise adjustment of the collisional properties of an atomic sample. Furthermore, the ramp of a magnetic field over a Feshbach resonance allows for the creation of molecules out of atomic samples [Herbig *et al.*, 2003; Regal *et al.*, 2003; Köhler *et al.*, 2006]. Feshbach resonances have been widely studied in single species experiments (for an overview see Chin *et al.*, 2010). However, during the last decade, a variety of Feshbach resonances between different alkaline species have been already identified for a variety of Bose-Bose [Thalhammer *et al.*, 2008; Marzok *et al.*, 2009; Pilch *et al.*, 2009; Cho *et al.*, 2013; Wang *et al.*, 2013], Bose-Fermi mixtures [Inouye *et al.*, 2004; Stan *et al.*, 2004; Ferlaino *et al.*, 2006; Deh *et al.*, 2008; Deh *et al.*, 2010; Schuster *et al.*, 2012; Park *et al.*, 2012] as well as for the Fermi-Fermi mixture of ^{6}Li-^{40}K [Wille *et al.*, 2008]. While the broad intraspecies Feshbach resonances in ^{133}Cs [Chin *et al.*, 2004a; Berninger *et al.*, 2012] and ^{6}Li [Jochim *et al.*, 2002; O'Hara *et al.*, 2002; Bartenstein

et al., 2005; Ottenstein *et al.*, 2008; Zürn *et al.*, 2012] are well-explored, only little has been known about the interspecies interaction properties of Li and Cs. The elastic scattering properties of ^{7}Li-^{133}Cs were studied by means of thermalization measurements at zero magnetic field [Mudrich *et al.*, 2002], where an elastic cross section of $\sigma = 8(4) \times 10^{-12}$ cm^2 for interspecies collisions was deduced. However, the tunability of the interspecies scattering properties via tuning the magnetic field has yet remained unexplored for the two possible combinations ^{6}Li-^{133}Cs and ^{7}Li-^{133}Cs. The ability of preparing optically trapped ^{6}Li -^{133}Cs mixtures in the μK temperature regime, as described in the previous chapter, gave access to search for Feshbach resonances in this Bose-Fermi mixture.

This chapter starts with reviewing the scattering theory, as required for describing ultracold collisions. Furthermore, the interactions during a scattering event of ultracold atoms as well as the origin of Feshbach resonances are described. After briefly mentioning the intraspecies scattering properties of ^{6}Li and ^{133}Cs , which are also present in a ^{6}Li -^{133}Cs mixture, the different interspecies loss mechanisms of a trapped ensemble are introduced. Since several of these loss mechanisms depend on the scattering length, a change of the loss rate in a certain magnetic field region is an indication for a Feshbach resonance. The investigation of collisional losses in an optically trapped ^{6}Li -^{133}Cs mixture led to the observation of nineteen interspecies Feshbach resonances by scanning a homogeneous magnetic field (Feshbach spectroscopy). The obtained resonances could be assigned to s- and p-wave molecular channels by a coupled channels calculation, performed by Prof. E. Tiemann, resulting in an accurate determination of ^{6}Li ^{133}Cs ground state potentials. In the last section three special magnetic field regions are discussed in detail at which the combinations of inter- and intraspecies scattering lengths provide testbeds for different model systems.

4.1 Collisions of ultracold atoms

In order to understand the underlying physics of a Feshbach resonance, the theoretical description of scattering of ultracold atoms is summarized in this section. Cases, in which the binding energy of a closed molecular state coincides with the energy of colliding free atoms are of particular interest. This results in enhanced scattering rates, if a coupling between the collisional channel and the bound state exists. A tunability of the scattering process can be obtained, if the different intermediate states have different magnetic moments, leading to the appearance of

magnetic Feshbach resonances.

4.1.1 Basic scattering theory

This section briefly reviews the scattering theory, following closely the review article Dalibard, 1999. The two-body wavefunction $\psi(\vec{r})$ of two colliding particles with a reduced mass μ, interacting through the potential $V(\vec{r})$ can be obtained by solving the Schrödinger equation

$$\left[\frac{\hbar^2}{2\mu}\vec{\nabla}^2 + V(\vec{r})\right]\psi(\vec{r}) = \frac{\hbar^2 k^2}{2\mu}\psi(\vec{r}) \tag{4.1}$$

for a wave vector k.

Commonly, the interaction potential vanishes for large internuclear distances and the wavefunction can be expressed at low temperatures as a sum of an incoming plane wave and an outgoing spherical wave with an angle dependent scattering amplitude $f(\theta, k)$:

$$\psi(\vec{r}) = e^{ikr} + f(\theta, k)\frac{e^{ikr}}{r}. \tag{4.2}$$

This enables the calculation of the differential cross-section $d\sigma(k)/d\Omega$ for scattering at a solid angle Ω:

$$\frac{d\sigma(k)}{d\Omega} = |f(\theta, k)|^2. \tag{4.3}$$

Assuming spherically symmetric potentials, it is convenient rewriting $\psi(\vec{r})$ in a basis set of the relative angular momentum l via

$$\psi(\vec{r}) = \sum_{l=0}^{\infty}\sum_{m=-l}^{l} Y_l^m(\theta, \phi)\frac{u_{k,l,m}(r)}{r}, \tag{4.4}$$

with spherical harmonics $Y_l^m(\theta, \phi)$. A solution for the scattering amplitude $f(\theta, k)$ can be obtained by inserting eq. 4.4 into eq. 4.1 and subsequently solving the Schrödinger equation for the radial component $u_{k,l,m}(r)$. In the limit of large internuclear separations, the scattering amplitude is given by

$$f(\theta, k) = \frac{1}{2ik}\sum_{l=0}^{\infty}(2l+1)(e^{2i\delta_l} - 1)P_l(cos(\theta)), \tag{4.5}$$

where P_l denotes the Legendre polynomials. The phase shift δ_l between the incoming and outgoing wave is an important parameter that accumulates all details of the

scattering event. Special care needs to be taken if the particles are identical. In the case of bosons, the wavefunction needs to be symmetrized, whereas for fermions an anti-symmetrized wavefunction is required. The differential cross-section is then given by

$$\frac{d\sigma(k)}{d\Omega} = |f(\theta, k) + \epsilon f(\theta - \pi, k)|^2, \tag{4.6}$$

with $\epsilon = +1$ for systems of identical bosons and $\epsilon = -1$ for fermionic systems.

Scattering length and cross sections

At ultracold temperatures, collisional contributions from higher order partial waves (l>0) are suppressed by the centrifugal barrier. A further integration over the angle θ gives access to the so called s-wave scattering length a. This property is defined by

$$a = -\lim_{k \to 0} \frac{tan[\delta_0(k)]}{k} \tag{4.7}$$

for the collisional zero energy limit ($k \to 0$). This single, universal parameter describes the whole scattering event in the ultracold domain.

The total elastic cross section can be then written as

$$\sigma_0(k) = \begin{cases} \dfrac{4\pi a^2}{1 + k^2 a^2} & \text{for distinguishable particles} \\ \dfrac{8\pi a^2}{1 + k^2 a^2} & \text{for identical bosons} \\ 0 & \text{for identical fermions.} \end{cases} \tag{4.8}$$

Scattering in a Bose- Fermi mixture

In the case of an ultracold mixture experiment, the scattering properties of the sample are determined by the inter- and intraspecies scattering lengths. The situation for an ultracold Bose-Fermi mixture of identical bosons and fermions is depicted in Fig. 4.1. Collisions of the bosons among each other are described by the scattering length a_{BB} and the interspecies scattering properties are given by the intraspecies scattering length a_{FB}. The interspecies scattering length a_{FF} of the fermions is zero.

4.1.2 Interactions at ultracold collisions

The interatomic interactions of two colliding atoms are in general a complicated mixture of electrostatic forces between the negatively charged electronic clouds and

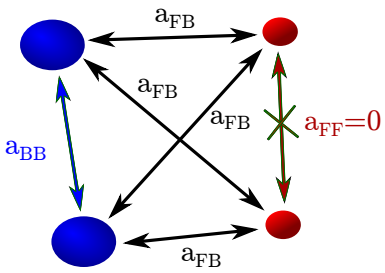

Figure 4.1: Scattering lengths in a Bose-Fermi mixture at ultracold temperatures. The scattering length for identical fermions is zero ($a_{FF} = 0$), whereas interactions between identical bosons and between bosons and fermions can occur.

the positively charged nuclei as well as couplings of angular momenta. In order to obtain the scattering length at a certain magnetic field, the internal energies and the Coulomb forces have to be considered. Taking all contributions into account, the Hamiltonian, which describes a binary collision event in the presence of a magnetic field, can be expressed as (see e.g. Stoof *et al.*, 1988; Moerdijk *et al.*, 1995; Timmermans *et al.*, 1999; Köhler *et al.*, 2006)

$$H = T + H_{\mathrm{hf}}(r) + H_{\mathrm{Z}} + \sum_{S=0,1} P_S V_S(r) + V_{dip}(\vec{r}) \tag{4.9}$$

with an operator T, representing the relative kinetic energy of the atom pair, the Born-Oppenheimer potentials V_S for the singlet (S=0) and triplet (S=1) states with their projection operators P_S, the hyperfine interaction H_{hf} of atom A and B, the magnetic Zeeman interaction term H_{Z} for the electrons and the nuclei, and a magnetic dipole spin-spin interaction term $V_{dip}(\vec{r})$. The individual terms are described in the following more in detail.

Born-Oppenheimer potential curves

The electrostatic forces of two colliding atoms can be separated into two parts: At large internuclear distances, the atoms experience Van-der-Waals interactions, generated by introduced dipole-dipole interactions. This attractive interaction is commonly written as a power series of $1/r$:

$$V_{VdW}(R) = -C_6/r^6 - C_8/r^8 - C_{10}/r^{10} \tag{4.10}$$

with dispersion coefficients C_6, C_8 and C_{10}.

If the two atoms approach each other, the electronic clouds start to overlap. At

these distances, the orientation of the electron spins $\mathbf{s}_1$ and $\mathbf{s}_2$ couple to a total spin $\mathbf{S} = \mathbf{s}_1 + \mathbf{s}_2$, resulting in singlet (S=0) and triplet states (S=1) for ground state alkaline atoms with $s = 1/2$. Since the triplet (singlet) spin wave function is symmetric (antisymmetric) against particle exchange, the fermionic nature of the electrons requires a (antisymmetric) symmetric spatial wave function. The reduced (enhanced) wave function amplitude at short distances in the triplet (singlet) configuration leads therefor to a smaller (larger) Coulomb repulsion for the electrons, which is usually described by an exchange interaction term. At very small distances the potential curves are repulsive due to the interactions of the positively charged nuclei and the Pauli blocking of the electrons.

A method for describing the electrostatic Coulomb interaction is based on the application of the "Born-Oppenheimer approximation" [Born and Oppenheimer, 1927], where the large mass difference allows for a separation of the electronic and nuclear degrees of freedom. The small electron mass leads to a nearly instantaneous arrangement of the electronic cloud. The dynamics of the collision process is then given by the movement of the atomic nuclei in electro-static potentials, which is, however, influenced by the arrangement of the electrons. The kinematics is often described by introducing relative coordinates and considering the movement of an atom with reduced mass μ in Born-Oppenheimer potential curves (BOpc) $V(r)$, where r is the internuclear separation. The exchange interaction manifests itself in the BOpc as a splitting into a singlet and a triplet component at short internuclear distances. This splitting is depicted in Fig. 4.2, where the energetically lowest states $X^1\Sigma^+$ and $a^3\Sigma^+$ of LiCs are shown.

Initial theoretical investigations of the ground state potential curves of LiCs were performed by *ab initio* calculations [Korek *et al.*, 2000, Aymar and Dulieu, 2005]. The description was improved by spectroscopic data based on Fourier-transform spectroscopy [Staanum *et al.*, 2007]. In addition, photoassociation spectroscopy [Grochola *et al.*, 2009] with ^{7}Li^{133}Cs provided a more accurate value of the dissociation energy.

Hyperfine interaction

The hyperfine interaction arises from the coupling of the nuclear spin $\vec{i}_\alpha$ of each atom α with the electronic angular momentum $\vec{j}_\alpha$. For alkaline atoms in their electronic ground states, where $\vec{j}_\alpha = \vec{s}_\alpha$ is valid, the hyperfine interaction can be written as

$$H_{\mathrm{hf}}(r) = \sum_{\alpha=A,B} a_\alpha(r)\vec{s}_\alpha \cdot \vec{i}_\alpha/\hbar^2 \tag{4.11}$$

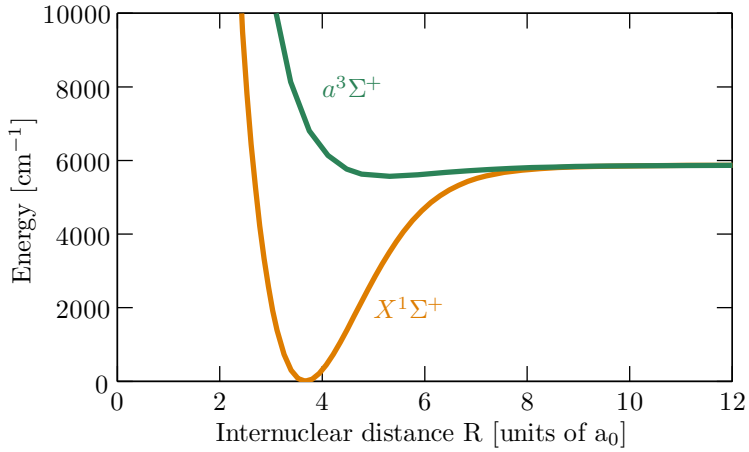

Figure 4.2: Ground state potential energy curves of LiCs, showing the singlet $X^1\Sigma^+$ and the triplet $a^3\Sigma^+$ state. The exchange interaction leads to a splitting at short internuclear distances. The long range part is dominated by the Van-der-Waals interaction. The curves were plotted by using the data points provided in Ref. Staanum *et al.*, 2007.

with a species and r dependent coupling constant $a_\alpha(r)$.

Zeeman interaction

The tunability of the scattering length in the vicinity of a magnetic Feshbach resonance needs interactions with external magnetic fields. This is provided by the Zeeman interaction, describing the interaction of the magnetic moments of the involved atoms with an external field of strength B via

$$H_Z(R) = \sum_{\alpha=A,B} (g_{s\alpha} s_{z\alpha} + g_{i\alpha} i_{z\alpha}) \mu_B B/\hbar, \tag{4.12}$$

with the gyromagnetic ratio $g_{s\alpha}$ ($g_{i\alpha}$) of the electron (nucleus) and Bohr's magneton μ_B.

In general, the combination of Hyperfine and Zeeman interaction is not diagonal in $\mathbf{S}^2$ which enables a coupling between the singlet and triplet states [Timmermans *et al.*, 1999], as required for the appearance of Feshbach resonances (see Sec. 4.1.3).

Dipole spin-spin interaction

In addition, dipolar couplings, arising from magnetic coupling of the spins as well as from first and second order spin-orbit couplings, occur. The different interactions

can be combined in an effective form [Strauss *et al.*, 2010]

$$V_{\text{dip}}(r) = \frac{2}{3}\lambda(r)(3S_Z^2 - S^2), \tag{4.13}$$

where S_Z is the total electron spin projected onto the molecular axis. The function λ contains the direct magnetic spin-spin interaction as the first term and second order spin-orbit contribution as the second term

$$\lambda = -\frac{3}{4}\alpha^2 \left(\frac{1}{r^3} + a_{\text{SO}} \exp\left(-br\right)\right), \tag{4.14}$$

with α being the universal fine structure constant and constants a_{SO} and b.

4.1.3 Origin of a Feshbach resonance

This subsection summarizes the approach for theoretically describing a Feshbach resonance of Moerdijk *et al.*, 1995, while using the notation of this reference. For solving the Schrödinger equation of the scattering event, it is convenient to split the Hamiltonian given in equation 4.9 in two parts:

$$H = H_0 + V_{int}. \tag{4.15}$$

An internal part H_0 with eigenstates $\{\alpha\beta\}$, which converges at large internuclear distances to product states of separate atoms in internal states $|\alpha\rangle$ and $|\beta\rangle$, and a coupling part V_{int}, which describes the coupling between the different channels $\{\alpha\beta\}$. The total scattering state Ψ can than be written as a sum

$$\Psi = \sum_{\{\alpha\beta\}} \Psi_{\{\alpha\beta\}}(\vec{r})|\{\alpha\beta\}\rangle \tag{4.16}$$

with $\vec{r}$ dependent coefficients $\Psi_{\{\alpha\beta\}}$.

Insertion of equation 4.16 into the Schrödinger equation results in a set of coupled differential equations for the relative motional wave functions $\Psi_{\{\alpha\beta\}}$, which motivates coupled channel calculations. In order to be accessible, the energy of a channel needs to be lower than the kinetic energy E at the asymptote of the colliding pair. This leads to a classification of the different channels into "open" and "closed" ones. The complete Hilbert space can be subdivided in a closed channel subspace $\boldsymbol{Q}$ and an open channel subspace $\boldsymbol{P}$. By using the projection operators P and Q, which projects onto the open and closed channels subspace, respectively, a system of two

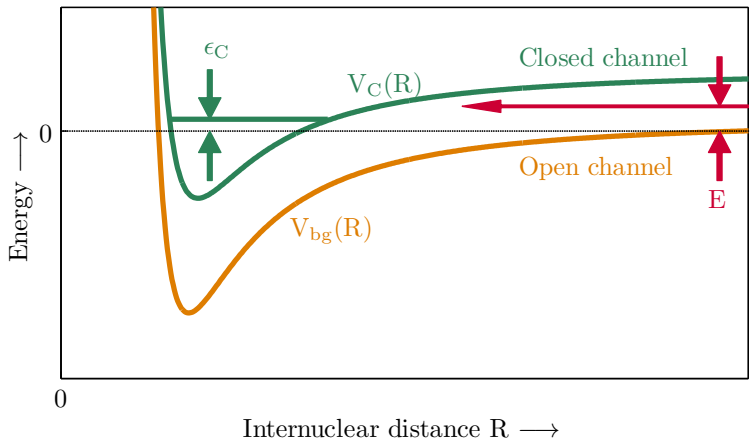

Figure 4.3: Principle of a Feshbach resonance. Feshbach resonances appear when the total energy E of two colliding atoms in an open channel, represented by the potential $V_{bg}(R)$ resonantly couples to a molecular state with energy ϵ_C in a closed channel $V_C(R)$. At ultracold collisions, where E $\approx$ 0, resonant coupling can be obtained by a magnetic field, if the two channels have different magnetic moments. Replotted from Chin *et al.*, 2010.

coupled equations is obtained from the Schrödinger equation:

$$(E - H_{PP})\Psi_P = H_{PQ}\Psi_Q \tag{4.17}$$

$$(E - H_{QQ})\Psi_Q = H_{QP}\Psi_P \tag{4.18}$$

with $\Psi_P = P\Psi$, $\Psi_Q = Q\Psi$, $H_{PP} = PHP$, $H_{QQ} = QHQ$, $H_{PQ} = PHQ$ and $H_{QP} = QHP$.

This system can be formally decoupled for the open channel states by introducing a Green operator $\frac{1}{E^+ - H_{QQ}}$ that generates an effective Hamiltonian

$$H_{eff} = H_{PP} + H_{PQ}\frac{1}{E^+ - H_{QQ}}H_{QP} \tag{4.19}$$

resulting in

$$(E - H_{eff})\Psi_P = 0. \tag{4.20}$$

The collision event described by equation 4.20 can be interpreted as bare scattering in the open channel P, arising from the first term, combined with a temporal propagation in a closed channel Q, represented by the second part.

This representation allows for the calculation of the scattering matrix element S^{ii}, which describes the scattering probability within a channel i. For the case where the total energy E of a colliding ultracold atomic pair is close to a discrete bound

state with energy ϵ_0 and only one open channel i exists, S_{ii} can be calculated via

$$S_{ii} = S_{ii}^0 \left(1 - \frac{i\Gamma}{E - \epsilon_0 - \delta + i/2\Gamma}\right) \tag{4.21}$$

with the scattering matrix element S_{ii}^0 for scattering in the bare open channel potential, a width Γ and a small resonance shift δ. Resonant enhancement is obtained, if the total collision energy E matches the sum of the bound state with energy ϵ_0 and the resonance shift δ.

Magnetic Feshbach resonances appear, if the two relevant potentials have different magnetic moments. An external magnetic field allows in such a case to fulfill the resonance condition by introducing a relative shift of the potential offsets in a way, that a bound state energy becomes degenerate with the collisional energy. The magnetic field dependence of the scattering length a can be deduced by a further treatment of the scattering matrix element S^{ii}. For magnetic Feshbach resonances with a center at B_0 the tunability of the scattering length by a magnetic field of strength B is given by [Moerdijk *et al.*, 1995,Timmermans *et al.*, 1999]:

$$a = a_0 \left(1 - \frac{\Delta}{B - B_0}\right) \tag{4.22}$$

where a_0 represents the background scatting length and Δ the width of the resonance.

4.2 Intraspecies scattering lengths of ^{6}Li and ^{133}Cs

Scattering of ^{6}Li and ^{133}Cs in their energetic lowest states has been widely investigated during the last decade and an overview can be found in a review article [Chin *et al.*, 2010]. Therefore, only a short summary is given here, including the recent results of Berninger *et al.*, 2012 and Zürn *et al.*, 2012, focusing on s-wave resonances in the energetically lowest spin states.

Intraspecies scattering length and three-body loss minima of ^{133}Cs

Interactions of ultracold ensembles of ^{133}Cs atoms, prepared in their energetically lowest spin state $|\mathrm{F} = 3, \mathrm{m_F} = 3\rangle$, can be accurately tuned due to the existence of three broad Feshbach resonances and a large background scattering length ($\approx 2000a_0$). At low fields, the behavior of the scattering length is dominated by a $\Delta = 28.7$ G broad s-wave Feshbach resonance located at $\mathrm{B_{res}} = -11.7$ G with a zero

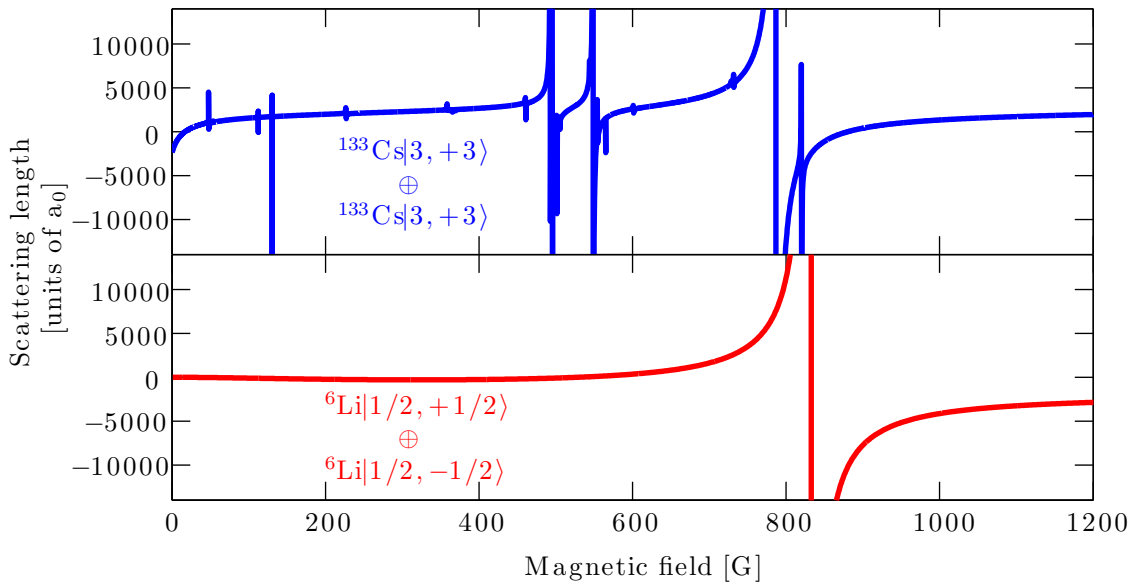

Figure 4.4: Magnetic field dependence of the scattering length for ^{133}Cs atoms (upper panel) [Berninger *et al.*, 2012] in the state $|F = 3, m_F = 3\rangle$ and for ^{6}Li mixtures (lower panel) [Zürn *et al.*, 2012] in the channel $|1/2, +1/2\rangle \oplus |1/2, -1/2\rangle$. Besides several small higher angular momentum Feshbach resonances, three broad s-waves at $B_{res} = -11.7$,$B_{res} = 548.8$, and $B_{res} = 786.8$ exist for ^{133}Cs and an extremely broad Feshbach resonance at $B_{res} = 832$ G for ^{6}Li . Various small features for both species, including a narrow s-wave resonance at $B_{res} = 543.8$ for Li, are not resolved. The ^{133}Cs scattering lengths were provided by courtesy of Prof. Julienne [Julienne, 2012].

crossing at $B_{zero} = 17.1$ G [Vuletić *et al.*, 1999, Chin *et al.*, 2004b, Lange *et al.*, 2009]. More recently, the field region above 250 G was explored experimentally [Berninger *et al.*, 2011,Berninger *et al.*, 2012], where two s-wave resonances, one at $B_{res} = 548.78$ G and another one at $B_{res} = 786.8$ G with a zero crossing at $B_{zero} = 880.9$ G were observed. The scattering length behavior of ^{133}Cs in the $|F = 3, m_F = 3\rangle$ state is depicted in Fig. 4.4.

Intraspecies scattering length of ^{6}Li

The fermionic nature of ^{6}Li suppresses intraspecies collisions in spin polarized samples at temperatures below the p- wave barrier. To observe elastic collisions, it is therefore convenient to work with mixtures of different spin states, where s-wave scattering appears. For the collisions within the channel $|F = 1/2, m_F = +1/2\rangle \oplus |1/2, -1/2\rangle$, corresponding to the lowest hyperfine states at zero magnetic fields, the scattering length almost vanishes ($|a| < 100\ a_0$ for magnetic field below

B < 100 G). At higher magnetic fields however, the scattering length of this system can be adjusted sensitively via a $\Delta = 262$ G broad Feshbach resonance located at $B_{res} = 832$ and a very narrow feature at 543 G [Zürn *et al.*, 2012, Jochim *et al.*, 2002, Bartenstein *et al.*, 2005, O'Hara *et al.*, 2002]. The magnetic field dependence of the ^{6}Li scattering length is shown in Fig. 4.4.

4.3 Loss processes of ultracold mixtures

The observation time of ultracold samples is limited by various loss phenomena. Such losses occur mainly via inelastic collisions with other atoms, since the released kinetic energy commonly extends the trap depth. Depending on how many trapped atoms are involved during a collision, they are classified as *One-body-*,*Two-body-* and *Three-body losses*. The fact that several loss mechanisms depend on the scattering length make loss measurements suitable for identifying Feshbach resonances.

One-body losses

A one-body loss of a trapped atom is independent of the surrounding trapped atoms. In ultracold experiments, these losses arise from collisions with remaining "hot" atoms from the background gas, as well as due to the absorption of photons from an optical dipole trap.

Two-body losses

Two-body losses occur, if the internal structure of one atom changes within a collision. The change of internal energy is converted into kinetic energy, which commonly extends the trapping potential and leads to a loss of the pair. Such processes can be a limiting factor for preparing dense gases. For insistence, the abnormal large spin relaxation rates of ^{133}Cs in the $m_F = -3$ prevented the observation of Bose-Einstein condensation in magnetic traps [Söding *et al.*, 1998; Guéry-Odelin *et al.*, 1998]. However, these losses can be avoided, if the atoms are prepared in their energetically lowest state $m_F = 3$. This state is a high-field-seeking state what prevents the use of magnetic traps.

Three-body losses

At high densities, three-body losses can be the dominating loss mechanism. They arise, when three particles collide and two of them form a molecule. The resulting

binding energy is converted into kinetic energy. Large elastic cross-sections are associated with high loss rates. This manifest itself in a scaling of the three-body loss coefficient $\beta_{3\mathrm{BD}}$ with the scattering length a [Fedichev *et al.*, 1996; D'Incao and Esry, 2005]:

$$\beta_{3\mathrm{BD}} \propto C(a,T)a^4 \tag{4.23}$$

where $C(a)$ contains a modulation via the Efimov effect at low temperatures T. The large tunability of the ^{133}Cs scattering length enabled the demonstration of the a^4 scaling of the three-body loss coefficient [Weber *et al.*, 2003b]. For preparing dense and cold ^{133}Cs gases, such as Bose-Einstein condensations [Weber *et al.*, 2003a] the modulation of $\beta_{3\mathrm{BD}}$ via $C(a)$ is important. $C(a)$ shows loss minima at magnetic fields of about $\mathrm{B_{3bd}} = 21$ G and $\mathrm{B_{3bd}} = 893$ G [Kraemer *et al.*, 2004; Berninger *et al.*, 2011; Berninger *et al.*, 2012]. Performing evaporative cooling of a ^{133}Cs cloud at these fields minimizes trap losses, whereas large elastic scattering cross sections still lead to high thermalization rates. In the case of ^{6}Li , three-body recombination events can play also an important role during evaporation in a two component Fermi gas. As described in Sec. 3.1.2, a weakly bound, universal dimer state exists at large positive scattering lengths, which can be populated via three-body recombination. This enables the application of efficient evaporative cooling schemes.

Evaporational losses in the LiCs- mixture

Besides the discussed loss mechanism, a further loss mechanism is present for an optically trapped ^{6}Li -^{133}Cs mixture at the conditions, which have been present during the loss spectroscopy measurements, that are described in the following section. As depicted in Fig. 3.9, the different polarizabilities of ^{133}Cs and ^{6}Li for light at 1070 nm results in effective trap depths of $U_{\mathrm{Cs}}/\mathrm{k_B} = 40\ \mu$K and $U_{\mathrm{Li}}/\mathrm{k_B} = 10\ \mu$K at a laser power of 0.9 W, which was applied during the Feshbach measurements. Because the two species were prepared at temperatures $T_{\mathrm{Cs}} = 8\ \mu$K and $T_{\mathrm{Li}} = 2\ \mu$K, respectively (see also Sec. 3.5), the ^{6}Li trap depth is comparable with the ^{133}Cs temperature and thermalization via interspecies elastic collisions can therefore lead to a loss of ^{6}Li . The thermalization rate is proportional to the elastic, interspecies collision rate Γ_{el}. Below the unitary limit, the interspecies collisional cross section $\Gamma_{el} \propto a_{LiCs}^2$ depends on the scattering length a_{LiCs}. The evaporational losses $\dot{N}_{Li}^{evap}$ of ^{6}Li show for sufficiently low scattering lengths a_{LiCs} a dependency of the latter as

$$\dot{N}_{Li}^{evap} \propto a_{LiCs}^2 \tag{4.24}$$

which is advantageous for identifying Feshbach resonance by monitoring ^{6}Li losses. The temperatures during the measurements for the Feshbach resonances were above the temperature, where an influence of the Efimov effect is expected, and an increase of three-body losses is a signature for a Feshbach resonance.

4.4 Observation of interspecies ^{6}Li - ^{133}Cs Feshbach resonances

This section describes the experimental investigation of Feshbach resonances in an ultracold ^{6}Li -^{133}Cs mixture by trap loss spectroscopy. The observed loss features have been analyzed via a couple channels calculation and the results of this calculation are summarized in addition.

Trap loss spectroscopy

In order to investigate Feshbach resonances, a trapped ^{6}Li -^{133}Cs mixture, containing $N_{\mathrm{Cs}} = 5 \cdot 10^4$ ^{133}Cs and $N_{\mathrm{Cs}} = 2 \cdot 10^5$ ^{6}Li atoms at temperatures of $T_{\mathrm{Cs}} = 8$ μK and $T_{\mathrm{Li}} = 2$ μK is prepared via applying the sequentially loading scheme of the Li dipole trap, which is described in detail in Sec.3.5. Furthermore, the ^{6}Li sample is afterwards spin polarized by removing one spin component at a high magnetic field (see Sec. 3.5.3). As described in Sec. 4.3 a Feshbach resonance manifests itself as an enhancement of atomic losses due to an increase of the inelastic three-body recombination rate. In addition, the increase in the elastic scattering cross section on a resonance leads to a significant heating of ^{6}Li by the much hotter ^{133}Cs atoms, resulting in loss of ^{6}Li atoms because of the lower trap depth for this species. Working with comparable ^{6}Li and ^{133}Cs atom densities, the larger visibility of Feshbach resonances is thus expected by monitoring the ^{6}Li atom number during the measurements.

After the preparation of the sample, Feshbach spectroscopy is performed by ramping the magnetic field to a desired value and waiting for a variable hold time between 60 and 2000 ms, which is experimentally optimized to achieve ^{6}Li loss signals between 15 % and 55 %[1]. This results in a clear signature of the resonances, without saturating the loss signal. For four very weak loss features, the ^{133}Cs density in the optical dipole trap was furthermore increased by factors of $1.5 - 3$ by using

[1] The exact conditions are listed in Table 4.1.

longer loading times of the ^{133}Cs MOT. The remaining fraction of ^{6}Li atoms is monitored via high-field absorption imaging providing selectivity on the spin state.

A total of nineteen loss maxima for the energetically two lowest ^{6}Li (^{133}Cs) entrance channels $|\mathrm{F} = 1/2, \mathrm{m_F} = 1/2\rangle$ and $|1/2, -1/2\rangle$ ($|3, 2\rangle$ and $|3, 3\rangle$) were found, all within the range between 650 G and 950 G. Fig. 4.5 shows four ^{6}Li loss spectra in the field region, where the broadest loss features were obtained. In addition scans over narrow features, where four of them showing a doublet structure, are depicted in Fig. 4.6. In order to exclude that the loss features are a signature of an interspecies ^{6}Li Feshbach resonance, ^{133}Cs was removed with a resonant light pulse during the Raman-sideband cooling phase. In addition, the measurement was performed under identical conditions with the other ^{6}Li $\mathrm{m_f}$ component. Furthermore, the measurement was repeated with only ^{133}Cs in the trap, to ensure that the observed ^{6}Li losses are not associated with ^{133}Cs intraspecies Feshbach resonances, which might indirectly influence the number of optically trapped ^{6}Li atoms. Positions and widths of the losses were determined by Gaussian fits, and the results are listed in Table 4.1. Trapping both spin components of ^{6}Li simultaneously with ^{133}Cs atoms for 500 ms, the full accessible field range between 0 G and 1300 G was scanned with a step size of 150 mG, yielding no observable additional interspecies loss features.

In addition to the presented measurements, the Chin group in Chicago reported shortly after our achievement [Repp *et al.*, 2013] about the observation of the five s-wave resonances in the spin channels $^6\mathrm{Li}\,|1/2, -1/2\rangle \oplus^{133}\mathrm{Cs}\,|3, 3\rangle$ and $^6\mathrm{Li}\,|1/2, +1/2\rangle \oplus^{133}\mathrm{Cs}\,|3, 3\rangle$ at magnetic fields, which are consistent with our measurements [Tung *et al.*, 2013].

Assignment of the resonances

The obtained resonances were analyzed in a coupled channels (cc) calculation, which was performed by Prof. E. Tiemann. Therefore only a brief summary is given here. The analysis was done in a similar way to previous calculations on other alkaline systems (see, e.g., Marzok *et al.*, 2009; Schuster *et al.*, 2012), using the atomic parameters for Li and Cs as compiled by Arimondo *et al.*, 1977.

Precise determination of Feshbach resonances and scattering lengths relies on accurate potential curves for the $a^3\Sigma^+$ and $X^1\Sigma^+$ states of ^{6}Li ^{133}Cs . Therefore, both potentials were constructed in a power series of the internuclear separation R, similar to the parametrization of NaK ground state curves [Gerdes *et al.*, 2008]. In a series of iterations between cc calculations for the Feshbach resonances and single channel calculations of rovibrational levels within the singlet and triplet potential,

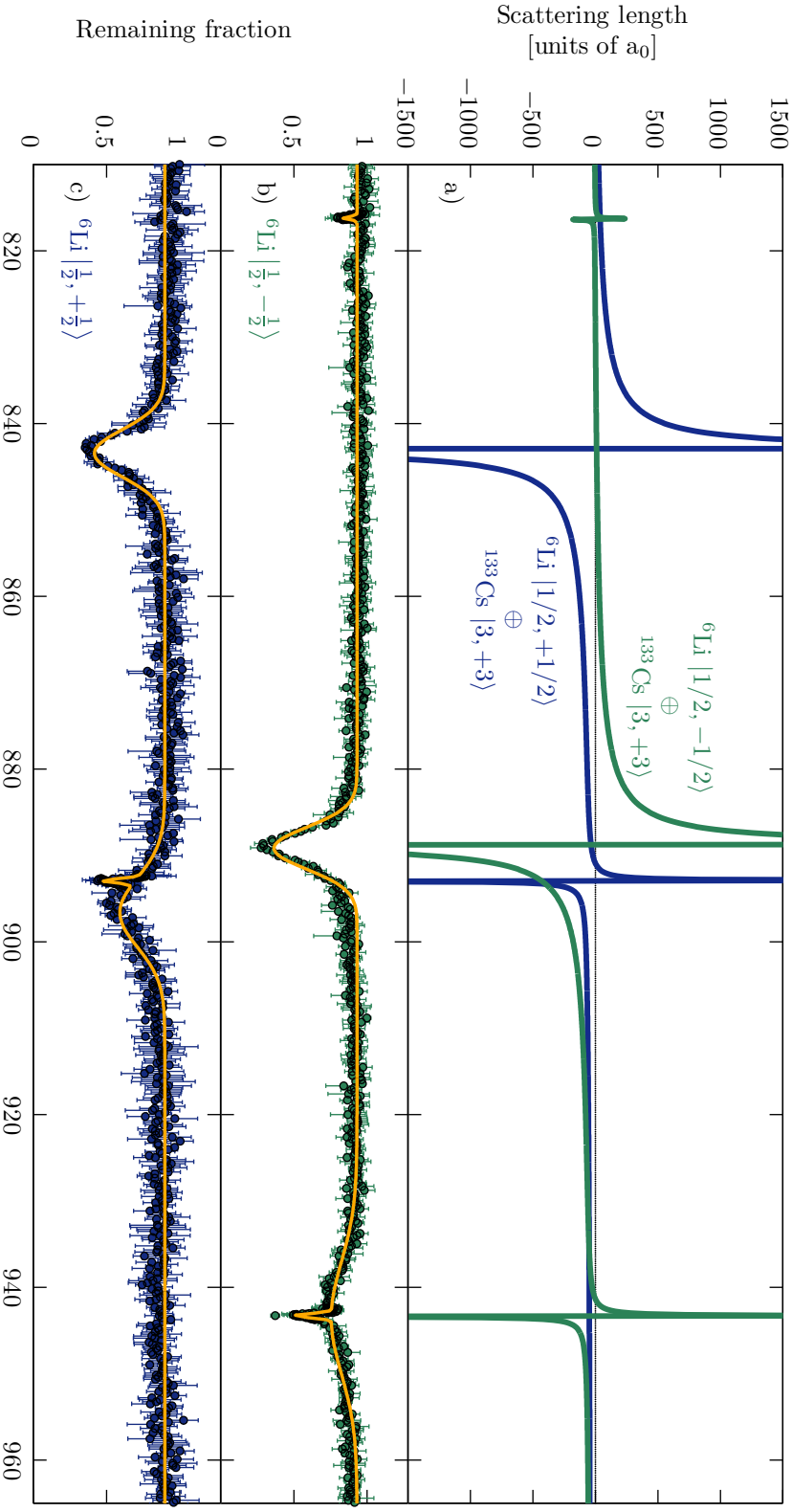

Figure 4.5: Broad interspecies ^{6}Li -^{133}Cs Feshbach resonances. (a) Calculated magnetic field dependence of scattering lengths for the entrance channels Li $|1/2,1/2\rangle \oplus$ Cs $|3,3\rangle$ (blue line) and Li $|1/2,-1/2\rangle \oplus$ Cs $|3,3\rangle$ (green line). (b) and (c) Remaining fraction of Li atoms, normalized to a sample without Cs, in the state $|1/2,-1/2\rangle$ and $|1/2,1/2\rangle$, respectively, after a hold time of 100 ms at the given magnetic field. The broad loss features at 943 G in b) and 893 G in c) arise from a Feshbach resonances of a small amount of Cs in the $|3,2\rangle$ state. The data points are an average over five randomized measurements. Center positions and widths of the loss features are obtained by fitting a sum of Gaussians (orange lines).

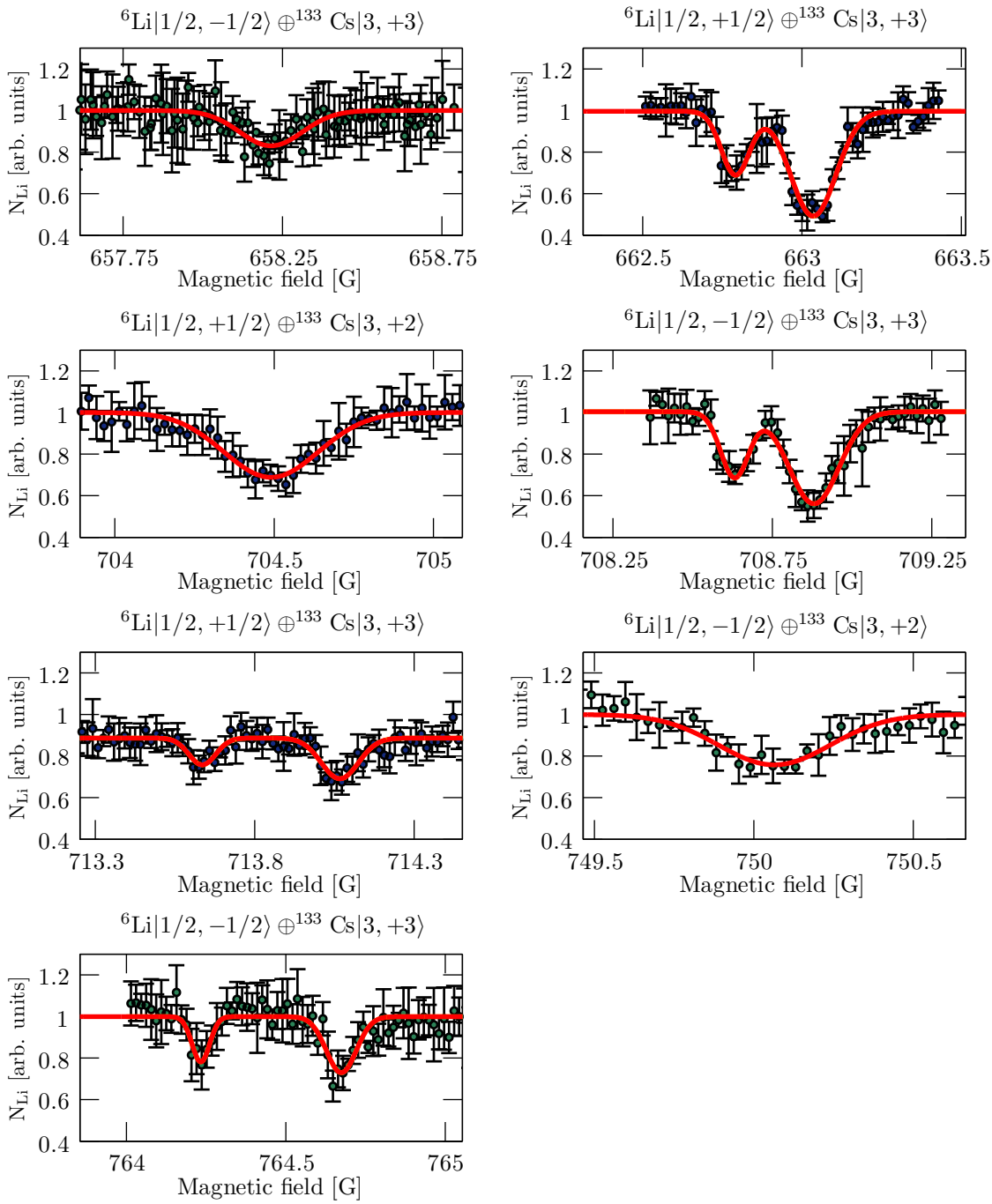

Figure 4.6: Trap loss spectra of the interspecies ^{6}Li -^{133}Cs p-wave resonances. All resonances were measured under different conditions (number of ^{133}Cs atoms in the trap and hold time), which are listed in Table 4.1 and normalized to the offset lines. The individual entrance channels were assigned by the coupled channels calculation.

the description of the potentials was improved by fitting the underlying coefficients to match the locations of the Feshbach resonances and simultaneously the 6498 rovibrational transitions from laser-induced fluorescence Fourier-transform spectroscopy of the previous work [Staanum *et al.*, 2007].

The resulting resonances are listed in Table 4.1 by their deviation $\delta = \mathrm{B}_{\mathrm{res}}^{\mathrm{exp}} - \mathrm{B}_{\mathrm{res}}^{\mathrm{theo}}$, and the resulting scattering length dependence on the magnetic field is depicted in Figure 4.5. $\mathrm{B}_{\mathrm{res}}^{\mathrm{theo}}$ is the peak position of the two-body collision rate at a kinetic energy of 2 μK. The fit used the experimental uncertainty for the weighting. The values are given in Tab. 4.1 and they consist of statistical errors, which were deduced by the 95% confidence interval of the gaussian fits to the loss features. Furthermore a systematic error for the center position of ± 0.1 G originates from the calibration plus an additional ± 0.1 G from day to day drifts have been included. The fit resulted in a reduced chi-squared of 0.75 for all Feshbach resonances, which is very satisfactory, since only three resonances are slightly beyond the experimental uncertainties. It was checked that the s-wave resonances will not shift by more than -0.02 G, choosing a kinetic energy of the entrance channel of 20 nK instead of 2 μK, as it is adequate from the experimental conditions. The redefined potential curves reflect scattering lengths for ^{6}Li - ^{133}Cs (^{7}Li - ^{133}Cs) of $\mathrm{a}_{\mathrm{singlet}} = 30.252(100)$ a_0 ($\mathrm{a}_{\mathrm{singlet}} = 45.477(150)$ a_0) in the singlet potential and $\mathrm{a}_{\mathrm{triplet}} = -34.259(200)$ a_0 ($\mathrm{a}_{\mathrm{triplet}} = 908.6(100)$ a_0) in the triplet potential.

As shown in Fig. 4.6, the splitting of four p-wave resonances could be resolved in the experiment, which originates from different projections of the rotational angular momentum l onto the space fixed axis. A fit to the function

$$\lambda = -\frac{3}{4}\alpha^2 \left(\frac{1}{r^3} + a_{\mathrm{SO}} \exp\left(-br\right) \right) \tag{4.25}$$

(see Eq. 4.14) resulted in $a_{\mathrm{SO}} = -8.0$ au and $b = 0.8$ au.

All Feshbach resonances originate from the least bound levels below the atom pair asymptote 2s $^2S_{1/2}(f_{\mathrm{Li}} = 1/2)$ + 6s $^2S_{1/2}(f_{\mathrm{Cs}} = 3)$ and are significant mixtures of the triplet-singlet manifold shown by an expectation value 0.7 of the total electron spin. Thus only the projection $\mathrm{m_F}$ of the total angular momentum and the rotational angular momentum l are good quantum numbers. The total angular momentum f, excluding l at zero magnetic field, and, due to the strong Cs hyperfine coupling, the angular momentum $G = S + i_{Cs}$ are also good quantum numbers which further justifies the assignment given in Table 4.1.

To characterize the resonance profiles, the resonance parameters for truly elastic scattering channels of two body collisions at the chosen kinetic energy, background

scattering length a_{bg} and the field difference between the resonance position and its zero crossing Δ are additionally given in Table 4.1. Both were determined by fitting the conventional function of the scattering length as function of the magnetic field B:

$$a = a_{\mathrm{bg}}(1 + \frac{\Delta}{B - B_{\mathrm{res}}} + ...), \tag{4.26}$$

using as many terms as resonances are present in this channel. The channels ^{6}Li $|1/2, 1/2\rangle \oplus^{133}$ Cs $|3, 2\rangle$ and ^{6}Li $|1/2, -1/2\rangle \oplus^{133}$ Cs $|3, 2\rangle$ have significant inelastic contributions, thus such simple representation, as described by equation 4.26, of the scattering length as function of B will not be appropriate.

Besides two weak and broad features at 937 G and 988 G in the s-wave entrance channels ^{6}Li $|1/2, \pm 1/2\rangle \oplus^{133}$ Cs $|3, 2\rangle$ and a very sharp feature at 1019 G for the ^{6}Li $|1/2, 1/2\rangle$ state, the cc model suggests a series of d-wave resonances in the field region below 400 G, which all were not detected in the scan over the full field range. No further s- wave resonances for magnetic fields up to 1300 G are expected for the studied entrance channels.

In addition to the cc- calculation, which precisely reproduces all observed resonance positions, an initial attempt to assign the resonances via a weighted least-square fit to a simple, undressed Asymptotic Bound State Model (ABM) [Wille *et al.*, 2008; Tiecke *et al.*, 2010], performed by R. Pires, does not provide a satisfactory agreement with the full set of observed resonance positions, reproducing magnetic field values of the resonances only within a range of 13 G. The ABM yields for $l = 0$ least bound state energies of $\epsilon_0^0 = 3323$ MHz for singlet and $\epsilon_1^0 = 3945$ MHz for triplet state, and for $l = 1$ $\epsilon_0^1 = 2795$ MHz for singlet and $\epsilon_1^1 = 3455$ MHz for triplet state and a singlet-triplet wavefunction overlap of $\zeta = 0.759$. These values deviate significantly from the cc calculation results of $\epsilon_0^0 = 1566$ MHz, $\epsilon_1^0 = 3942$ MHz, $\epsilon_0^1 = 1159$ MHz, $\epsilon_1^1 = 3372$ MHz and $\zeta = 0.866$. In order to minimize the influence of the coupling between resonant channels and continuum of the (broad) s-wave resonances, only the p-wave resonances were fitted, resulting in reduced deviations with $\epsilon_0^0 = 2546$ MHz, $\epsilon_1^0 = 3978$ MHz, $\epsilon_0^1 = 1431$ MHz, $\epsilon_1^1 = 3626$ MHz and $\zeta = 0.845$. These discrepancies, together with the fact that a global shift is obtained from the resonance spectrum by about -60 G when using the values of the cc calculation in the ABM, indicate that a further investigation of the ABM is required.

4.5 Relative tunability of interactions in an ultracold ^{6}Li -^{133}Cs mixture

Three of the observed s-wave resonances provide a unique tunability of the ^{6}Li - ^{133}Cs mixture. The two resonances at 896.6 G and 889.2 G are very close to a zero crossing of the Cs scattering length at 880.2 G, which originates from a very broad s-wave resonance at 787 G [Lee *et al.*, 2007; Berninger *et al.*, 2012]. As the fermionic nature of ^{6}Li suppresses intraspecies collisions in a spin-polarized sample, an intriguing system featuring only tunable interspecies interactions can be created. In addition, the Feshbach resonance at 843.5 G overlaps with the broad intraspecies Feshbach resonances in ^{6}Li at 832.18 G [Zürn *et al.*, 2012] which results in a system with large scattering length both between Cs and the energetically lowest Li state, as well as between the two lowest Li states. Additionally, the coincidence between an Efimov three-body loss minimum at 893 G [Berninger *et al.*, 2011] and two interspecies Feshbach resonances allows for the realization of cooling schemes for ^{6}Li -^{133}Cs mixtures where ^{133}Cs atoms are evaporated with minimized losses, while effectively cooling a ^{6}Li sample sympathetically [Mudrich *et al.*, 2002]. For reaching a quantum degenerate ^{6}Li - ^{133}Cs mixture following this approach, losses during thermalization have to be avoided. Therefore, it might be appropriate to implement species selective optical potentials [LeBlanc and Thywissen, 2007] by using two different wavelengths. This would allow for creating similar trap depths for ^{6}Li and ^{133}Cs .

Entrance channel	B_{res}^{exp}[G]	ΔB^{exp} [G]	N_{Cs}	t_{Hold} [ms]	Li Loss [%]	δ [G]	Δ [G]	a_{bg} [a_0]	m_F	f	G	l
^{6}Li $\|1/2,+1/2\rangle$	662.79(1)	0.10(2)	5×10^4	500	30	-0.04	-	-	7/2	9/2	7/2	1
$\oplus$ ^{133}Cs $\|3,+3\rangle$	663.04(1)	0.17(2)	5×10^4	500	50	-0.02	-	-	9/2	9/2	7/2	1
	713.63(2)	0.10(3)	5×10^4	1000	15	-0.05	-	-	9/2	7/2	7/2	1
	714.07(1)	0.14(3)	5×10^4	1000	30	-0.05	-	-	9/2	7/2	7/2	1
	843.5(4)	6.4(1)	5×10^4	100	50	0.51	60.4	-28.5	7/2	9/2	7/2	0
	892.87(7)*	0.4(2)	5×10^4	60	20	-0.11	4.6	-28.5	7/2	7/2	7/2	0
^{6}Li $\|1/2,-1/2\rangle$	658.21(5)	0.2(1)	14×10^4	1000	20	0.07	-	-	7/2	9/2	7/2	1
$\oplus$ ^{133}Cs $\|3,+3\rangle$	708.63(1)	0.10(2)	5×10^4	500	30	-0.05	-	-	5/2	7/2	7/2	1
	708.88(1)	0.18(2)	5×10^4	500	45	-0.03	-	-	7/2	7/2	7/2	1
	764.23(1)	0.07(3)	5×10^4	2000	20	-0.06	-	-	7/2	5/2	7/2	1
	764.67(1)	0.11(3)	5×10^4	2000	25	-0.05	-	-	7/2	5/2	7/2	1
	816.24(2)	0.20(4)	5×10^4	250	45	-0.12	0.36	-28.4	5/2	9/2	7/2	0
	889.2(2)	5.7(5)	5×10^4	100	55	0.46	59.9	-28.4	5/2	7/2	7/2	0
	943.26(3)	0.38(7)	5×10^4	100	45	-0.12	4.3	-28.4	5/2	5/2	7/2	0
^{6}Li $\|1/2,+1/2\rangle$	704.49(3)	0.35(9)	8×10^4	1000	30	0.07	-	-	7/2	9/2	7/2	1
$\oplus$ ^{133}Cs $\|3,+2\rangle$	896.6(7)	10(2)	5×10^4	100	30	0.68	-	-	5/2	9/2	7/2	0
^{6}Li $\|1/2,-1/2\rangle$	750.06(6)	0.4(2)	8×10^4	1000	25	0.06	-	-	5 /2	7/2	7/2	1
$\oplus$ ^{133}Cs $\|3,+2\rangle$	853.85(1)	0.15(3)	8×10^4	500	40	-0.17	-	-	3 /2	9/2	7/2	0
	943.5(1.1)**	15**(3)	5×10^4	100	20	2.21	-	-	3/2	7/2	7/2	0

Table 4.1: List of interspecies Li-Cs Feshbach resonances for combinations of the entrance channels ^{133}Cs $|f=3,m_f=+2\rangle$, ^{133}Cs $|3,+3\rangle$, ^{6}Li $|1/2,-1/2\rangle$ and ^{6}Li $|1/2,+1/2\rangle$. The experimentally obtained positions and widths are deduced by fitting Gaussian functions with the center at the magnetic field B_{res}^{exp} and the FWHM ΔB^{exp} to the recorded loss spectra. Statistical errors are deduced by the 95% confidence interval of the fit. A systematic error for the center position of ±0.1 G originates from the calibration plus an additional ±0.1 G from day to day drifts. The resonance positions B_{res}^{theo} derived from coupled channels calculations are given as deviations $\delta = B_{res}^{exp} - B_{res}^{theo}$ with respect to the observations, showing excellent agreement. The assigned quantum numbers of the involved molecular states are explained in the text. For the purely elastic channels of two body collisions at the chosen kinetic energy, the background scattering lengths a_{bg} and zero crossings of the scattering lengths with respect to the divergence position for 1 nK kinetic energy is shown. (*) The loss feature at 892.87 G overlaps with a Cs 3-body loss minimum at 893(1) G [Berninger *et al.*, 2011]. This might have a minor effect on the amount of losses due to slightly different ^{133}Cs densities. (**) The fit is not unique, depending on the amount of data points which were considered around the small loss feature at 943.26 G. For the cc-calculation the averaged value 942.6(1.0) G from several profile simulations was used.

Chapter 5

Conclusion and perspectives

At the beginning of this thesis photoassociated LiCs molecules were widely studied, where for instance the formation of LiCs molecules in their rovibrational ground state by a single photoassocation step was demonstrated [Deiglmayr *et al.*, 2008b] or the permanent electric dipole moment of deeply bound dimers was deduced [Deiglmayr *et al.*, 2010a] (see Chapter A for a complete overview). However, the experiments were performed at temperatures of $T \approx$ 10 μK or higher. Motivated by the achievements on photoassociated LiCs molecules, a move of the equipment from the University of Freiburg to Heidelberg was used, for a re-design of the about 15 years old experimental apparatus in order to prepare ^{6}Li -^{133}Cs mixtures at much higher phase-space densities

Starting with an empty laboratory, new vacuum and laser systems were designed and set up in order to laser cool the two species. A key element is a double species Zeeman slower, which accounts for the different required magnetic fields due to the large mass imbalance of the two species. The performance of the system was characterized by monitoring the loading dynamics of the magneto-optical traps. Loading rates into the MOTs of $\mathrm{R_{Cs}} = 2.1 \cdot 10^{8}$ atoms/s for ^{133}Cs and a corresponding rate of $\mathrm{R_{Li}} = 1.3 \cdot 10^{8}$ atoms/s for ^{6}Li after a compression phase were obtained at typical operation conditions. The achieved loading rates are sufficient for ensuring fast experimental cycle times. Moreover, degenerate Raman-Sideband Cooling (DRSC) for ^{133}Cs was implemented at the setup in order to further cool and spin polarize the atoms. This results in samples containing $2 \cdot 10^{7}$ atoms at temperatures of $T \approx$ 1 μK after loading a ^{133}Cs MOT for 1 s. Stern-Gerlach measurements allowed one to deduce the degree of spin purity of the samples, where 85% of the atoms are after DRSC were found to be in the energetically lowest spin state $|F = 3, m_F = 3\rangle$ whereas about 15% populated the state $|F = 3, m_F = 2\rangle$.

The phase-space densities were dramatically increased by further evaporatively cooling the atoms in optical dipole traps. In order to account for different conditions after laser cooling as well as for the contrary requirements during the evaporation, two optical dipole traps have been set up in the course of this thesis. Evaporative cooling of ^{133}Cs in a dipole trap, that was optimized for that species, resulted in the best schemes in atom numbers of $N_{\mathrm{Cs}} = 7 \cdot 10^4$ at temperatures of $T_{\mathrm{Cs}} = 100$ nK. However, the corresponding phase-space density of $\rho_{\mathrm{Cs}} = 4 \cdot 10^{-2}$ is below the critical phase-space density for obtaining Bose-Einstein condensation. An onset of quantum degeneracy was probably prevented by the small trapping frequencies and a modification of the trapping potential might be advantageous for further experiments. Quantum degeneracy was realized in a trap that was set up for ^{6}Li . Evaporatively cooling a two-spin component Fermi gas of ^{6}Li led to the observation of a bimodal density distribution, where condensate fractions up to 30% were deduced.

The combined trapping of an ultracold Bose-Fermi mixture of ^{6}Li -^{133}Cs was demonstrated for the first time in our experiment in the frame of this thesis[1]. This was realized by first transferring and evaporatively cooling ^{6}Li atoms in a trap to temperatures of $T_{\mathrm{Li}} = 2.5$ μK where $N_{\mathrm{Li}} = 10^5$ ^{6}Li atoms remained. A ^{133}Cs MOT was loaded at a slightly different position, which was afterwards overlapped with the trap center where Cs atoms were further cooled and spin polarized by DRSC. At this stage $N_{\mathrm{Cs}} = 5 \cdot 10^4$ ^{133}Cs and $N_{\mathrm{Li}} = 2 \cdot 10^5$ ^{6}Li atoms were trapped at temperatures of $T_{\mathrm{Cs}} = 8$ μK and $T_{\mathrm{Li}} = 2$ μK, respectively. A further measurement of the trapping frequencies allowed to deduce atomic peak densities of $n_{\mathrm{Cs}} = 3 \cdot 10^{11}$ cm^{-3} and $n_{\mathrm{Li}} = 1 \cdot 10^{12}$ cm^{-3}.

A main result of this thesis is the exploration of interspecies Feshbach resonances in the Li-Cs system. The ability of preparing trapped ^{6}Li -^{133}Cs mixtures enabled trap loss spectroscopy measurements, where the Feshbach resonances were identified by observing an enhancement of atomic loss. A total of nineteen interspecies loss maxima for the energetically two lowest ^{6}Li (^{133}Cs) entrance channels $|F = 1/2, m_f = 1/2\rangle$ and $|1/2, -1/2\rangle$ ($|3, 2\rangle$ and $|3, 3\rangle$) were found, all within the range between 650 G and 950 G. Shortly after our realization [Repp *et al.*, 2013], the Chin group in Chicago reported of at the observation of five Feshbach resonances at positions, which are consistent with our results [Tung *et al.*, 2013]. A collaboration with Prof. E. Tiemann from the University of Hannover, who analyzed our data by a couple channels calculation, led to an assignment of all the found resonances to s- and p-wave molecular channels. While the interspecies scattering length for most

[1]Shortly after our realization [Repp *et al.*, 2013], the Chin group in Chicago also reported on the preparation of an ultracold ^{6}Li -^{133}Cs mixture [Tung *et al.*, 2013].

of the magnetic field regions nearly vanishes ($a \approx -30\ a_o$), the field region between 800 G and 950 G is of particular interest. Two 60 G broad[2], two 5 G broad and one 0.5 G broad Feshbach resonances with s-wave character between ^{133}Cs atoms in their energetically lowest spin state and ^{6}Li atoms in either of the two lowest spin states allow for a precise tuning of the collisional properties.

5.1 Perspectives

The broad interspecies ^{6}Li -^{133}Cs Feshbach resonances give access to study of different effects of few and many-body physics in ultracold ^{6}Li -^{133}Cs mixtures. Since deeply bound LiCs molecules [Deiglmayr *et al.*, 2008b] have a permanent dipole moment of 5.5 D [Aymar and Dulieu, 2005; Deiglmayr *et al.*, 2010a], the largest among all alkaline combinations, the most prominent application relies on the formation of a dipolar quantum gas (for review articles see [Baranov, 2008; Pupillo *et al.*, 2008b; Lahaye *et al.*, 2009; Baranov *et al.*, 2012]) of LiCs molecules. Opposed to molecules, Fröhlich polarons [Fröhlich, 1954; for a review see Devreese and Alexandrov, 2009] can be investigated by using the fact that one of the scattering lengths is found in a magnetic field region, where a nearly ideal gas of Cs can be prepared. Furthermore, the precise tunability of the interspecies scattering length is considered to be promising for the investigation of the Efimov effect [Braaten and Hammer, 2007], where the large mass difference of ^{6}Li and ^{133}Cs is advantageous for the observation of a whole series of resonances [D'Incao and Esry, 2006]. This section will present these different possibilities in detail.

5.1.1 Dipolar molecules

Insight into many-body phenomena are expected from polar molecules at high phase-space densities, due the long-range and anisotropic character of the dipole-dipole interaction (for a review see e.g. [Carr *et al.*, 2009]). Interesting perspectives are for instance the study of two- dimensional samples [Micheli *et al.*, 2007]. Depending on the strength of the dipolar interactions, transitions to super-fluid phases and, if repulsive dipolar interactions dominate over the kinetic energy, even crystalline phases are expected [Büchler *et al.*, 2007]. Simulation of condensed matter systems becomes feasible [Pupillo *et al.*, 2008b] where novel, tunable potentials for additional particles can be generated [Pupillo *et al.*, 2008a]. Besides two dimensional systems,

[2]Here, the widths are given as distance of the calculated resonance positions and the calculated zero crossing of the scattering lengths.

dipolar molecules are considered also to be an excellent candidate for the investigation of interacting one-dimensional tubes, where novel spatial ordering effects are predicted [Dalmonte *et al.*, 2010; Astrakharchik *et al.*, 2008]. Furthermore, these molecules are considered to be an excellent candidate for the realization quantum computing schemes [DeMille, 2002].

This section shortly reviews the dipolar interaction and compares the different dipole moments that are present in ultracold systems, demonstrating the outstanding character of deeply bound LiCs molecules. The reader is also referred to Chapter A. Besides a brief overview over molecular formation schemes and a summarize the results of the measurements on photoassociated LiCs molecules, also a short introduction in ultracold reactions can be found there.

Dipolar interactions

For particles possessing permanent dipole moments additional forces exist, that arise from the dipole-dipole interaction. The potential for two dipoles, separated by a distance $\vec{R}$ can be expressed by [Lahaye *et al.*, 2009]

$$U_{dd}(\vec{R}) = \frac{C_{dd}}{4\pi}\frac{(\vec{e_1}\cdot\vec{e_2})R^2 - 3(\vec{e_1}\vec{R})(\vec{e_2}\vec{R})}{R^5} \tag{5.1}$$

with unit vectors $\vec{e_1}$ and $\vec{e_2}$ and a coupling constant C_{dd} (see Fig. 5.1 a)). If the system is polarized via an external field, all dipoles are aligned parallel and the resulting potential is given by [Lahaye *et al.*, 2009]:

$$U_{dd}(\vec{R}) = \frac{C_{dd}}{4\pi}\frac{1-3\cos^2(\theta)}{R^3} \tag{5.2}$$

Here, θ denotes the angle between the polarization axis and the relative position (see Fig. 5.1 b)). As depicted in Fig. 5.1 c) and d), the forces are anisotropic and have attractive (repulsive) character for angles smaller (larger) than the "magic angle" $\theta = \arccos(1/\sqrt{3}) \approx 55°$.

Besides changing the electric field strength, tunability can be reached, if a static field with magnitude E_z is combined with an oscillating field of amplitude E_{xy} in perpendicular direction. In the adiabatic limit, where the orientation of the dipoles follows the direction of the field, a time averaged potential [Giovanazzi *et al.*, 2002]

$$\langle U_{dd}(\vec{R})\rangle_t = \frac{C_{dd}}{4\pi}\frac{1-3\cos^2(\theta)}{R^3}\frac{3\cos^2\phi - 1}{2} \tag{5.3}$$

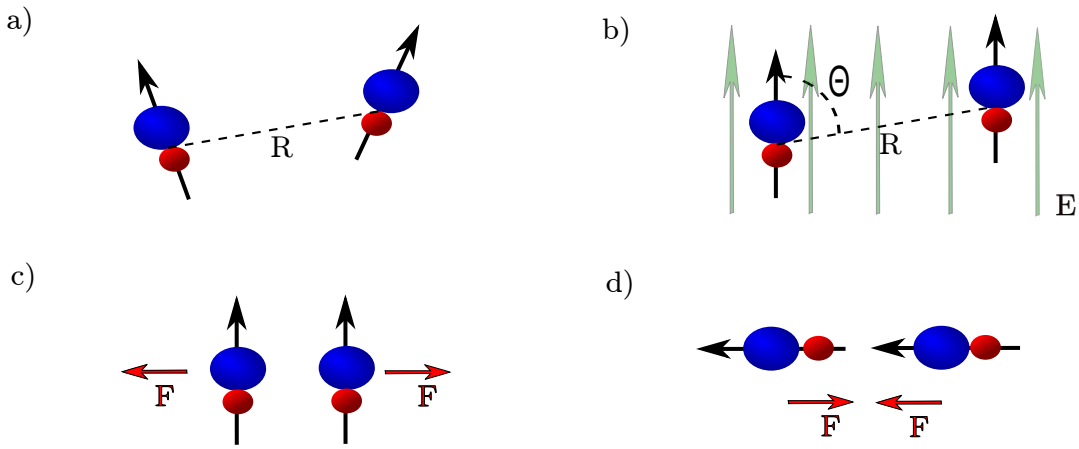

Figure 5.1: Dipole-dipole interaction of two molecules. (a) The dipoles are arranged arbitrarily in a non polarized configuration. (b) An external electric field orientates the molecules, leading to a polarized sample. (c,d) Due to the anisotropic nature, the forces are repulsive in a "side by side" arrangement (c) and attractive in a "head-to-tail" configuration (d). Modified replotted from Lahaye *et al.*, 2009.

is created, which can be varied by changing the ratio of the field amplitudes $\phi = \arctan(E_{xy}/E_z)$.

The strength of the interaction strongly depends on the coupling constant C_{dd} between the dipoles. For magnetic (electric) dipoles, with permanent magnetic (electric) dipole moments μ (d), C_{dd} is given by $C_{dd}^{mag} = \mu_0\mu^2$ ($C_{dd}^{el} = d^2/\epsilon_0$) [Lahaye *et al.*, 2009], where μ (ϵ_0) denotes the magnetic (electric) vacuum permeability. Typical permanent electric dipole moments are on the order of $e \cdot a_0{}^3$ while for magnetic dipoles, typically $\mu \approx \mu_B$. The ratio of the magnetic versus the electric coupling constant can thus be estimated via [Lahaye *et al.*, 2009]:

$$\frac{C_{dd}^{mag}}{C_{dd}^{el}} \approx \frac{\mu_0\mu^2}{d^2/\epsilon_0} \approx \alpha^2 \approx 10^{-4} \tag{5.4}$$

Therefore, much higher forces are expected by using electric dipole moments.

The permanent dipole moment of polar molecules

A suitable system for studying dipolar effects are alkaline heteronuclear dimers in their lowest vibrational states, which are on the order of several Debye [Aymar and Dulieu, 2005]. Experiments with deeply bound ground state LiCs molecules with about d=5.5 D, containing the largest permanent dipole moment among all alkaline

[3] e denotes the electron charge and a_o the Bohr radius.

combinations are very promising. This can be seen in Fig 5.2 which depicts the vibrational quantum number dependence of the dipole moment of all heteronuclear alkaline dimers as well as a measurement of the permanent dipole moment of deeply bound LiCs molecules.

However, for observing dipolar effects an ensemble needs to be polarized by an external electric field. In order to induce a dipole moment in the laboratory frame, the effective polarizabilities $\bar{\alpha}$ have to be considered. A study of heteronuclear alkaline dimers in their vibrational ground state shows that RbCs molecules have effective polarizabilities $\bar{\alpha}_{RbCs} = 597.6$ a.u., which is significantly larger than $\bar{\alpha}_{LiCs} = 368.8$ a.u., as calculated for LiCs [Deiglmayr *et al.*, 2008a]. A further investigation of the field dependence of the induced electric dipole moment d showed that already at electric fields $E \approx 2$ kV/cm LiCs molecules exhibit the electric dipole moment of RbCs at infinite fields. A fields of $E \approx 20$ kV/cm, which might be experimentally accessible, LiCs molecules have an induced dipole moment of $d_{LiCs} > 4$ D, which extends all other stable heteronuclear molecules at this field [Julienne *et al.*, 2011].

LiCs molecules have been already excessively studied in a series of experiments via performing photoassociation [Jones *et al.*, 2006; Ulmanis *et al.*, 2012] at an early stage of this thesis [Deiglmayr *et al.*, 2008b; Deiglmayr *et al.*, 2009a; Deiglmayr *et al.*, 2009b; Grochola *et al.*, 2009; Deiglmayr *et al.*, 2010a; Deiglmayr *et al.*, 2010b; Deiglmayr *et al.*, 2011a; Deiglmayr *et al.*, 2011b] which are reviewed in Sec. A. However, the phase-space densities had been too low in these experiments in order to observe dipolar many-body effects. The obtained interspecies Feshbach resonances, which have been described in the previous chapter, make the investigation of dipolar effects in a sample of deeply bound LiCs feasible. Having the ability of ramping a magnetic field over a Feshbach resonance allows for the transfer of an atomic sample into a sample, that consists of weakly bound molecules [Herbig *et al.*, 2003; Regal *et al.*, 2003; Köhler *et al.*, 2006]. These dimers can be further converted into deeply bound molecules via a coherent stimulated rapid adiabatic passage (STIRAP)[Ni *et al.*, 2008; Danzl *et al.*, 2008; Lang *et al.*, 2008]. A more detailed description of this two processes can be found in Sec. A.1.1. Since chemical reactions between two LiCs molecules are expected to decay into homonuclear Li_2 and Cs_2 dimers in a chemical reaction [Żuchowski and Hutson, 2010], special care needs to be taken on the selection of the trapping potential, when working with dense molecular samples. This is discussed in Sec. A.2.

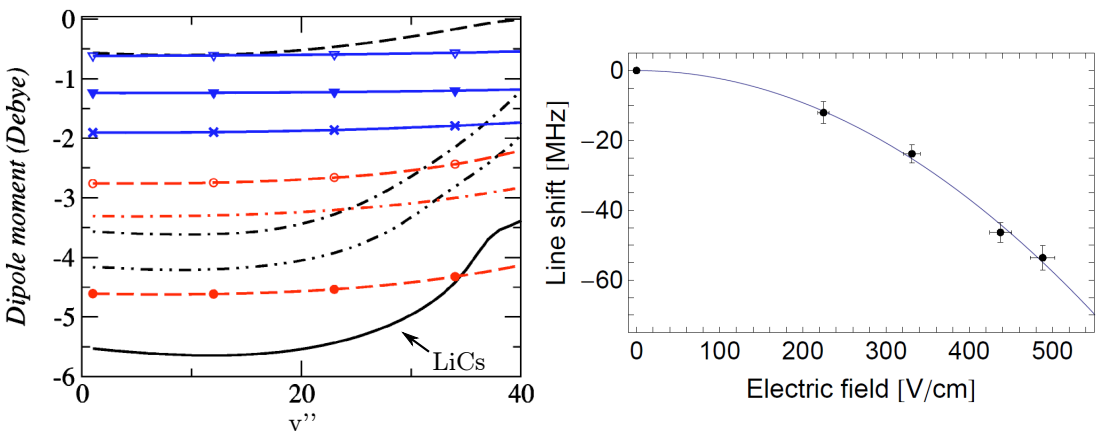

Figure 5.2: Permanent electric dipole moment. Left: The variation of the permanent dipole moment for ground state molecules for various heteronuclear alkaline combinations in respect to the vibrational quantum number v'' is shown. The dipole moment of LiCs corresponds to the black solid line. Reprinted with permission from Aymar and Dulieu, 2005. Copyright 2005, American Institute of Physics. Right: Measurement of the permanent electric dipole moment of LiCs molecules in the state $X^1\Sigma^+, v'' = 2, J'' = 0$ by monitoring the Stark shift of transitions to the $B^1\Pi, v' = 18, J' = 1$ level. The quadratic field dependence corresponds to a permanent electric dipole moment of 5.5(2) D. Adapted from Deiglmayr *et al.*, 2010a.

Other dipolar quantum gases

Weaker, but still significant magnetic dipole-dipole interactions exist in the ultracold regime of elements with a complex electron shell structure. The expansion dynamics and the collapse of BECs was used to observe such magnetic dipole-dipole interactions. Initial experiments investigated Chromium samples [Stuhler *et al.*, 2005; Beaufils *et al.*, 2008], which have a permanent magnetic dipole moment of $\mu = 6\ \mu_B$. More recently dipolar effects were observed by investigating Dysprosium [Lu *et al.*, 2011] and Erbium [Aikawa *et al.*, 2012], which have permanent magnetic dipole moments of $\mu = 10\ \mu_B$ and $\mu = 7\ \mu_B$, respectively. However, the largest interactions of neutral atoms are provided by Rydberg atoms [Lahaye *et al.*, 2009].

5.1.2 Modeling Fröhlich type polarons

A fundamental problem in solid state physics is the dynamics of an electron moving in a charged ion lattice. Due to the Coulomb forces, the electron interacts with the lattice core atoms and excites lattice phonons by polarizing the surrounding media, while the back action of the resulting polarizing field influences the electron

movement. The combined system of lattice phonons and electrons, can be treated as a quasi-particle, a so called Fröhlich polaron, which is described by the Fröhlich Hamiltonian [Fröhlich, 1954; for a review see Devreese and Alexandrov, 2009]. The mobility of the polaron is thereby characterized via introducing an effective mass $m_{eff} > m_{el}$, which is larger than the electron mass m_{el}. Depending on the coupling strength, two regimes are classified: Delocalized states exist within the so called *weakly coupled regime*, whereas in the *strongly coupled regime*, a diverging effective mass leads to self-trapped states of the polarons.

Insight to the Fröhlich polaron can be provided by experiments with ultracold mixtures, since the underlying Hamiltonian of an impurity in a BEC can be directly mapped to the Fröhlich Hamiltonian [Cucchietti and Timmermans, 2006; Tempere *et al.*, 2009]. The lattice phonons are represented by Bogoliubov modes in the Bose-Einstein condensate, whereas Feshbach resonances allow for a precise adjustment of the modeled phonon-electron coupling strength [Tempere *et al.*, 2009]

$$\alpha = 15^{1/5} \left(\frac{N_B \cdot a_{bb}}{\bar{a}_{HO}} \right)^{1/5} \frac{a_{IB}^2}{a_{BB} \cdot \bar{a}_{HO}}, \tag{5.5}$$

by varying the Boson-Boson (Boson-Impurity) scattering lengths a_{BB} (a_{IB}). Further tunability of α can be achieved by changing the number of particles in the BEC N_B as well as the harmonic oscillator length $\bar{a}_{HO} = \sqrt{\hbar/m_B\bar{\omega}_B}$ for Bosons of mass m_B, which are confined in an optical trap with a mean trapping frequency $\bar{\omega}_B$.

Interesting prospectives rely on the possibility of reaching the strongly coupled regime, which corresponds to $\alpha \gtrsim 1$. For sufficiently low temperatures, Tempere *et al.*, 2009 predicts a dramatic increase of the effective polaron mass for $\alpha > 3$. Similar to solid state systems, self-localized phenomena of the impurity are also expected in the ultracold regime for strong couplings [Sacha and Timmermans, 2006], where the tunability of the coupling strengths give access to phase diagrams of the level of the impurities' localization, including a collapse of the BEC at extreme interactions [Kalas and Blume, 2006].

Furthermore, the dynamics of a fermionic impurity in a BEC within the weak coupling regime can be studied. As predicted by a semi-classical treatment, depending on whether the velocity of the impurity is above or below the sound velocity of the BEC, damping occurs [Dasenbrook and Komnik, 2013].

Experiments of a ^{6}Li impurity in a ^{133}Cs BEC at magnetic fields of about $B =$ 890 G are very promising for reaching the strong coupling regime. As depicted in Fig. 5.3, $\alpha \gtrsim 1$ is reached for magnetic fields $B \approx$ 886 G - 892 G, while assum-

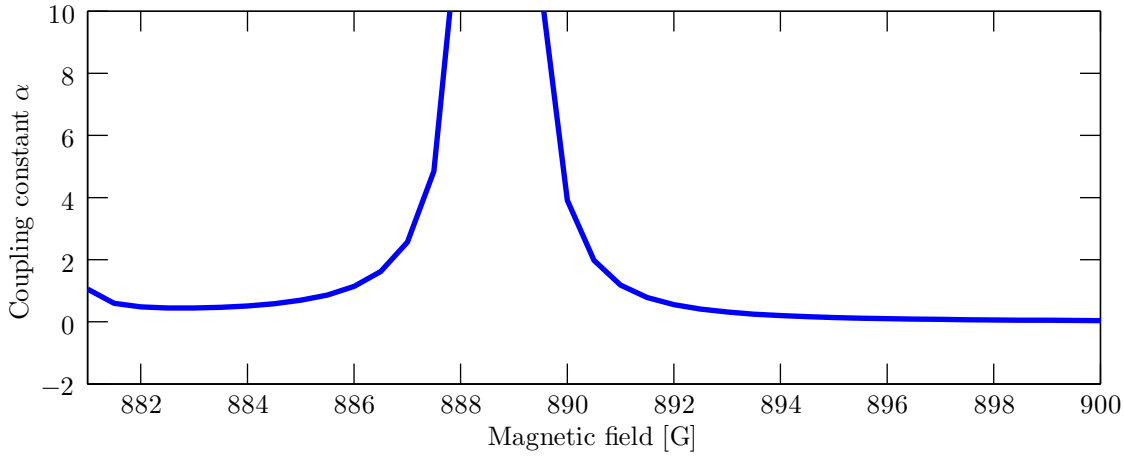

Figure 5.3: Calculated magnetic field dependence of the polaron coupling constant α of a ^{6}Li impurity interacting with a ^{133}Cs BEC . The strong coupling regime ($\alpha \gtrsim 1$; see text) is reached for fields $B \approx 886$ G - 892 G. The dependence was derived by Equation 5.5 for a ^{6}Li impurity in the $|1/2; -1/2\rangle$ state in Cs BEC, containing $N_B = 10^5$ particles in a potential with an average trapping frequency $\omega_{Cs}^{-} = 2\pi \cdot 100$ Hz. The behavior of α reflects the zero crossing of the ^{133}Cs scattering length at 881 G as well as the ^{6}Li -^{133}Cs Feshbach resonance at 889 G. The underlying ^{133}Cs scattering lengths [Berninger *et al.*, 2012] were provided by courtesy of Prof. Julienne [Julienne, 2012].

ing realistic experimental conditions. In the considered region, the ^{133}Cs scattering length [Berninger *et al.*, 2011] is positive. This allows for the creation of BECs, and in addition three-body losses of ^{133}Cs are minimized in the considered region, due to an Efimov three-body loss minimum at 893 G [Berninger *et al.*, 2011].

The coincidence of an interspecies ^{6}Li -^{133}Cs Feshbach resonance at 843 and an intraspecies ^{6}Li Feshbach resonance at 832 G [Zürn *et al.*, 2012] results in a system with large scattering lengths both between ^{133}Cs and the energetically lowest ^{6}Li state, as well as between the two lowest ^{6}Li states. This scenario might be additionally suitable for studying self-localization of bosonic impurities immersed in a two-component superfluid Fermi gas [Targońska and Sacha, 2010].

In a pioneering experiment, K impurities in a one-dimensional Rb Bose gas were investigated, however, no change of the impurity trapping frequency was observed [Catani *et al.*, 2012]. This is in contrast to the expectation, where the variation of the interaction strengths results in a change of the effective mass which manifests itself in a change of the trapping frequency. In contrast, polaronic behavior of so-called Fermi-polarons was demonstrated in slightly different systems in the ultracold domain: Using spin imbalanced Fermi-Fermi mixtures of the same species, an increase of the effective mass [Nascimbène *et al.*, 2009] and a modified radio-frequency

spectrum, arising from the polaron [Schirotzek *et al.*, 2009] was observed. More recently, attractive [Koschorreck *et al.*, 2012] as well as repulsive [Kohstall *et al.*, 2012] Fermi- polarons were identified by working with spin mixtures of K and Fermi-Fermi mixtures of Li-K, respectively.

5.1.3 Efimov states in systems with large mass imbalance

The ability to accurately tune the interspecies scattering length via broad interspecies s-wave Feshbach resonances gives the opportunity of studying universal few-body physics by investigating the Efimov effect (for reviews see Braaten and Hammer, 2007 and Ferlaino *et al.*, 2011), which was originally proposed in the context of nuclear physics [Efimov, 1971; Efimov, 1979]. In the universal regime, where binary interactions are characterized by the single parameter a, the scattering length, an infinite series of three body states exist for diverging scattering lengths. This series is characterized by a universal scaling of the binding energies E_N and E_{N+1} between the states N and $N+1$ at the Feshbach resonance ($a = \infty$) where the states are separated by

$$\frac{E_{N+1}}{E_N} = \exp(-2\pi/S_0). \tag{5.6}$$

The property $\exp(\pi/S_0)$ (≈ 22.7 for bosonic systems of equal mass) denotes the geometrical factor. For negative scattering lengths, an additional universal connection exists between the values of a, where the binding energies E_N and E_{N+1} are zero and crosses the tri-atomic threshold at a_N and a_{N+1}, respectively:

$$\frac{a_{N+1}}{a_N} = \exp(-\pi/S_0). \tag{5.7}$$

Further relations exist for the crossing of the Efimov states with the binding energy of the universal dimer state at positive scattering lengths, as well as with an additional three-body recombination minimum (see [Ferlaino *et al.*, 2011] for an overview). An overview of the Efimov scenario for identical particles is depicted in Fig. 5.4.

After an initial experiment with ^{133}Cs [Kraemer *et al.*, 2006] , Efimov features were confirmed by subsequent investigations using various homonuclear alkaline systems [Ottenstein *et al.*, 2008; Knoop *et al.*, 2009; Huckans *et al.*, 2009; Zaccanti *et al.*, 2009; Williams *et al.*, 2009; Gross *et al.*, 2009; Ferlaino *et al.*, 2009; Lompe *et al.*, 2010; Nakajima *et al.*, 2011; Berninger *et al.*, 2011; Gross *et al.*, 2011; Roy *et al.*, 2013] as well as K-Rb mixtures [Barontini *et al.*, 2009]. However, a series of Efimov states has so far not been observed, since a precise tuning of the scattering length by about two orders of magnitude is required for equal mass systems.

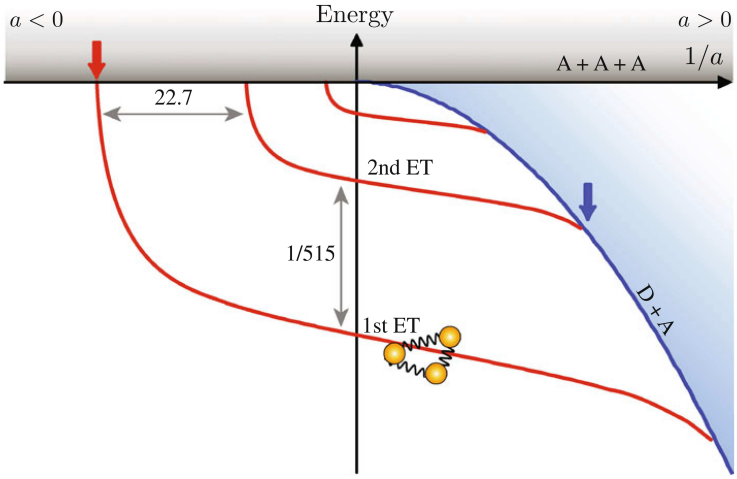

Figure 5.4: Efimov scenario for identical particles. The binding energy of three body Efimov states (red lines) and the binding energy of a universal dimer state (blue line) is shown as a function of the inverse scattering length 1/a. For systems of identical atoms the first two states, at which the states cross the scattering continuum at attractive interactions (a<0) are spaced by a factor of 22.7, whereas the large mass difference in the Li-Cs system leads to a reduction to 4.9 [D'Incao and Esry, 2006]. Reprinted with kind permission from Springer Science and Business Media from Ferlaino *et al.*, 2011 .

An improved situation arises by preparing ultracold mixtures containing constituents with large mass ratios, where a reduction of the scaling is expected for increased mass ratios [D'Incao and Esry, 2006; Helfrich *et al.*, 2010]. Most promising are thus experiments dealing with ^{6}Li and ^{133}Cs , where the extreme mass ratio of $m_{Cs}/m_{Li} \approx 22$ results in an advantageous geometrical factor of $\exp(\pi/S_0) \approx 4.9$ for Cs-Cs-Li Efimov states [D'Incao and Esry, 2006]. Therefore the amount of resonances, in a given scattering length interval is increased, while precise adjustment of the scattering length can be provided via the 60 G broad Feshbach resonances at 843 G and 889 G.

As pointed out for several ^{133}Cs Feshbach resonances by Berninger *et al.*, 2011 as well as recently for ^{39}K by Roy *et al.*, 2013 and more general for different homonuclear systems by Chin, 2011, the first Efimov state a_0 can be connected for all systems with the van-der-Waals radius R_{vdW} via $a_0 \approx -10\ R_{vdW}$. An observation of the Efimov effect in Li-Cs mixtures could clarify if such a universal behavior of the underlying so-called three-body parameter also holds for heteronuclear systems, as recently proposed by Wang *et al.*, 2012.

Furthermore, the Li-Cs system is well suited for measuring the energy dependencies of the Efimov states via collision experiments [Wang *et al.*, 2010]. An open

question is the possibility of the appearance of universal Efimov resonances containing more than three particles, as it could be seen for ^{133}Cs , where four-body [Ferlaino *et al.*, 2009] and even five-body resonances [Zenesini *et al.*, 2012] were detected.

Appendix A

Ultracold LiCs molecules: Formation, molecular collisions and dipolar effects

As already described in Sec. 5.1.1 deeply bound heteronuclear molecules can be very promising for the investigating of many-body phenomena, which arise from the long-range and anisotropic dipole-dipole interaction [for a review see e.g. Carr *et al.*, 2009], or for the implementation of quantum computing schemes [DeMille, 2002]. As also mentioned in Sec. 5.1.1 deeply bound LiCs molecules processes the largest permanent electric dipole moment among all alkaline dimers [Aymar and Dulieu, 2005; Deiglmayr *et al.*, 2010a]. It is therefore seen as an excellent candidate to explore dipolar effects. Using a previous version of the experimental apparatus, extensive knowledge about the properties of the LiCs molecule was obtained at the University of Freiburg [Kraft, 2006; Lange, 2008; Deiglmayr, 2009]. Initially the photoassociation (PA) [Jones *et al.*, 2006; Ulmanis *et al.*, 2012] of LiCs molecules by the cooling light in overlapped Li and Cs MOTs [Kraft *et al.*, 2006] was observed. At an early stage of this thesis the formation of ultracold LiCs molecules was then optimized by a detailed experimental investigation of the molecular structure [Grochola *et al.*, 2009; Deiglmayr *et al.*, 2009b; Deiglmayr *et al.*, 2010a] leading to the formation of LiCs molecules in the rovibrational ground state [Deiglmayr *et al.*, 2008b]. In these experiments the molecules were detected by ionizing them in a resonant-enhanced multi-photon ionization scheme, followed mass-selective detection in a time-of-flight spectrometer [Kraft *et al.*, 2007]. This sections summarize these results, which are described in detail in the PhD thesis of Johannes Deiglmayr [Deiglmayr, 2009] and are part of the review article Ulmanis *et al.*, 2012. Due to

the ability of interspecies Li-Cs Feshbach resonances enables the preparation of LiCs samples via magnetoassocation instead of photoassocation techniques where much higher molecular phase-space densities can be reached.

This chapter starts with a brief overview over photoassocation and magnetoassociation schemes more in detail and reviews the formation of LiCs molecules in the excited state via photoassocation. Subsequent spontaneous decay led to the observation of deeply bound state molecules. Afterwards, an introduction in inelastic collisions at ultracold temperatures of heteronuclear alkaline dimers is given, which can lead to losses in molecular sample. The last part reviews the observation of dipolar effects of LiCs molecules.

A.1 Formation of deeply bound, ultracold molecules

An experimental challenge is the preparation of dense samples of polar molecular at ultracold temperatures. Molecules in the mK range have been yet obtained by the application of direct cooling methods, such as Buffer-gas cooling [Weinstein *et al.*, 1998], Stark decelerating [van de Meerakker *et al.*, 2005] or Billiard-like collisions [Strecker and Chandler, 2008]. Colder molecular temperatures in the μK regime are reached by performing photoassociation at an initially laser- cooled atomic mixtures of two species [for reviews see Jones *et al.*, 2006; Ulmanis *et al.*, 2012]. However the highest phase-space densities of heteronuclear molecules have so far been reached via applying the combination of magnetoassociation and STIRAP techniques on dense and ultracold K-Rb [Ni *et al.*, 2008] and Rb-Cs mixtures [Innsbruck group, unpublished yet, see Debatin *et al.*, 2011 and Takekoshi *et al.*, 2012 for principal procedure].

A.1.1 Synthesis of ultra cold molecules out of ultracold atoms

This section gives a short overview over the photoassociation and magnetoassocation technique, which were so far used for creating molecules out of ultracold atomic samples. Both processes are depicted in Fig. A.1.

- **Photoassocation.** During a photoassociation process (for reviews see e.g. [Jones *et al.*, 2006; Ulmanis *et al.*, 2012]), an excited bound molecular state AB^* is formed out of colliding atoms A and B by first absorbing a resonant photon of energy $h\nu$:

$$A + B + h\nu \mapsto AB^*. \tag{A.1}$$

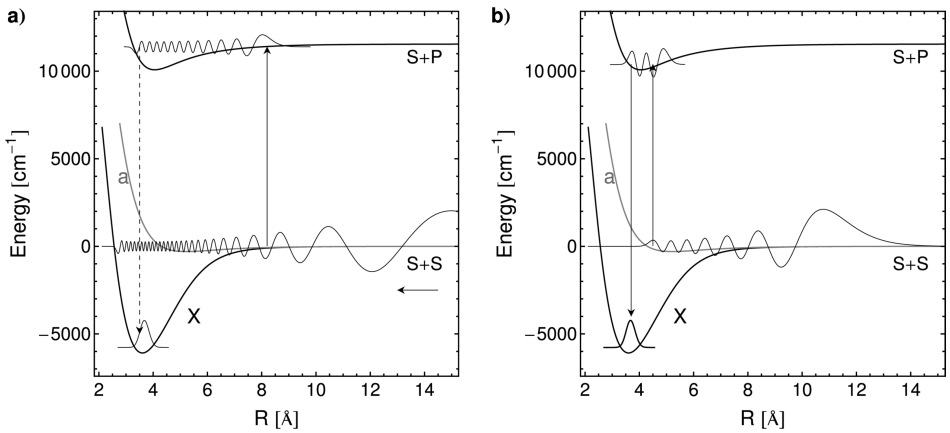

Figure A.1: (a) Photoassocation and (b) magnetoassocation and Raman transfer. In photoassocation, an excited molecular state is populated via the absorption of a photon during a collision of an atomic pair. Molecular levels in the ground state are populated by a following spontaneous decay process. In magnetoassocation, a weakly bound molecular state is prepared by ramping a magnetic field over a Feshbach resonance in an atomic sample. The population can be coherently transfered into deeper states via a stimulated Raman transfers by making use of two pulsed laser beams. Taken from Ulmanis *et al.*, 2012.

A subsequent emission of a photon $h\nu^*$ can either lead to a relaxation into rovibrational levels in the electronic ground state

$$AB^* \mapsto AB + h\nu^* \tag{A.2}$$

or form unbound pairs. The process is depicted in Fig. A.1. The ground state population distribution in this process is given by the wavefunction overlap between the involved states and the collisional wavefunction. Therefore enhanced molecule formation rates might be reached by modifying the scattering wavefunction via Feshbach resonances [Pellegrini *et al.*, 2008].

By applying photoassocation, deeply bound ground state molecules have been created for K_2 [Nikolov *et al.*, 2000], RbCs [Sage *et al.*, 2005], LiCs [Deiglmayr *et al.*, 2008b], Cs_2 [Viteau *et al.*, 2008] and KRb [Aikawa *et al.*, 2010], whereas only for LiCs a single photoassocation step was required (see Sec A.1.2). However, since incoherent processes are involved during photoassocation, the phase-space density is not conserved what limits the possibility of achieving a molecular quantum gas.

- **Magnetoassocation and Raman transfer.** In contrast to photoassocation,

a completely coherent scheme for creating deeply bound molecules out of an atomic ensemble is the combination of magnetoassocation followed by a subsequent transfer into low lying states. In the magnetoassociation step, weakly bound Feshbach molecules [Herbig *et al.*, 2003; Regal *et al.*, 2003; Köhler *et al.*, 2006] are created by ramping a magnetic field over a Feshbach resonance. A coupling to deeper levels by two laser pulses allows for the transfer of population via a stimulated rapid adiabatic passage (STIRAP). The scheme is depicted in Fig. A.1. By a proper selection of laser frequencies and polarizations, full control over the final quantum state, like rovibration and molecular hyperfine levels, can be achieved.

This technology was used for generating deeply bound homonuclear molecules of Cs_2 in the singlet [Danzl *et al.*, 2008] and Rb_2 in the triplet state [Lang *et al.*, 2008] as well as the heteronuclear molecules KRb [Ni *et al.*, 2008] and RbCs [Innsbruck group, unpublished yet, see Debatin *et al.*, 2011 and Takekoshi *et al.*, 2012 for principal procedure] in their energetically lowest states. The observed Feshbach resonances are quite promising for preparing LiCs molecules by following this approach. However, suitable optical transitions for an efficient STIRAP process need to be identified. For further experiments with LiCs it will important to select a good trapping wavelength, where heating effects from scattering of photons are minimized. A bad mode-matching of the potentials during the STIRAP transfer must be avoided. They can arise, if the Feshbach molecules and ground state molecules experience different trap depths due to unequal polarizabilities.

A.1.2 Photoassociation of LiCs molecules

The photoassociation technique was extensively applied at the previous experimental setup in order to produce LiCs molecules in the $B^1\Pi$ state. Spontaneous decay led to the population of levels in the $X^1\Sigma^+$ potential. Molecules in the absolute vibrational and rotational ground state $X^1\Sigma^+$, $v'' = 0; J'' = 0$ could be produced in a single photoassociation step. The spectroscopy of the $B^1\Pi$ state as well as the formation of deeply bound levels in the $X^1\Sigma^+$ are reviewed in this section.

Photoassociation spectroscopy of the $B^1\Pi$ state

This subsection summarizes the following publications:

- *A. Grochola, A. Pashov, J. Deiglmayr, M. Repp, E. Tiemann, R. Wester, M.*

Weidemüller
The $B^1\Pi$ state in LiCs studied by photoassociation spectroscopy
Journal of Chemical Physics **131**, 054304 (2009)

- *J. Deiglmayr, P. Pellegrini, A. Grochola, M. Repp, R. Côté, O. Dulieu, R. Wester, M. Weidemüller*
  Influence of a Feshbach resonance on the photoassociation of LiCs
  New Journal of Physics **11**, 055034 (2009)
  Erratum: New Journal of Physics **12**, 079802 (2010)

An improved potential energy curve of the $B^1\Pi$ state of LiCs, which was initially investigated by Fourier transform spectroscopy [Stein *et al.*, 2008], was gained by performing photoassociation spectroscopy [Grochola *et al.*, 2009]. A total of 54 resonances could be observed, which were assigned to rovibrational levels $v' = 35; J' = 2$ to the $v' = 0; J' = 2$ level.

Combined information from the spectroscopy of ultracold and hot molecules [Staanum *et al.*, 2007] allowed us to derive an improved value for the dissociation energy of the ground state, $D_0 = 5783.495(5)$ cm^{-1}. The newer values significantly improved the quality of the coupled channel calculations for predicting and interpreting the LiCs Feshbach resonances.

Absolute molecule formation rates were furthermore extracted, resulting in unexpectedly large values for photoassociation into low lying states of the $B^1\Pi$ potential [Deiglmayr *et al.*, 2009a]. The fact that the inner turning point of the lowest triplet state potential $a^3\Sigma^+$ matches the Condon points of the $B^1\Pi$ potential, indicates significant contributions from the triplet component of the scattering wave function. An initial attempt of explaining the high rates via perturbation of the singlet scattering function by a broad Feshbach resonance turned out to fail [Deiglmayr *et al.*, 2010b] and a strong singlet-triplet mixing within the excited $B^1\Pi$ state is considered to be more reasonable.

Formation of ultracold polar molecules in the rovibrational ground state

This subsection summarizes the following publications:

- *J. Deiglmayr, A. Grochola, M. Repp, K. Mörtlbauer, C. Glück, J. Lange, O. Dulieu, R. Wester, M. Weidemüller*
  Formation of ultracold polar molecules in the rovibrational ground state
  Physical Review Letters **101**, 133004 (2008)

- *J. Deiglmayr, M. Repp, A. Grochola, K. Mörtlbauer, C. Glück, O. Dulieu, J. Lange, R. Wester, M. Weidemüller*
  Formation of ultracold dipolar molecules in the lowest vibrational levels by photoassociation
  Faraday Discussions **142**, 335 (2009)

The ability of photoassociating low lying levels within the $B^1\Pi$ potential, allowed for the investigation of deeply bound states in the $X^1\Sigma^+$ potential, since reasonable spontaneous decay rates exist. By performing photoassociation via the $v'' = 4; J'' = 1$ level of the $B^1\Pi$ state, molecules in their absolute vibrational and rotational ground state $v'' = 0; J'' = 0$ $X^1\Sigma^+$ were detected [Deiglmayr *et al.*, 2008b; Deiglmayr *et al.*, 2009b]. A production rate of 10^2 molecules/s in their rovibrational groundstate was deduced.

A.2 Ultracold molecular collisions

Molecular collisions are influenced at ultracold temperatures by quantum mechanics [Krems, 2008; Julienne *et al.*, 2011] where statistics and threshold laws pay an important role [Ospelkaus *et al.*, 2010]. This can be used to control molecular collisions by external magnetic [Knoop *et al.*, 2010] or, if the molecules are further polar, by external electric fields [de Miranda *et al.*, 2011]. Besides their prospectives in order to manipulate collisions, a disadvantage of molecular collisions in the ultracold domain is that they can lead to a loss of the molecule out of a trap. This is caused by the fact that the reaction energy is converted into kinetic energy that extends usually the trapping potential and leads therefore to a loss. A challenge of ultracold molecular experiments is the preparation of ensembles with suppressed losses. For homonuclear dimers, inelastic collisions are energetically forbidden, if the molecules are prepared in their energetically lowest state. The situation differs for heteronuclear dimers, formed by atomic constituents A and B. They can undergo a chemical reaction

$$2\mathrm{AB} \longmapsto 2\mathrm{A} + 2\mathrm{B} + \Delta\mathrm{E} \tag{A.3}$$

where pairs of homonuclear molecules are formed, if the reaction energy ΔE has a positive sign. A study by Żuchowski and Hutson, 2010 led to a classification of alkaline dimers into stable and instable ones, depending on if chemical reactions are

allowed or not:

$$\Delta \mathrm{E} \begin{cases} < 0 & \text{for LiNa, LiK, LiRb, LiCs and KRb} \quad \text{"}\textit{unstable}\text{"} \\ > 0 & \text{for KNa, NaRb, NaCs, KCs and RbCs} \quad \text{"}\textit{stable}\text{"} \end{cases} \tag{A.4}$$

Inelastic two body loss coefficients for these alkaline molecular reactions were calculated by Julienne *et al.*, 2011. Working in a two dimensional configuration, the repulsive dipolar forces in a "side to side" configuration dramatically suppress inelastic collisions of LiCs molecules. Already dipole moments of 1 D, which requires moderate electric fields below 2 kV/cm, result in a loss coefficient $K_2 \approx 10^{-7}$ cm^2/s for LiCs molecules, confined in a trap with a trapping frequency of $\omega = 30$ kHz. At lower fields, the quantum nature of the particles matters. Small loss rates are expected for fermions, which already have been observed at two pioneering experiments by using KRb molecules [Ospelkaus *et al.*, 2010; de Miranda *et al.*, 2011].

Furthermore, collisions vanish when molecules are formed in deep optical lattices with an occupation per lattice side of one or less, as demonstrated for Rb_2 [Lang *et al.*, 2008], Cs_2 [Danzl *et al.*, 2010] and KRb [Chotia *et al.*, 2012]. In addition, more sophisticated schemes, like the suppression of collisions via blue-shielding by an RF-field [Gorshkov *et al.*, 2008], might be applied.

Inelastic collisions of ultracold polar LiCs molecules with Cs atoms in an optical dipole trap

This subsection summarizes the following publication:

- *J. Deiglmayr, M. Repp, R. Wester, O. Dulieu, M. Weidemüller*
  Inelastic collisions of ultracold polar LiCs molecules with caesium atoms in an optical dipole trap
  Physical Chemistry Chemical Physics **13**, 19101 (2011)

The possibility of trapping LiCs molecules in a quasi-electrostatic dipole trap together with Cs atoms allowed for deducing rate coefficients for atom-molecule collisions. By performing photoassociation via the $v' = 26; J' = 1$ $B^1\Pi$ level and $v' = 28; J' = 1$ $B^1\Pi$ inelastic two-body loss coefficients $K_{v'=26}^{Cs-LiCs} = (2.3 \pm 0.3 \pm 0.5) \cdot 10^{-10}$cm^3/s [1] and $K_{v'=28}^{Cs-LiCs} = (2.8 \pm 0.4 \pm 0.5) \cdot 10^{-10}$cm^3/s, respectively, were extracted [Deiglmayr *et al.*, 2011b]. Surprisingly, the rates are on the same order of magnitude as rate coefficients for $Cs_2 - Cs$ [Staanum *et al.*, 2006; Zahzam *et al.*,

[1] The first error denotes the statistical error and the second one is the experimental uncertainty.

2006], RbCs – Cs and RbCs – Rb [Hudson *et al.*, 2008] collisions, which were measured under similar conditions. This observation could be explained by a universal model [Idziaszek and Julienne, 2010], showing that the inelastic loss rates are determined by the long-range forces, if at short-range chemical forces lead to an inelastic decay into other channels with unit probability. The obtained LiCs-Cs collision rates were about three times larger than unitarity limited rates, as found for s-waves by applying the universal model. Good agreement is found, if contributions of p-wave collision are taken into account, which is justified by the collisional temperature, at which the measurements were performed.

A.3 Dipolar effects

The low phase-space density in photoassociation experiments prevented the study of dipolar many-body effects with deeply bound molecules. However, applying this technique allowed to determine the permanent dipole moment of deeply bound LiCs molecules as well as the observation of population redistribution effects in deply bound LiCs molecules. Both results are shortly reviewed.

Permanent dipole moment of deeply bound LiCs molecules

This subsection summarizes the following publication:

- *J. Deiglmayr, A. Grochola, M. Repp, O. Dulieu, R. Wester, M. Weidemüller*
  Permanent dipole moment of LiCs in the ground state,
  Physical Review A **82**, 335 (2010)

The permanent electric dipole moment of LiCs could be extracted by measuring the Stark shift of optical transitions in the presence of an electric field. For the $v'' = 2$ and $v'' = 3$ states within the $X^1\Sigma^+$ potential the permanent electric dipole moment could be measured to be 5.5(2) D and 5.3(2) D, respectively [Deiglmayr *et al.*, 2010a]. The measurement of the Stark shift for the $v'' = 2$ vibrational level of the $X^1\Sigma^+$ potential is shown in Fig. 5.2.

Population redistribution in optically trapped polar molecules

This subsection summarizes the following publication:

- *J. Deiglmayr, M. Repp, O. Dulieu, R. Wester, M. Weidemüller*
  Population redistribution in optically trapped polar molecules
  European Physical Journal D **65**, 99 (2011)

The large permanent dipole moment of deeply bound Li-Cs molecules, leads to a strong coupling between internal states, as well as to the black-body radiation field of the environment. In contrast to most of the other alkaline dimers, this latter coupling is important in the case of LiCs, as the spectral density of the black-body radiation at room temperature has a significant amplitude at the frequencies of vibrational transitions between low lying levels of the $X^1\Sigma^+$ state. Using a trapped ensemble of LiCs molecules, the population dynamics was state-selectively investigated and a qualitative agreement with a rate model was found [Deiglmayr *et al.*, 2011a]. Further experiments with rovibrational ground-state molecules might be influenced by the black-body radiation, where depletion lifetimes of 59 s are expected [Vanhaecke and Dulieu, 2007].

Appendix B

Zeeman Slower

As described in Sec. 2.2, a Zeeman slower, consisting out of four helical coils is set up at our experimental setup, that is used for a sequential MOT loading scheme. A photo of the slower is shown in Fig. B.1. This chapter gives a more detailed description of the simulation of the deceleration process. Furthermore, the parametrization of the helical coils is part of this chapter.

B.1 Calculating the optimal field profiles

The forces $\mathbf{F}$ in a Zeeman slower can be described via [Metcalf and van der Straten, 2003] $\mathbf{F} = \hbar\mathbf{k}\gamma_p$ where $\mathbf{k} = 2\pi/\lambda$ denotes the wave vector of the light with a wavelength λ and

$$\gamma_p = \frac{S_0\gamma/2}{1 + S_0 + 4(\Delta/\gamma)^2} \tag{B.1}$$

the excitation rate for a two level atom with a decay rate of the excited state $1/\gamma$. The saturation parameter $S_0 = I/I_{sat}$ is the ratio between the light intensity I and the saturation intensity of the transition I_{sat}. The total detuning

$$\Delta = \Delta_{Laser} + \Delta_{Doppler} + \Delta_{Zeeman} \tag{B.2}$$

is the sum of the shifts which arise from detuning the laser by Δ_{Laser} from the atomic resonance, a Doppler shift $\Delta_{Doppler} = -\mathbf{k}\cdot\mathbf{v}$ that is seen by an atom of a velocity $\mathbf{v}$ in its rest frame as well as a total Zeeman shift of the atomic levels Δ_{Zeeman} in the presence of a magnetic field. The position and velocity dependent deceleration for an atom with a mass m in a Zeeman slower therefore can be cal-

Figure B.1: Helical Slower.

culated via $\mathbf{a} = \eta\mathbf{F}/m = \eta \cdot \mathbf{a}_{max}$, where $\eta = 0...1$ is a safety factor that ensures that the deceleration process does not brake down at any position. As a first step for designing the helical coils, the required fields for effectively decelerating ^{6}Li and ^{133}Cs atoms have been calculated. Therefore, the deceleration process was inverted in a numerical simulation by virtually accelerating atoms towards the oven with a starting velocity v_{start} at the MOT center, with individual settings for the two species. The magnetic fields for the slowing process around the experimental chamber are mainly determined by the chamber (MOT coil) dimensions and desired gradient for loading the MOT. Therefore the simulation started by first accelerating the atoms only by the radial fields of the MOT coils (see Sec. 2.3 for details) at the given currents. After a distance d_{min}, where fields from additional coils could be provided, the acceleration at each position d afterwards was maximized to $\eta \cdot a_{max}$ by applying additional fields and optimizing $\Delta_{Zeeman}(d)$. The Zeeman shift for the optical transition $6^2\mathrm{S}_{1/2}, F = 4, m_F = 4 \rightarrow 6^2\mathrm{P}_{3/2}, F = 5, m_F = 5$ in ^{133}Cs was calculated by the formulas given in Steck, 2008 for the low field region. For ^{6}Li the required fields are large enough, that the atomic transitions are well described in the Paschen-Back regime, resulting in good quantum numbers J, m_J and I, m_I and were calculated by the formulas given in Gehm, 2003 for the transitions $2^2\mathrm{S}_{1/2}, J = 1/2, m_J = 1/2 \rightarrow 2^2\mathrm{P}_{3/2}, J = 3/2, m_J = 3/2$. Closed optical transitions with $\Delta m_I = 0$ for the three $m_I = -1$,$m_I = 0$ and $m_I = +1$, sublevels are possible in the Paschen-Back regime. The fields for the ^{6}Li configuration was optimized for decelerating all three m_I states by adapting the field slope in a way that one m_I state is accelerated with $\eta \cdot a_{max}$ while allowing a smaller deceleration for the other states. The used atomic constants as well as the used parameters for the simulation are given in Table B.1 .

B.2 Simulating the deceleration process

As a last step in the simulation process, the deceleration of ^{6}Li and ^{133}Cs using the individual configurations was checked. Therefore, the atoms started at the oven with

Parameter	^{6}Li	^{133}Cs
λ	671 nm [Gehm, 2003]	852 nm [Steck, 2008]
γ	$2\pi \cdot 5.8$ MHz [Gehm, 2003]	$2\pi \cdot 5.2$ MHz [Steck, 2008]
I_{MOT}	97.7 A	30 A
$I_{Helices}^{outer}$	75 A	30 A
$I_{Helices}^{inner}$	75 A	0 A
$I_{Adaption}$	-1 A	4.5 A
$\partial B_{MOT}^{axial}/\partial z$	31.1 G/cm	9.5 G/cm
S_0	2.5	10
η	0.5	0.5
δ_{Laser}	$-2\pi \cdot 70$ MHz	$-2\pi \cdot 35$ MHz
v_{start}	48 m/s	23 m/s
d_{min}	0.125 m	0.075 m/s

Table B.1: Atomic properties (upper part) and parameters (lower part) used for simulating the optimal fields for the two species. The differences in S_0 arise from different available laser powers on the experiment and the differences in v_{start} assuming higher MOT capture velocities of an ^{6}Li MOT due to the smaller mass.

certain velocity classes $\mathrm{v_{oven}}$. The deceleration process was modeled by numerically integrating the differential

$$dv/dt = \eta \cdot a_{max}(\Delta(v, d)) \tag{B.3}$$

until the atoms reached the MOT center. In addition, the influence of the transversal heating due to photon scattering was investigated. Therefore an increase of the rms value of the transversal velocity $dv_{\mathrm{transversal}}^{\mathrm{rms}}$ by scattering N photons was calculated via [Joffe *et al.*, 1993]:

$$dv_{\mathrm{transversal}}^{\mathrm{rms}}/dt = \sqrt{N/3} \cdot v_{\mathrm{rec}}. \tag{B.4}$$

The capture velocities $\mathrm{v}_{\mathrm{capture}}^{\mathrm{Slower}}$ of the slower were obtained by regarding the maximum velocity class, for which the two species could still be decelerated. The position dependent velocities and the radial extensions of the atomic beam are plotted in the middle and lower panels in Fig. 2.4 and the obtained results are summarized in Tab. B.2.

Species	^{133}Cs	^{6}Li $m_J = +1$	^{6}Li $m_J = 0$	^{6}Li $m_J = -1$
η	0.525	0.525	0.525	0.525
$v^{\text{Slower}}_{\text{capture}}$	150 m/s	650 m/s	625 m/s	575 m/s
v^{MOT}	24 m/s	49 m/s	44 m/s	40 m/s
$r^{\text{MOT}}_{\text{transversal}}$	1.4 mm	3.8 mm	4.6 mm	5.4 mm

Table B.2: Results of simulating the slowing process for the different species. $v^{\text{Slower}}_{\text{capture}}$ is the maximal velocity classes for atoms at the oven section for which slowing for a given safety factor η is possible. v^{MOT} is the obtained velocity and $r^{\text{MOT}}_{\text{transversal}}$ the rms value of the beam radius for atoms leaving the oven with $v^{\text{Slower}}_{\text{capture}}$. η is slightly higher as used for simulating the optimal fields (see Tab. B.1) taking small deviations in the field profile and numerical inaccuracies into account.

B.3 Parametrization of the helical coils

For generating the magnetic fields, a design was chosen, which consists of four interleaving coils made of helical profiles [Bell *et al.*, 2010] with radii of $R_1 = 19.5$ mm, $R_2 = 29.5$ mm, $R_3 = 47.5$ mm and $R_4 = 57.5$ mm. The variable pitch coils are parametrized similarly to the original work of Bell *et al.*, 2010, with two additional parameters, j (j=1...4), for labeling the various coils and $\alpha_j = \pm 1$, which describes the winding orientation :

$$\mathbf{r}_j(p) = \{x_j(p), y_j(p), z_j(p)\} \tag{B.5}$$

$$x_j(p) = R_j \cdot cos[\theta_j(p)] \tag{B.6}$$

$$y_j(p) = \alpha_j \cdot R_j \cdot sin[\theta_j(p)] \tag{B.7}$$

$$z_j(p) = c_{j,7} \cdot p + c_{j,8} \tag{B.8}$$

$$\theta_j(p) = \sum_{m=0...6} c_{j,m} \cdot p^m \tag{B.9}$$

with an free parameter $p \epsilon [0, 2\pi]$, coil radii R_j and transverse (longitudinal) coordinates z (x,y) relative to the coil axis. The magnetic field of such a coil at a position $\mathbf{r'}_j = d\mathbf{r}_j + \{0, 0, z'\}$ for a current I_j and a magnetic permeability μ can be calculated by employing the Biot-Savart law [Bell *et al.*, 2010]:

$$\mathbf{B}_j(\mathbf{r'}_j) = \frac{\mu I_j}{4\pi} \int_0^{2\pi} \frac{(d\mathbf{r'}_j/dp_j) \times \mathbf{r'}_j}{r'^3} dp_j. \tag{B.10}$$

For symmetry reasons, the radial components cancels and thus only the transversal field components at the coils axis were calculated.

The required fields for decelerating ^{133}Cs are much smaller than for ^{6}Li and the $B_j(z')$ decreases with larger radius for a given current. Therefore, the profiles of outer two coils have first been optimized for matching the ^{133}Cs slowing configuration with a moderate current of 30 A, while no current is flowing in the inner two coils. In a second step, the profiles of the inner two helical coils were adapted for matching the ^{6}Li slowing configuration with a current of 75 A, where a field from the outer two coils, operating at a current of 75 A, was taken into account. The obtained parameters are listed in Tab. B.3.

	j=1	j=2	j=3	j=4
R_j	19.5 mm	29.5 mm	47.5 mm	57.5 mm
$c_{j,0}$	π	π	π	π
$c_{j,1}$	-11.75	-11.75	-6.5	-6.5
$c_{j,2}$	-5.75	-5.75	-19.0	-19.0
$c_{j,3}$	-1.635	-1.635	4.03	4.03
$c_{j,4}$	$8.855 \cdot 10^{-1}$	$8.855 \cdot 10^{-1}$	$-2.49 \cdot 10^{-1}$	$-2.49 \cdot 10^{-1}$
$c_{j,5}$	$-1.699 \cdot 10^{-1}$	$-1.699 \cdot 10^{-1}$	$-7.82 \cdot 10^{-2}$	$-7.82 \cdot 10^{-2}$
$c_{j,6}$	$1.157 \cdot 10^{-2}$	$1.157 \cdot 10^{-2}$	$1.025 \cdot 10^{-2}$	$1.025 \cdot 10^{-2}$
$c_{j,7}$	$-5.57 \cdot 10^{-2}$ m	$-5.57 \cdot 10^{-2}$ m	$-7.27 \cdot 10^{-2}$ m	$-7.27 \cdot 10^{-2}$ m
$c_{j,8}$	$-1.56 \cdot 10^{-1}$ m	$-1.56 \cdot 10^{-1}$ m	$-1.65 \cdot 10^{-1}$ m	$-1.65 \cdot 10^{-1}$ m
α_j	+1	-1	+1	-1

Table B.3: Parameters for the four helices j=1...4 with radii R_i. The different coefficients $c_{j,7}$ for the inner and outer layers reflect the different lengths of the two inner and outer layers and the coefficients $c_{j,8}$ the distance from the MOT. $c_{j,0}$ is a global orientation of a helix and the α_j reflect the fact that the inner and outer coils are connected at the chamber side.

Bibliography

[Aikawa *et al.*, 2010] Aikawa, K., Akamatsu, D., Hayashi, M., Oasa, K., Kobayashi, J., Naidon, P., Kishimoto, T., Ueda, M., and Inouye, S. (2010). *Coherent Transfer of Photoassociated Molecules into the Rovibrational Ground State.* Phys. Rev. Lett. **105**, 203001.

[Aikawa *et al.*, 2012] Aikawa, K., Frisch, A., Mark, M., Baier, S., Rietzler, A., Grimm, R., and Ferlaino, F. (2012). *Bose-Einstein Condensation of Erbium.* Phys. Rev. Lett. **108**, 210401.

[Anderson *et al.*, 1995] Anderson, M. H., Ensher, J. R., Matthews, M. R., Wieman, C. E., and Cornell, E. A. (1995). *Observation of Bose-Einstein Condensation in a Dilute Atomic Vapor.* Science **269**, 198.

[Arimondo *et al.*, 1977] Arimondo, E., Inguscio, M., and Violino, P. (1977). *Experimental determinations of the hyperfine structure in the alkali atoms.* Rev. Mod. Phys. **49**, 31.

[Astrakharchik *et al.*, 2008] Astrakharchik, G. E., Morigi, G., De Chiara, G., and Boronat, J. (2008). *Ground state of low-dimensional dipolar gases: Linear and zigzag chains.* Phys. Rev. A **78**, 063622.

[Aymar and Dulieu, 2005] Aymar, M. and Dulieu, O. (2005). *Calculation of accurate permanent dipole moments of the lowest* $^{1,3}\Sigma^+$ *states of heteronuclear alkali dimers using extended basis sets.* The Journal of Chemical Physics **122**, 204302.

[Baranov, 2008] Baranov, M. (2008). *Theoretical progress in many-body physics with ultracold dipolar gases.* Physics Reports **464**, 71 .

[Baranov *et al.*, 2012] Baranov, M. A., Dalmonte, M., Pupillo, G., and Zoller, P. (2012). *Condensed Matter Theory of Dipolar Quantum Gases.* Chemical Reviews **112**, 5012.

[Bardeen *et al.*, 1957] Bardeen, J., Cooper, L. N., and Schrieffer, J. R. (1957). *Theory of Superconductivity.* Phys. Rev. **108**, 1175.

[Barontini *et al.*, 2009] Barontini, G., Weber, C., Rabatti, F., Catani, J., Thalhammer, G., Inguscio, M., and Minardi, F. (2009). *Observation of Heteronuclear Atomic Efimov Resonances.* Phys. Rev. Lett. **103**, 043201.

[Bartenstein *et al.*, 2005] Bartenstein, M., Altmeyer, A., Riedl, S., Geursen, R., Jochim, S., Chin, C., Denschlag, J. H., Grimm, R., Simoni, A., Tiesinga, E., Williams, C. J., and Julienne, P. S. (2005). *Precise Determination of* ^{6}Li *Cold Collision Parameters by Radio-Frequency Spectroscopy on Weakly Bound Molecules.* Phys. Rev. Lett. **94**, 103201.

[Bartenstein *et al.*, 2004] Bartenstein, M., Altmeyer, A., Riedl, S., Jochim, S., Chin, C., Denschlag, J. H., and Grimm, R. (2004). *Crossover from a Molecular Bose-Einstein Condensate to a Degenerate Fermi Gas.* Phys. Rev. Lett. **92**, 120401.

[Beaufils *et al.*, 2008] Beaufils, Q., Chicireanu, R., Zanon, T., Laburthe-Tolra, B., Maréchal, E., Vernac, L., Keller, J.-C., and Gorceix, O. (2008). *All-optical production of chromium Bose-Einstein condensates.* Phys. Rev. A **77**, 061601.

[Bell *et al.*, 2010] Bell, S. C., Junker, M., Jasperse, M., Turner, L. D., Lin, Y.-J., Spielman, I. B., and Scholten, R. E. (2010). *A slow atom source using a collimated effusive oven and a single-layer variable pitch coil Zeeman slower.* Review of Scientific Instruments **81**, 013105.

[Benvenuti *et al.*, 1999] Benvenuti, C., Cazeneuve, J., Chiggiato, P., Cicoira, F., Escudeiro Santana, A., Johanek, V., Ruzinov, V., and Fraxedas, J. (1999). *A novel route to extreme vacua: The non-evaporable getter thin film coatings.* Vacuum **53**, 219.

[Bergeman *et al.*, 1987] Bergeman, T., Erez, G., and Metcalf, H. J. (1987). *Magnetostatic trapping fields for neutral atoms.* Phys. Rev. A **35**, 1535.

[Berninger *et al.*, 2011] Berninger, M., Zenesini, A., Huang, B., Harm, W., Nägerl, H.-C., Ferlaino, F., Grimm, R., Julienne, P. S., and Hutson, J. M. (2011). *Universality of the Three-Body Parameter for Efimov States in Ultracold Cesium.* Phys. Rev. Lett. **107**, 120401.

[Berninger *et al.*, 2012] Berninger, M., Zenesini, A., Huang, B., Harm, W., Nägerl, H.-C., Ferlaino, F., Grimm, R., Julienne, P. S., and Hutson, J. M. (2012).

Feshbach resonances, weakly bound states and coupled-channel potentials for cesium molecules at high magnetic field. arXiv:1212.5584.

[Bijlsma *et al.*, 2000] Bijlsma, M. J., Heringa, B. A., and Stoof, H. T. C. (2000). *Phonon exchange in dilute Fermi-Bose mixtures: Tailoring the Fermi-Fermi interaction.* Phys. Rev. A **61**, 053601.

[Bloch *et al.*, 2008] Bloch, I., Dalibard, J., and Zwerger, W. (2008). *Many-body physics with ultracold gases.* Rev. Mod. Phys. **80**, 885.

[Born and Oppenheimer, 1927] Born, M. and Oppenheimer, R. (1927). *Zur Quantentheorie der Molekeln.* Annalen der Physik **389**, 457.

[Bourdel *et al.*, 2004] Bourdel, T., Khaykovich, L., Cubizolles, J., Zhang, J., Chevy, F., Teichmann, M., Tarruell, L., Kokkelmans, S. J. J. M. F., and Salomon, C. (2004). *Experimental Study of the BEC-BCS Crossover Region in Lithium 6.* Phys. Rev. Lett. **93**, 050401.

[Braaten and Hammer, 2007] Braaten, E. and Hammer, H.-W. (2007). *Efimov physics in cold atoms.* Annals of Physics **322**, 120 .

[Bradley *et al.*, 1995] Bradley, C. C., Sackett, C. A., Tollett, J. J., and Hulet, R. G. (1995). *Evidence of Bose-Einstein Condensation in an Atomic Gas with Attractive Interactions.* Phys. Rev. Lett. **75**, 1687.

[Büchler *et al.*, 2007] Büchler, H. P., Demler, E., Lukin, M., Micheli, A., Prokof'ev, N., Pupillo, G., and Zoller, P. (2007). *Strongly Correlated 2D Quantum Phases with Cold Polar Molecules: Controlling the Shape of the Interaction Potential.* Phys. Rev. Lett. **98**, 060404.

[Carr *et al.*, 2009] Carr, L. D., DeMille, D., Krems, R. V., and Ye, J. (2009). *Cold and ultracold molecules: science, technology and applications.* New Journal of Physics **11**, 055049.

[Catani *et al.*, 2008] Catani, J., De Sarlo, L., Barontini, G., Minardi, F., and Inguscio, M. (2008). *Degenerate Bose-Bose mixture in a three-dimensional optical lattice.* Phys. Rev. A **77**, 011603.

[Catani *et al.*, 2012] Catani, J., Lamporesi, G., Naik, D., Gring, M., Inguscio, M., Minardi, F., Kantian, A., and Giamarchi, T. (2012). *Quantum dynamics of impurities in a one-dimensional Bose gas.* Phys. Rev. A **85**, 023623.

[Chin, 2011] Chin, C. (2011). *Universal scaling of Efimov resonance positions in cold atom systems.* arXiv:1111.1484.

[Chin *et al.*, 2004a] Chin, C., Bartenstein, M., Altmeyer, A., Riedl, S., Jochim, S., Denschlag, J. H., and Grimm, R. (2004a). *Observation of the Pairing Gap in a Strongly Interacting Fermi Gas.* Science **305**, 1128.

[Chin *et al.*, 2009] Chin, C., Flambaum, V. V., and Kozlov, M. G. (2009). *Ultracold molecules: new probes on the variation of fundamental constants.* New Journal of Physics **11**, 055048.

[Chin and Grimm, 2004] Chin, C. and Grimm, R. (2004). *Thermal equilibrium and efficient evaporation of an ultracold atom-molecule mixture.* Phys. Rev. A **69**, 033612.

[Chin *et al.*, 2010] Chin, C., Grimm, R., Julienne, P., and Tiesinga, E. (2010). *Feshbach resonances in ultracold gases.* Rev. Mod. Phys. **82**, 1225.

[Chin *et al.*, 2004b] Chin, C., Vuletić, V., Kerman, A. J., Chu, S., Tiesinga, E., Leo, P. J., and Williams, C. J. (2004b). *Precision Feshbach spectroscopy of ultracold* Cs_2. Phys. Rev. A **70**, 032701.

[Cho *et al.*, 2013] Cho, H.-W., McCarron, D. J., Köppinger, M. P., Jenkin, D. L., Butler, K. L., Julienne, P. S., Blackley, C. L., Le Sueur, C. R., Hutson, J. M., and Cornish, S. L. (2013). *Feshbach spectroscopy of an ultracold mixture of* ^{85}Rb *and* ^{133}Cs. Phys. Rev. A **87**, 010703.

[Chotia *et al.*, 2012] Chotia, A., Neyenhuis, B., Moses, S. A., Yan, B., Covey, J. P., Foss-Feig, M., Rey, A. M., Jin, D. S., and Ye, J. (2012). *Long-Lived Dipolar Molecules and Feshbach Molecules in a 3D Optical Lattice.* Phys. Rev. Lett. **108**, 080405.

[Chu, 1998] Chu, S. (1998). *Nobel Lecture: The manipulation of neutral particles.* Rev. Mod. Phys. **70**, 685.

[Cohen-Tannoudji, 1998] Cohen-Tannoudji, C. N. (1998). *Nobel Lecture: Manipulating atoms with photons.* Rev. Mod. Phys. **70**, 707.

[Cornell and Wieman, 2002] Cornell, E. A. and Wieman, C. E. (2002). *Nobel Lecture: Bose-Einstein condensation in a dilute gas, the first 70 years and some recent experiments.* Rev. Mod. Phys. **74**, 875.

[Courteille *et al.*, 1998] Courteille, P., Freeland, R. S., Heinzen, D. J., van Abeelen, F. A., and Verhaar, B. J. (1998). *Observation of a Feshbach Resonance in Cold Atom Scattering.* Phys. Rev. Lett. **81**, 69.

[Cucchietti and Timmermans, 2006] Cucchietti, F. M. and Timmermans, E. (2006). *Strong-Coupling Polarons in Dilute Gas Bose-Einstein Condensates.* Phys. Rev. Lett. **96**, 210401.

[Dalibard, 1999] Dalibard, J. (1999). *Collisional dynamics of ultra-cold atomic gases.* In: M. Inguscio, S. S. and Wieman, C. E. (Eds.), *Proceedings of the International School of Physics Enrico Fermi* Vol. Course CXL , p. 321. IOS Press, Amsterdam.

[Dalmonte *et al.*, 2010] Dalmonte, M., Pupillo, G., and Zoller, P. (2010). *One-Dimensional Quantum Liquids with Power-Law Interactions: The Luttinger Staircase.* Phys. Rev. Lett. **105**, 140401.

[Danzl *et al.*, 2008] Danzl, J. G., Haller, E., Gustavsson, M., Mark, M. J., Hart, R., Bouloufa, N., Dulieu, O., Ritsch, H., and Nägerl, H.-C. (2008). *Quantum Gas of Deeply Bound Ground State Molecules.* Science **321**, 1062.

[Danzl *et al.*, 2010] Danzl, J. G., Mark, M. J., Haller, E., Gustavsson, M., Hart, R., Aldegunde, J., Hutson, J. M., and Nägerl, H.-C. (2010). *An ultracold high-density sample of rovibronic ground-state molecules in an optical lattice.* Nat Phys **6**, 265.

[Dasenbrook and Komnik, 2013] Dasenbrook, D. and Komnik, A. (2013). *Semiclassical polaron dynamics of impurities in ultracold gases.* Phys. Rev. B **87**, 094301.

[Davis *et al.*, 1995] Davis, K. B., Mewes, M. O., Andrews, M. R., van Druten, N. J., Durfee, D. S., Kurn, D. M., and Ketterle, W. (1995). *Bose-Einstein Condensation in a Gas of Sodium Atoms.* Phys. Rev. Lett. **75**, 3969.

[de Miranda *et al.*, 2011] de Miranda, M. H. G., Chotia, A., Neyenhuis, B., Wang, D., Queéméner, G., Ospelkaus, S., Bohn, J. L., Ye, J., and Jin, D. S. (2011). *Controlling the quantum stereodynamics of ultracold bimolecular reactions.* Nat Phys **7**, 502.

[Debatin *et al.*, 2011] Debatin, M., Takekoshi, T., Rameshan, R., Reichsöllner, L., Ferlaino, F., Grimm, R., Vexiau, R., Bouloufa, N., Dulieu, O., and Nägerl, H.-

C. (2011). *Molecular spectroscopy for ground-state transfer of ultracold RbCs molecules.* Phys. Chem. Chem. Phys. **13**, 18926.

[Deh *et al.*, 2010] Deh, B., Gunton, W., Klappauf, B. G., Li, Z., Semczuk, M., Van Dongen, J., and Madison, K. W. (2010). *Giant Feshbach resonances in* ^{6}Li-^{85}Rb *mixtures.* Phys. Rev. A **82**, 020701.

[Deh *et al.*, 2008] Deh, B., Marzok, C., Zimmermann, C., and Courteille, P. W. (2008). *Feshbach resonances in mixtures of ultracold* ^{6}Li *and* ^{87}Rb *gases.* Phys. Rev. A **77**, 010701.

[Deiglmayr, 2009] Deiglmayr, J. (2009). *Structure, formation, and interactions of ultracold polar molecules.* PhD thesis Albert-Ludwigs-Universität Freiburg im Breisgau, Germany.

[Deiglmayr *et al.*, 2008a] Deiglmayr, J., Aymar, M., Wester, R., Weidemüller, M., and Dulieu, O. (2008a). *Calculations of static dipole polarizabilities of alkali dimers: Prospects for alignment of ultracold molecules.* The Journal of Chemical Physics **129**, 064309.

[Deiglmayr *et al.*, 2010a] Deiglmayr, J., Grochola, A., Repp, M., Dulieu, O., Wester, R., and Weidemüller, M. (2010a). *Permanent dipole moment of LiCs in the ground state.* Phys. Rev. A **82**, 032503.

[Deiglmayr *et al.*, 2008b] Deiglmayr, J., Grochola, A., Repp, M., Mörtlbauer, K., Glück, C., Lange, J., Dulieu, O., Wester, R., and Weidemüller, M. (2008b). *Formation of Ultracold Polar Molecules in the Rovibrational Ground State.* Phys. Rev. Lett. **101**, 133004.

[Deiglmayr *et al.*, 2009a] Deiglmayr, J., Pellegrini, P., Grochola, A., Repp, M., Côté, R., Dulieu, O., Wester, R., and Weidemüller, M. (2009a). *Influence of a Feshbach resonance on the photoassociation of LiCs.* New Journal of Physics **11**, 055034.

[Deiglmayr *et al.*, 2010b] Deiglmayr, J., Pellegrini, P., Grochola, A., Repp, M., Côté, R., Dulieu, O., Wester, R., and Weidemüller, M. (2010b). *Influence of a Feshbach resonance on the photoassociation of LiCs.* New Journal of Physics **12**, 079802. Erratum.

[Deiglmayr *et al.*, 2011a] Deiglmayr, J., Repp, M., Dulieu, O., Wester, R., and Weidemüller, M. (2011a). *Population redistribution in optically trapped polar*

molecules. The European Physical Journal D - Atomic, Molecular, Optical and Plasma Physics **65**, 99.

[Deiglmayr *et al.*, 2009b] Deiglmayr, J., Repp, M., Grochola, A., Mörtlbauer, K., Glück, C., Dulieu, O., Lange, J., Wester, R., and Weidemüller, M. (2009b). *Formation of ultracold dipolar molecules in the lowest vibrational levels by photoassociation.* Faraday Discuss. **142**, 335.

[Deiglmayr *et al.*, 2011b] Deiglmayr, J., Repp, M., Wester, R., Dulieu, O., and Weidemüller, M. (2011b). *Inelastic collisions of ultracold polar LiCs molecules with caesium atoms in an optical dipole trap.* Phys. Chem. Chem. Phys. **13**, 19101.

[DeMarco and Jin, 1999] DeMarco, B. and Jin, D. S. (1999). *Onset of Fermi Degeneracy in a Trapped Atomic Gas.* Science **285**, 1703.

[DeMille, 2002] DeMille, D. (2002). *Quantum Computation with Trapped Polar Molecules.* Phys. Rev. Lett. **88**, 067901.

[DeMille *et al.*, 2000] DeMille, D., Bay, F., Bickman, S., Kawall, D., Krause, D., Maxwell, S. E., and Hunter, L. R. (2000). *Investigation of PbO as a system for measuring the electric dipole moment of the electron.* Phys. Rev. A **61**, 052507.

[DePue *et al.*, 2000] DePue, M. T., Winoto, S. L., Han, D. J., and Weiss, D. S. (2000). *Transient compression of a MOT and high intensity fluorescent imaging of optically thick clouds of atoms.* Opt. Comm. **180**, 73.

[Devreese and Alexandrov, 2009] Devreese, J. T. and Alexandrov, A. S. (2009). *Fröhlich polaron and bipolaron: recent developments.* Reports on Progress in Physics **72**, 066501.

[D'Incao and Esry, 2005] D'Incao, J. P. and Esry, B. D. (2005). *Scattering Length Scaling Laws for Ultracold Three-Body Collisions.* Phys. Rev. Lett. **94**, 213201.

[D'Incao and Esry, 2006] D'Incao, J. P. and Esry, B. D. (2006). *Enhancing the observability of the Efimov effect in ultracold atomic gas mixtures.* Phys. Rev. A **73**, 030703.

[Żuchowski and Hutson, 2010] Żuchowski, P. S. and Hutson, J. M. (2010). *Reactions of ultracold alkali-metal dimers.* Phys. Rev. A **81**, 060703.

[Drewsen *et al.*, 1994] Drewsen, M., Laurent, P., Nadir, A., Santarelli, G., Clairon, A., Castin, Y., Grison, D., and Salomon, C. (1994). *Investigation of sub-Doppler cooling effects in a cesium magneto-optical trap.* Applied Physics B **59**, 283.

[Duarte *et al.*, 2011] Duarte, P. M., Hart, R. A., Hitchcock, J. M., Corcovilos, T. A., Yang, T.-L., Reed, A., and Hulet, R. G. (2011). *All-optical production of a lithium quantum gas using narrow-line laser cooling.* Phys. Rev. A **84**, 061406.

[Efimov, 1971] Efimov, V. (1971). *Weakly bound states of three resonantly-interacting particles.* Sov. J. Nuc. Phys. **12**, 589.

[Efimov, 1979] Efimov, V. (1979). *Low-energy properties of three resonantly interacting particles.* Sov. J. Nuc. Phys. **29**, 546.

[Fedichev *et al.*, 1996] Fedichev, P. O., Reynolds, M. W., and Shlyapnikov, G. V. (1996). *Three-Body Recombination of Ultracold Atoms to a Weakly Bound s Level.* Phys. Rev. Lett. **77**, 2921.

[Ferlaino *et al.*, 2006] Ferlaino, F., D'Errico, C., Roati, G., Zaccanti, M., Inguscio, M., Modugno, G., and Simoni, A. (2006). *Feshbach spectroscopy of a* K-Rb *atomic mixture.* Phys. Rev. A **73**, 040702.

[Ferlaino *et al.*, 2009] Ferlaino, F., Knoop, S., Berninger, M., Harm, W., D'Incao, J. P., Nägerl, H.-C., and Grimm, R. (2009). *Evidence for Universal Four-Body States Tied to an Efimov Trimer.* Phys. Rev. Lett. **102**, 140401.

[Ferlaino *et al.*, 2011] Ferlaino, F., Zenesini, A., Berninger, M., Huang, B., Nägerl, H.-C., and Grimm, R. (2011). *Efimov Resonances in Ultracold Quantum Gases.* Few-Body Systems **51**, 113.

[Fernandes *et al.*, 2012] Fernandes, D. R., Sievers, F., Kretzschmar, N., Wu, S., Salomon, C., and Chevy, F. (2012). *Sub-Doppler laser cooling of fermionic 40 K atoms in three-dimensional gray optical molasses.* EPL (Europhysics Letters) **100**, 63001.

[Fröhlich, 1954] Fröhlich, H. (1954). *Electrons in lattice fields.* Advances in Physics **3**, 325.

[Gehm, 2003] Gehm, M. E. (2003). *Properties of* ^{6}*Li.* available online "AT WWW.PHYSICS.NCSU.EDU/JET/TECHDOCS/PDF/PROPERTIESOFLI.PDF".

[Gerdes *et al.*, 2008] Gerdes, A., Hobein, M., Knöckel, H., and Tiemann, E. (2008). *Ground state potentials of the NaK molecule.* Eur. Phys. J. D **49**, 67.

[Giovanazzi *et al.*, 2002] Giovanazzi, S., Görlitz, A., and Pfau, T. (2002). *Tuning the Dipolar Interaction in Quantum Gases.* Phys. Rev. Lett. **89**, 130401.

[Goldwin *et al.*, 2004] Goldwin, J., Inouye, S., Olsen, M. L., Newman, B., DePaola, B. D., and Jin, D. S. (2004). *Measurement of the interaction strength in a Bose-Fermi mixture with* ^{87}Rb *and* ^{40}K. Phys. Rev. A **70**, 021601.

[Gorshkov *et al.*, 2008] Gorshkov, A. V., Rabl, P., Pupillo, G., Micheli, A., Zoller, P., Lukin, M. D., and Büchler, H. P. (2008). *Suppression of Inelastic Collisions Between Polar Molecules With a Repulsive Shield.* Phys. Rev. Lett. **101**, 073201.

[Granade *et al.*, 2002] Granade, S. R., Gehm, M. E., O'Hara, K. M., and Thomas, J. E. (2002). *All-Optical Production of a Degenerate Fermi Gas.* Phys. Rev. Lett. **88**, 120405.

[Greiner *et al.*, 2002] Greiner, M., Mandel, O., Esslinger, T., Hansch, T. W., and Bloch, I. (2002). *Quantum phase transition from a superfluid to a Mott insulator in a gas of ultracold atoms.* Nature **415**, 39.

[Greiner *et al.*, 2003] Greiner, M., Regal, C. A., and Jin, D. S. (2003). *Emergence of a molecular Bose-Einstein condensate from a Fermi gas.* Nature **426**, 537.

[Grimm *et al.*, 2000] Grimm, R., Weidemüller, M., and Ovchinnikov, Y. B. (2000). *Optical Dipole Traps for Neutral Atoms.* Advances In Atomic, Molecular, and Optical Physics **42**, 95 .

[Grochola *et al.*, 2009] Grochola, A., Pashov, A., Deiglmayr, J., Repp, M., Tiemann, E., Wester, R., and Weidemüller, M. (2009). *Photoassociation spectroscopy of the* $B^1\Pi$ *state of LiCs.* The Journal of Chemical Physics **131**, 054304.

[Gross *et al.*, 2009] Gross, N., Shotan, Z., Kokkelmans, S., and Khaykovich, L. (2009). *Observation of Universality in Ultracold* ^{7}Li *Three-Body Recombination.* Phys. Rev. Lett. **103**, 163202.

[Gross *et al.*, 2011] Gross, N., Shotan, Z., Machtey, O., Kokkelmans, S., and Khaykovich, L. (2011). *Study of Efimov physics in two nuclear-spin sublevels of* ^{7}Li. Comptes Rendus Physique **12**, 4 .

[Guéry-Odelin *et al.*, 1998] Guéry-Odelin, D., Söding, J., Desbiolles, P., and Dalibard, J. (1998). *Is Bose-Einstein condensation of atomic cesium possible?* EPL (Europhysics Letters) **44**, 25.

[Gustavsson, 2008] Gustavsson, M. (2008). *A quantum gas with tunable interactions in an optical lattice.* PhD thesis University of Innsbruck, Insbruck, Austria.

[Gustavsson *et al.*, 2008] Gustavsson, M., Haller, E., Mark, M. J., Danzl, J. G., Rojas-Kopeinig, G., and Nägerl, H.-C. (2008). *Control of Interaction-Induced Dephasing of Bloch Oscillations.* Phys. Rev. Lett. **100**, 080404.

[Hadzibabic *et al.*, 2006] Hadzibabic, Z., Kruger, P., Cheneau, M., Battelier, B., and Dalibard, J. (2006). *Berezinskii-Kosterlitz-Thouless crossover in a trapped atomic gas.* Nature **441**, 1118.

[Hadzibabic *et al.*, 2002] Hadzibabic, Z., Stan, C. A., Dieckmann, K., Gupta, S., Zwierlein, M. W., Görlitz, A., and Ketterle, W. (2002). *Two-Species Mixture of Quantum Degenerate Bose and Fermi Gases.* Phys. Rev. Lett. **88**, 160401.

[Heck, 2012] Heck, R. (2012). *All-Optical Formation of an Ultracold Gas of Fermionic Lithium Close to Quantum Degeneracy.* Diploma thesis Ruprecht-Karls-Universität Heidelberg, Germany.

[Helfrich *et al.*, 2010] Helfrich, K., Hammer, H.-W., and Petrov, D. S. (2010). *Three-body problem in heteronuclear mixtures with resonant interspecies interaction.* Phys. Rev. A **81**, 042715.

[Heraeus, 2013] Heraeus (2013). *Suprasil and Infrasil -Material Grades for the Infrared Spectrum.* online available at WWW.HERAEUS-QUARZGLAS.COM.

[Herbig *et al.*, 2003] Herbig, J., Kraemer, T., Mark, M., Weber, T., Chin, C., Nägerl, H.-C., and Grimm, R. (2003). *Preparation of a Pure Molecular Quantum Gas.* Science **301**, 1510.

[Hoogerland *et al.*, 1996] Hoogerland, M., Driessen, J., Vredenbregt, E., Megens, H., Schuwer, M., Beijerinck, H., and van Leeuwen, K. (1996). *Bright thermal atomic beams by laser cooling: A 1400-fold gain in beam flux.* Applied Physics B **62**, 323.

[Huckans *et al.*, 2009] Huckans, J. H., Williams, J. R., Hazlett, E. L., Stites, R. W., and O'Hara, K. M. (2009). *Three-Body Recombination in a Three-State Fermi Gas with Widely Tunable Interactions.* Phys. Rev. Lett. **102**, 165302.

[Hudson *et al.*, 2008] Hudson, E. R., Gilfoy, N. B., Kotochigova, S., Sage, J. M., and DeMille, D. (2008). *Inelastic Collisions of Ultracold Heteronuclear Molecules in an Optical Trap.* Phys. Rev. Lett. **100**, 203201.

[Hung, 2011] Hung, C.-L. (2011). *In situ probing of two-dimensional quantum gases.* PhD thesis Universiy of Chicago, United States.

[Hung *et al.*, 2008] Hung, C.-L., Zhang, X., Gemelke, N., and Chin, C. (2008). *Accelerating evaporative cooling of atoms into Bose-Einstein condensation in optical traps.* Phys. Rev. A **78**, 011604.

[Idziaszek and Julienne, 2010] Idziaszek, Z. and Julienne, P. S. (2010). *Universal Rate Constants for Reactive Collisions of Ultracold Molecules.* Phys. Rev. Lett. **104**, 113202.

[Inouye *et al.*, 1998] Inouye, S., Andrews, M. R., Stenger, J., Miesner, H.-J., Stamper-Kurn, D. M., and Ketterle, W. (1998). *Observation of Feshbach resonances in a Bose-Einstein condensate.* Nature **392**, 151.

[Inouye *et al.*, 2004] Inouye, S., Goldwin, J., Olsen, M. L., Ticknor, C., Bohn, J. L., and Jin, D. S. (2004). *Observation of Heteronuclear Feshbach Resonances in a Mixture of Bosons and Fermions.* Phys. Rev. Lett. **93**, 183201.

[Jochim, 2004] Jochim, S. (2004). *Bose-Einstein Condensation of Molecules.* PhD thesis University of Innsbruck, Insbruck, Austria.

[Jochim *et al.*, 2003a] Jochim, S., Bartenstein, M., Altmeyer, A., Hendl, G., Chin, C., Denschlag, J. H., and Grimm, R. (2003a). *Pure Gas of Optically Trapped Molecules Created from Fermionic Atoms.* Phys. Rev. Lett. **91**, 240402.

[Jochim *et al.*, 2003b] Jochim, S., Bartenstein, M., Altmeyer, A., Hendl, G., Riedl, S., Chin, C., Hecker Denschlag, J., and Grimm, R. (2003b). *Bose-Einstein Condensation of Molecules.* Science **302**, 2101.

[Jochim *et al.*, 2002] Jochim, S., Bartenstein, M., Hendl, G., Denschlag, J. H., Grimm, R., Mosk, A., and Weidemüller, M. (2002). *Magnetic Field Control of Elastic Scattering in a Cold Gas of Fermionic Lithium Atoms.* Phys. Rev. Lett. **89**, 273202.

[Joffe *et al.*, 1993] Joffe, M. A., Ketterle, W., Martin, A., and Pritchard, D. E. (1993). *Transverse cooling and deflection of an atomic beam inside a Zeeman slower.* J. Opt. Soc. Am. B **10**, 2257.

[Jones *et al.*, 2006] Jones, K. M., Tiesinga, E., Lett, P. D., and Julienne, P. S. (2006). *Ultracold photoassociation spectroscopy: Long-range molecules and atomic scattering.* Rev. Mod. Phys. **78**, 483.

[Julienne, 2012] Julienne, P. S. (2012). private communication.

[Julienne *et al.*, 2011] Julienne, P. S., Hanna, T. M., and Idziaszek, Z. (2011). *Universal ultracold collision rates for polar molecules of two alkali-metal atoms.* Phys. Chem. Chem. Phys. **13**, 19114.

[Kalas and Blume, 2006] Kalas, R. M. and Blume, D. (2006). *Interaction-induced localization of an impurity in a trapped Bose-Einstein condensate.* Phys. Rev. A **73**, 043608.

[Kerman *et al.*, 2000] Kerman, A. J., Vuletić, V., Chin, C., and Chu, S. (2000). *Beyond Optical Molasses: 3D Raman Sideband Cooling of Atomic Cesium to High Phase-Space Density.* Phys. Rev. Lett. **84**, 439.

[Ketterle, 2002] Ketterle, W. (2002). *Nobel lecture: When atoms behave as waves: Bose-Einstein condensation and the atom laser.* Rev. Mod. Phys. **74**, 1131.

[Ketterle *et al.*, 1999] Ketterle, W., Durfee, D. S., and Stamper-Kurn, D. M. (1999). *Making, probing and understanding Bose-Einstein condensates.* In: M. Inguscio, S. S. and Wieman, C. (Eds.), *Proceedings of the International School of Physics "Enrico Fermi"* Course CXL , pp. 67–176. IOS Press, Amsterdam.

[Ketterle and van Druten, 1996] Ketterle, W. and van Druten, N. J. (1996). *Evaporative cooling of atoms.* Advances in Atomic, Molecular, and Optical Physics **37**, 181.

[Knoop *et al.*, 2010] Knoop, S., Ferlaino, F., Berninger, M., Mark, M., Nägerl, H.-C., Grimm, R., D'Incao, J. P., and Esry, B. D. (2010). *Magnetically Controlled Exchange Process in an Ultracold Atom-Dimer Mixture.* Phys. Rev. Lett. **104**, 053201.

[Knoop *et al.*, 2009] Knoop, S., Ferlaino, F., Mark, M., Berninger, M., Schobel, H., Nägerl, H.-C., and Grimm, R. (2009). *Observation of an Efimov-like trimer resonance in ultracold atom-dimer scattering.* Nat Phys **5**, 227.

[Köhler *et al.*, 2006] Köhler, T., Góral, K., and Julienne, P. S. (2006). *Production of cold molecules via magnetically tunable Feshbach resonances.* Rev. Mod. Phys. **78**, 1311.

[Kohnen, 2008] Kohnen, M. (2008). *Ultracold Fermi Mixtures in an Optical Dipole Trap.* Diploma thesis Ruprecht-Karls-Universität Heidelberg, Germany.

[Kohstall *et al.*, 2012] Kohstall, C., Zaccanti, M., Jag, M., Trenkwalder, A., Massignan, P., Bruun, G. M., Schreck, F., and Grimm, R. (2012). *Metastability and coherence of repulsive polarons in a strongly interacting Fermi mixture.* Nature **485**, 615.

[Korek *et al.*, 2000] Korek, M., Allouche, A. R., Fakhreddine, K., and Chaalan, A. (2000). *Theoretical study of the electronic structure of LiCs, NaCs, and KCs molecules.* Canadian Journal of Physics **78**, 977.

[Koschorreck *et al.*, 2012] Koschorreck, M., Pertot, D., Vogt, E., Frohlich, B., Feld, M., and Kohl, M. (2012). *Attractive and repulsive Fermi polarons in two dimensions.* Nature **485**, 619.

[Kraemer *et al.*, 2004] Kraemer, T., Herbig, J., Mark, M., Weber, T., Chin, C., Nägerl, H.-C., and Grimm, R. (2004). *Optimized production of a cesium Bose-Einstein condensate.* Applied Physics B: Lasers and Optics **79**, 1013. 10.1007/s00340-004-1657-5.

[Kraemer *et al.*, 2006] Kraemer, T., Mark, M., Waldburger, P., Danzl, J. G., Chin, C., Engeser, B., Lange, A. D., Pilch, K., Jaakkola, A., Nägerl, H.-C., and Grimm, R. (2006). *Evidence for Efimov quantum states in an ultracold gas of caesium atoms.* Nature **440**, 315.

[Kraft, 2006] Kraft, S. (2006). *Formation, trapping and interaction of ultracold molecules.* PhD thesis Albert-Ludwigs-Universität Freiburg im Breisgau, Germany.

[Kraft *et al.*, 2007] Kraft, S. D., Mikosch, J., Staanum, P., Deiglmayr, J., Lange, J., Fioretti, A., Wester, R., and Weidemüller, M. (2007). *A high resolution time-of-flight mass spectrometer for the detection of ultracold molecules.* Appl. Phys. B **89**, 453.

[Kraft *et al.*, 2006] Kraft, S. D., Staanum, P., Lange, J., Vogel, L., Wester, R., and Weidemüller, M. (2006). *Formation of ultracold LiCs molecules.* Journal of Physics B: Atomic, Molecular and Optical Physics **39**, S993.

[Krems, 2008] Krems, R. V. (2008). *Cold controlled chemistry.* Phys. Chem. Chem. Phys. **10**, 4079.

[Lahaye *et al.*, 2009] Lahaye, T., Menotti, C., Santos, L., Lewenstein, M., and Pfau, T. (2009). *The physics of dipolar bosonic quantum gases.* Reports on Progress in Physics **72**, 126401.

[Lang *et al.*, 2008] Lang, F., Winkler, K., Strauss, C., Grimm, R., and Denschlag, J. H. (2008). *Ultracold Triplet Molecules in the Rovibrational Ground State.* Phys. Rev. Lett. **101**, 133005.

[Lange *et al.*, 2009] Lange, A. D., Pilch, K., Prantner, A., Ferlaino, F., Engeser, B., Nägerl, H.-C., Grimm, R., and Chin, C. (2009). *Determination of atomic scattering lengths from measurements of molecular binding energies near Feshbach resonances.* Phys. Rev. A **79**, 013622.

[Lange, 2008] Lange, J. (2008). *Erzeugung ultrakalter LiCs-Moleküle durch Photoassoziation.* PhD thesis Albert-Ludwigs-Universität Freiburg im Breisgau, Germany.

[LeBlanc and Thywissen, 2007] LeBlanc, L. J. and Thywissen, J. H. (2007). *Species-specific optical lattices.* Phys. Rev. A **75**, 053612.

[Lee *et al.*, 2007] Lee, M. D., Köhler, T., and Julienne, P. S. (2007). *Excited Thomas-Efimov levels in ultracold gases.* Phys. Rev. A **76**, 012720.

[Lercher *et al.*, 2011] Lercher, A., Takekoshi, T., Debatin, M., Schuster, B., Rameshan, R., Ferlaino, F., Grimm, R., and Nägerl, H. (2011). *Production of a dual-species Bose-Einstein condensate of Rb and Cs atoms.* The European Physical Journal D **65**, 3.

[Lompe, 2008] Lompe, T. (2008). *An apparatus for the production of molecular Bose-Einstein condensates.* Diploma thesis Ruprecht-Karls-Universität Heidelberg, Germany.

[Lompe *et al.*, 2010] Lompe, T., Ottenstein, T. B., Serwane, F., Wenz, A. N., Zürn, G., and Jochim, S. (2010). *Radio-Frequency Association of Efimov Trimers.* Science **330**, 940.

[Lu *et al.*, 2011] Lu, M., Burdick, N. Q., Youn, S. H., and Lev, B. L. (2011). *Strongly Dipolar Bose-Einstein Condensate of Dysprosium.* Phys. Rev. Lett. **107**, 190401.

[Lu *et al.*, 1996] Lu, Z. T., Corwin, K. L., Renn, M. J., Anderson, M. H., Cornell, E. A., and Wieman, C. E. (1996). *Low-Velocity Intense Source of Atoms from a Magneto-optical Trap.* Phys. Rev. Lett. **77**, 3331.

[Luiten *et al.*, 1996] Luiten, O. J., Reynolds, M. W., and Walraven, J. T. M. (1996). *Kinetic theory of the evaporative cooling of a trapped gas.* Phys. Rev. A **53**, 381.

[Marti *et al.*, 2010] Marti, G. E., Olf, R., Vogt, E., Öttl, A., and Stamper-Kurn, D. M. (2010). *Two-element Zeeman slower for rubidium and lithium.* Phys. Rev. A **81**, 043424.

[Marzok *et al.*, 2009] Marzok, C., Deh, B., Zimmermann, C., Courteille, P. W., Tiemann, E., Vanne, Y. V., and Saenz, A. (2009). *Feshbach resonances in an ultracold* ^{7}Li *and* ^{87}Rb *mixture.* Phys. Rev. A **79**, 012717.

[McCarron *et al.*, 2011] McCarron, D. J., Cho, H. W., Jenkin, D. L., Köppinger, M. P., and Cornish, S. L. (2011). *Dual-species Bose-Einstein condensate of* ^{87}Rb *and* ^{133}Cs. Phys. Rev. A **84**, 011603.

[Metcalf and van der Straten, 2003] Metcalf, H. J. and van der Straten, P. (2003). *Laser cooling and trapping of atoms.* J. Opt. Soc. Am. B **20**, 887.

[Meyer, 2010] Meyer, K. (2010). *An optical dipole trap for a two-species quantum degenerate gas.* Diploma thesis Ruprecht-Karls-Universität Heidelberg, Germany.

[Micheli *et al.*, 2007] Micheli, A., Pupillo, G., Büchler, H. P., and Zoller, P. (2007). *Cold polar molecules in two-dimensional traps: Tailoring interactions with external fields for novel quantum phases.* Phys. Rev. A **76**, 043604.

[Modugno *et al.*, 2001] Modugno, G., Ferrari, G., Roati, G., Brecha, R. J., Simoni, A., and Inguscio, M. (2001). *Bose-Einstein Condensation of Potassium Atoms by Sympathetic Cooling.* Science **294**, 1320.

[Moerdijk *et al.*, 1995] Moerdijk, A. J., Verhaar, B. J., and Axelsson, A. (1995). *Resonances in ultracold collisions of* ^{6}Li, ^{7}Li, *and* ^{23}Na. Phys. Rev. A **51**, 4852.

[Mosk *et al.*, 2001] Mosk, A., Kraft, S., Mudrich, M., Singer, K., Wohlleben, W., Grimm, R., and Weidemüller, M. (2001). *Mixture of ultracold lithium and cesium atoms in an optical dipole trap.* Applied Physics B: Lasers and Optics **73**, 791.

[Mudrich *et al.*, 2004] Mudrich, M., Kraft, S., Lange, J., Mosk, A., Weidemüller, M., and Tiesinga, E. (2004). *Hyperfine-changing collisions in an optically trapped gas of ultracold cesium and lithium.* Phys. Rev. A **70**, 062712.

[Mudrich *et al.*, 2002] Mudrich, M., Kraft, S., Singer, K., Grimm, R., Mosk, A., and Weidemüller, M. (2002). *Sympathetic Cooling with Two Atomic Species in an Optical Trap.* Phys. Rev. Lett. **88**, 253001.

[Müller, 2011] Müller, R. (2011). *Towards an ultracold mixture of* ^{6}Li *and* ^{133}Cs. Diploma thesis Ruprecht-Karls-Universität Heidelberg, Germany.

[Nakajima *et al.*, 2011] Nakajima, S., Horikoshi, M., Mukaiyama, T., Naidon, P., and Ueda, M. (2011). *Measurement of an Efimov Trimer Binding Energy in a Three-Component Mixture of* ^{6}Li. Phys. Rev. Lett. **106**, 143201.

[Nascimbène *et al.*, 2009] Nascimbène, S., Navon, N., Jiang, K. J., Tarruell, L., Teichmann, M., McKeever, J., Chevy, F., and Salomon, C. (2009). *Collective Oscillations of an Imbalanced Fermi Gas: Axial Compression Modes and Polaron Effective Mass.* Phys. Rev. Lett. **103**, 170402.

[Ni *et al.*, 2008] Ni, K.-K., Ospelkaus, S., de Miranda, M. H. G., Pe'er, A., Neyenhuis, B., Zirbel, J. J., Kotochigova, S., Julienne, P. S., Jin, D. S., and Ye, J. (2008). *A High Phase-Space-Density Gas of Polar Molecules.* Science **322**, 231.

[Nikolov *et al.*, 2000] Nikolov, A. N., Ensher, J. R., Eyler, E. E., Wang, H., Stwalley, W. C., and Gould, P. L. (2000). *Efficient Production of Ground-State Potassium Molecules at Sub-mK Temperatures by Two-Step Photoassociation.* Phys. Rev. Lett. **84**, 246.

[Ockeloen *et al.*, 2010] Ockeloen, C. F., Tauschinsky, A. F., Spreeuw, R. J. C., and Whitlock, S. (2010). *Detection of small atom numbers through image processing.* Phys. Rev. A **82**, 061606.

[O'Hara *et al.*, 2002] O'Hara, K. M., Hemmer, S. L., Granade, S. R., Gehm, M. E., Thomas, J. E., Venturi, V., Tiesinga, E., and Williams, C. J. (2002). *Measurement of the zero crossing in a Feshbach resonance of fermionic* ^{6}Li. Phys. Rev. A **66**, 041401.

[Ospelkaus *et al.*, 2010] Ospelkaus, S., Ni, K.-K., Wang, D., de Miranda, M. H. G., Neyenhuis, B., Quéméner, G., Julienne, P. S., Bohn, J. L., Jin, D. S., and Ye, J. (2010). *Quantum-State Controlled Chemical Reactions of Ultracold Potassium-Rubidium Molecules.* Science **327**, 853.

[Ottenstein *et al.*, 2008] Ottenstein, T. B., Lompe, T., Kohnen, M., Wenz, A. N., and Jochim, S. (2008). *Collisional Stability of a Three-Component Degenerate Fermi Gas.* Phys. Rev. Lett. **101**, 203202.

[Papp *et al.*, 2008] Papp, S. B., Pino, J. M., and Wieman, C. E. (2008). *Tunable Miscibility in a Dual-Species Bose-Einstein Condensate.* Phys. Rev. Lett. **101**, 040402.

[Paredes *et al.*, 2004] Paredes, B., Widera, A., Murg, V., Mandel, O., Folling, S., Cirac, I., Shlyapnikov, G. V., Hansch, T. W., and Bloch, I. (2004). *Tonks-Girardeau gas of ultracold atoms in an optical lattice.* Nature **429**, 277.

[Park *et al.*, 2012] Park, J. W., Wu, C.-H., Santiago, I., Tiecke, T. G., Will, S., Ahmadi, P., and Zwierlein, M. W. (2012). *Quantum degenerate Bose-Fermi mixture of chemically different atomic species with widely tunable interactions.* Phys. Rev. A **85**, 051602.

[Pellegrini *et al.*, 2008] Pellegrini, P., Gacesa, M., and Côté, R. (2008). *Giant Formation Rates of Ultracold Molecules via Feshbach-Optimized Photoassociation.* Phys. Rev. Lett. **101**, 053201.

[Petrov, 2003] Petrov, D. S. (2003). *Three-body problem in Fermi gases with short-range interparticle interaction.* Phys. Rev. A **67**, 010703.

[Petrov *et al.*, 2005] Petrov, D. S., Salomon, C., and Shlyapnikov, G. V. (2005). *Scattering properties of weakly bound dimers of fermionic atoms.* Phys. Rev. A **71**, 012708.

[Phillips, 1998] Phillips, W. D. (1998). *Nobel Lecture: Laser cooling and trapping of neutral atoms.* Rev. Mod. Phys. **70**, 721.

[Phillips and Metcalf, 1982] Phillips, W. D. and Metcalf, H. (1982). *Laser Deceleration of an Atomic Beam.* Phys. Rev. Lett. **48**, 596.

[Pilch *et al.*, 2009] Pilch, K., Lange, A. D., Prantner, A., Kerner, G., Ferlaino, F., Nägerl, H.-C., and Grimm, R. (2009). *Observation of interspecies Feshbach resonances in an ultracold Rb-Cs mixture.* Phys. Rev. A **79**, 042718.

[Pinkse *et al.*, 1997] Pinkse, P. W. H., Mosk, A., Weidemüller, M., Reynolds, M. W., Hijmans, T. W., and Walraven, J. T. M. (1997). *Adiabatically Changing the Phase-Space Density of a Trapped Bose Gas.* Phys. Rev. Lett. **78**, 990.

[Pupillo *et al.*, 2008a] Pupillo, G., Griessner, A., Micheli, A., Ortner, M., Wang, D.-W., and Zoller, P. (2008a). *Cold Atoms and Molecules in Self-Assembled Dipolar Lattices.* Phys. Rev. Lett. **100**, 050402.

[Pupillo *et al.*, 2008b] Pupillo, G., Micheli, A., Büchler, H., and Zoller, P. (2008b). *Cold molecules: Creation and applications* chapter Condensed Matter Physics with Cold Polar Molecules. Taylor & Francis.

[Raab *et al.*, 1987] Raab, E. L., Prentiss, M., Cable, A., Chu, S., and Pritchard, D. E. (1987). *Trapping of Neutral Sodium Atoms with Radiation Pressure.* Phys. Rev. Lett. **59**, 2631.

[Regal *et al.*, 2004] Regal, C. A., Greiner, M., and Jin, D. S. (2004). *Observation of Resonance Condensation of Fermionic Atom Pairs.* Phys. Rev. Lett. **92**, 040403.

[Regal *et al.*, 2003] Regal, C. A., Ticknor, C., Bohn, J. L., and Jin, D. S. (2003). *Creation of ultracold molecules from a Fermi gas of atoms.* Nature **424**, 47.

[Repp *et al.*, 2013] Repp, M., Pires, R., Ulmanis, J., Heck, R., Kuhnle, E. D., Weidemüller, M., and Tiemann, E. (2013). *Observation of interspecies* ^{6}Li-^{133}Cs *Feshbach resonances.* Phys. Rev. A **87**, 010701.

[Roy *et al.*, 2013] Roy, S., Landini, M., Trenkwalder, A., Semeghini, G., Spagnolli, G., Simoni, A., Fattori, M., Inguscio, M., and Modugno, G. (2013). *Universality of the three-body Efimov parameter at narrow Feshbach resonances.* arXiv:1303.3843.

[Sacha and Timmermans, 2006] Sacha, K. and Timmermans, E. (2006). *Self-localized impurities embedded in a one-dimensional Bose-Einstein condensate and their quantum fluctuations.* Phys. Rev. A **73**, 063604.

[Sage *et al.*, 2005] Sage, J. M., Sainis, S., Bergeman, T., and DeMille, D. (2005). *Optical Production of Ultracold Polar Molecules.* Phys. Rev. Lett. **94**, 203001.

[Salzmann, 2007] Salzmann, W. (2007). *Photoassociation and coherent control of ultracold molecules by femtosecond pulses.* PhD thesis Albert-Ludwigs-Universität Freiburg, Germany.

[Schirotzek *et al.*, 2009] Schirotzek, A., Wu, C.-H., Sommer, A., and Zwierlein, M. W. (2009). *Observation of Fermi Polarons in a Tunable Fermi Liquid of Ultracold Atoms.* Phys. Rev. Lett. **102**, 230402.

[Schlöder *et al.*, 1999] Schlöder, U., Engler, H., Schünemann, U., Grimm, R., and Weidemüller, M. (1999). *Cold inelastic collisions between lithium and cesium in a two-species magneto-optical trap.* The European Physical Journal D **7**, 331.

[Schmidt, 2011] Schmidt, S. (2011). *Aufbau und Charakterisierung eines frequenzstabilisierten Diodenlasersystems zur Kühlung und Speicherung von Cs-Atomen.* Diploma thesis Ruprecht-Karls-Universität Heidelberg, Germany.

[Schreck *et al.*, 2001] Schreck, F., Khaykovich, L., Corwin, K. L., Ferrari, G., Bourdel, T., Cubizolles, J., and Salomon, C. (2001). *Quasipure Bose-Einstein Condensate Immersed in a Fermi Sea.* Phys. Rev. Lett. **87**, 080403.

[Schunck *et al.*, 2008] Schunck, C. H., Shin, Y.-i., Schirotzek, A., and Ketterle, W. (2008). *Determination of the fermion pair size in a resonantly interacting superfluid.* Nature **454**, 739.

[Schünemann *et al.*, 1999] Schünemann, U., Engler, H., Grimm, R., Weidemüller, M., and Zielonkowski, M. (1999). *Simple scheme for tunable frequency offset locking of two lasers.* Review of Scientific Instruments **70**, 242.

[Schünemann *et al.*, 1998] Schünemann, U., Engler, H., Zielonkowski, M., Weidemüller, M., and Grimm, R. (1998). *Magneto-optic trapping of lithium using semiconductor lasers.* Optics Communications **158**, 263 .

[Schuster *et al.*, 2012] Schuster, T., Scelle, R., Trautmann, A., Knoop, S., Oberthaler, M. K., Haverhals, M. M., Goosen, M. R., Kokkelmans, S. J. J. M. F., and Tiemann, E. (2012). *Feshbach spectroscopy and scattering properties of ultracold Li + Na mixtures.* Phys. Rev. A **85**, 042721.

[Serwane *et al.*, 2011] Serwane, F., Zürn, G., Lompe, T., Ottenstein, T. B., Wenz, A. N., and Jochim, S. (2011). *Deterministic Preparation of a Tunable Few-Fermion System.* Science **332**, 336.

[Silber *et al.*, 2005] Silber, C., Günther, S., Marzok, C., Deh, B., Courteille, P. W., and Zimmermann, C. (2005). *Quantum-Degenerate Mixture of Fermionic Lithium and Bosonic Rubidium Gases.* Phys. Rev. Lett. **95**, 170408.

[Söding *et al.*, 1998] Söding, J., Guéry-Odelin, D., Desbiolles, P., Ferrari, G., and Dalibard, J. (1998). *Giant Spin Relaxation of an Ultracold Cesium Gas.* Phys. Rev. Lett. **80**, 1869.

[Spiegelhalder *et al.*, 2010] Spiegelhalder, F. M., Trenkwalder, A., Naik, D., Kerner, G., Wille, E., Hendl, G., Schreck, F., and Grimm, R. (2010). *All-optical production of a degenerate mixture of* ^{6}Li *and* ^{40}K *and creation of heteronuclear molecules.* Phys. Rev. A **81**, 043637.

[Staanum *et al.*, 2006] Staanum, P., Kraft, S. D., Lange, J., Wester, R., and Weidemüller, M. (2006). *Experimental Investigation of Ultracold Atom-Molecule Collisions.* Phys. Rev. Lett. **96**, 023201.

[Staanum *et al.*, 2007] Staanum, P., Pashov, A., Knöckel, H., and Tiemann, E. (2007). $X^1\Sigma^+$ *and* $a^3\Sigma^+$ *states of LiCs studied by Fourier-transform spectroscopy.* Phys. Rev. A **75**, 042513.

[Stamper-Kurn *et al.*, 1998] Stamper-Kurn, D. M., Miesner, H.-J., Chikkatur, A. P., Inouye, S., Stenger, J., and Ketterle, W. (1998). *Reversible Formation of a Bose-Einstein Condensate.* Phys. Rev. Lett. **81**, 2194.

[Stan and Ketterle, 2005] Stan, C. A. and Ketterle, W. (2005). *Multiple species atom source for laser-cooling experiments.* Review of Scientific Instruments **76**, 063113.

[Stan *et al.*, 2004] Stan, C. A., Zwierlein, M. W., Schunck, C. H., Raupach, S. M. F., and Ketterle, W. (2004). *Observation of Feshbach Resonances between Two Different Atomic Species.* Phys. Rev. Lett. **93**, 143001.

[Steck, 2008] Steck, D. A. (2008). *Cesium D Line Data.* available online at HTTP://STECK.US/ALKALIDATA(revision 2.0.1, 2 May 2008).

[Stein *et al.*, 2008] Stein, A., Pashov, A., Staanum, P. F., Knöckel, H., and Tiemann, E. (2008). *The* $B^1\Pi$ *and* $D^1\Pi$ *states of LiCs studied by Fourier-transform spectroscopy.* The European Physical Journal D **48**, 177.

[Stoof *et al.*, 1988] Stoof, H. T. C., Koelman, J. M. V. A., and Verhaar, B. J. (1988). *Spin-exchange and dipole relaxation rates in atomic hydrogen: Rigorous and simplified calculations.* Phys. Rev. B **38**, 4688.

[Strauss *et al.*, 2010] Strauss, C., Takekoshi, T., Lang, F., Winkler, K., Grimm, R., Hecker Denschlag, J., and Tiemann, E. (2010). *Hyperfine, rotational, and vibrational structure of the* $a^3\Sigma_u^+$ *state of* $^{87}Rb_2$. Phys. Rev. A **82**, 052514.

[Strecker and Chandler, 2008] Strecker, K. E. and Chandler, D. W. (2008). *Kinematic production of isolated millikelvin molecules.* Phys. Rev. A **78**, 063406.

[Stuhler, 2001] Stuhler, J. (2001). *Kontinuierliches Laden einer Magnetfalle mit lasergekühlten Chromatomen.* PhD thesis Universität Konstanz, Germany.

[Stuhler *et al.*, 2005] Stuhler, J., Griesmaier, A., Koch, T., Fattori, M., Pfau, T., Giovanazzi, S., Pedri, P., and Santos, L. (2005). *Observation of Dipole-Dipole Interaction in a Degenerate Quantum Gas.* Phys. Rev. Lett. **95**, 150406.

[Taglieber *et al.*, 2008] Taglieber, M., Voigt, A.-C., Aoki, T., Hänsch, T. W., and Dieckmann, K. (2008). *Quantum Degenerate Two-Species Fermi-Fermi Mixture Coexisting with a Bose-Einstein Condensate.* Phys. Rev. Lett. **100**, 010401.

[Takekoshi *et al.*, 2012] Takekoshi, T., Debatin, M., Rameshan, R., Ferlaino, F., Grimm, R., Nägerl, H.-C., Le Sueur, C. R., Hutson, J. M., Julienne, P. S., Kotochigova, S., and Tiemann, E. (2012). *Towards the production of ultracold ground-state RbCs molecules: Feshbach resonances, weakly bound states, and the coupled-channel model.* Phys. Rev. A **85**, 032506.

[Targońska and Sacha, 2010] Targońska, K. and Sacha, K. (2010). *Self-localization of a small number of Bose particles in a superfluid Fermi system.* Phys. Rev. A **82**, 033601.

[Tempere *et al.*, 2009] Tempere, J., Casteels, W., Oberthaler, M. K., Knoop, S., Timmermans, E., and Devreese, J. T. (2009). *Feynman path-integral treatment of the BEC-impurity polaron.* Phys. Rev. B **80**, 184504.

[Tey *et al.*, 2010] Tey, M. K., Stellmer, S., Grimm, R., and Schreck, F. (2010). *Double-degenerate Bose-Fermi mixture of strontium.* Phys. Rev. A **82**, 011608.

[Thalhammer *et al.*, 2008] Thalhammer, G., Barontini, G., De Sarlo, L., Catani, J., Minardi, F., and Inguscio, M. (2008). *Double Species Bose-Einstein Condensate with Tunable Interspecies Interactions.* Phys. Rev. Lett. **100**, 210402.

[Tiecke *et al.*, 2010] Tiecke, T. G., Goosen, M. R., Ludewig, A., Gensemer, S. D., Kraft, S., Kokkelmans, S. J. J. M. F., and Walraven, J. T. M. (2010). *Broad Feshbach Resonance in the* ^{6}Li-^{40}**K** *Mixture.* Phys. Rev. Lett. **104**, 053202.

[Timmermans *et al.*, 1999] Timmermans, E., Tommasini, P., Hussein, M., and Kerman, A. (1999). *Feshbach resonances in atomic Bose-Einstein condensates.* Physics Reports **315**, 199 .

[Treutlein *et al.*, 2001] Treutlein, P., Chung, K. Y., and Chu, S. (2001). *High-brightness atom source for atomic fountains.* Phys. Rev. A **63**, 051401.

[Truscott *et al.*, 2001] Truscott, A. G., Strecker, K. E., McAlexander, W. I., Partridge, G. B., and Hulet, R. G. (2001). *Observation of Fermi Pressure in a Gas of Trapped Atoms.* Science **291**, 2570.

[Tung *et al.*, 2013] Tung, S.-K., Parker, C., Johansen, J., Chin, C., Wang, Y., and Julienne, P. S. (2013). *Ultracold mixtures of atomic ^6Li and ^{133}Cs with tunable interactions.* Phys. Rev. A **87**, 010702.

[Ulmanis *et al.*, 2012] Ulmanis, J., Deiglmayr, J., Repp, M., Wester, R., and Weidemüller, M. (2012). *Ultracold Molecules Formed by Photoassociation: Heteronuclear Dimers, Inelastic Collisions, and Interactions with Ultrashort Laser Pulses.* Chemical Reviews **112**, 4890.

[van de Meerakker *et al.*, 2005] van de Meerakker, S. Y. T., Smeets, P. H. M., Vanhaecke, N., Jongma, R. T., and Meijer, G. (2005). *Deceleration and Electrostatic Trapping of OH Radicals.* Phys. Rev. Lett. **94**, 023004.

[Vanhaecke and Dulieu, 2007] Vanhaecke, N. and Dulieu, O. (2007). *Precision measurements with polar molecules: the role of the black body radiation.* Molecular Physics **105**, 1723.

[Viteau *et al.*, 2008] Viteau, M., Chotia, A., Allegrini, M., Bouloufa, N., Dulieu, O., Comparat, D., and Pillet, P. (2008). *Optical Pumping and Vibrational Cooling of Molecules.* Science **321**, 232.

[Vuletić *et al.*, 1999] Vuletić, V., Kerman, A. J., Chin, C., and Chu, S. (1999). *Observation of Low-Field Feshbach Resonances in Collisions of Cesium Atoms.* Phys. Rev. Lett. **82**, 1406.

[Vuletić *et al.*, 2001] Vuletić, V., Kerman, A. J., Chin, C., and Chu, S. (2001). *Laser cooling: Beyond optical molasses and beyond closed transitions.* Vol. 551 , pp. 356–366. AIP Conference Proceedings.

[Wang *et al.*, 2013] Wang, F., Xiong, D., Li, X., Wang, D., and Tiemann, E. (2013). *Observation of Feshbach resonances between ultracold Na and Rb atoms.* arXiv:1303.0334.

[Wang *et al.*, 2012] Wang, J., D'Incao, J. P., Esry, B. D., and Greene, C. H. (2012). *Origin of the Three-Body Parameter Universality in Efimov Physics.* Phys. Rev. Lett. **108**, 263001.

[Wang *et al.*, 2010] Wang, Y., D'Incao, J. P., Nägerl, H.-C., and Esry, B. D. (2010). *Colliding Bose-Einstein Condensates to Observe Efimov Physics.* Phys. Rev. Lett. **104**, 113201.

[Weber *et al.*, 2003a] Weber, T., Herbig, J., Mark, M., Nägerl, H.-C., and Grimm, R. (2003a). *Bose-Einstein Condensation of Cesium.* Science **299**, 232.

[Weber *et al.*, 2003b] Weber, T., Herbig, J., Mark, M., Nägerl, H.-C., and Grimm, R. (2003b). *Three-Body Recombination at Large Scattering Lengths in an Ultracold Atomic Gas.* Phys. Rev. Lett. **91**, 123201.

[Weinstein *et al.*, 1998] Weinstein, J. D., deCarvalho, R., Guillet, T., Friedrich, B., and Doyle, J. M. (1998). *Magnetic trapping of calcium monohydride molecules at millikelvin temperatures.* Nature **395**, 148.

[Wille *et al.*, 2008] Wille, E., Spiegelhalder, F. M., Kerner, G., Naik, D., Trenkwalder, A., Hendl, G., Schreck, F., Grimm, R., Tiecke, T. G., Walraven, J. T. M., Kokkelmans, S. J. J. M. F., Tiesinga, E., and Julienne, P. S. (2008). *Exploring an Ultracold Fermi-Fermi Mixture: Interspecies Feshbach Resonances and Scattering Properties of* ^{6}Li *and* ^{40}K. Phys. Rev. Lett. **100**, 053201.

[Williams *et al.*, 2009] Williams, J. R., Hazlett, E. L., Huckans, J. H., Stites, R. W., Zhang, Y., and O'Hara, K. M. (2009). *Evidence for an Excited-State Efimov Trimer in a Three-Component Fermi Gas.* Phys. Rev. Lett. **103**, 130404.

[Wutz *et al.*, 1982] Wutz, M., Adam, H., and Walcher, W. (1982). *Theorie und Praxis der Vakuumtechnik* Vol. 2., völlig neubearb. u. erw. Aufl. / unt. Mitarb. von F. Fauser.

[Zaccanti *et al.*, 2009] Zaccanti, M., Deissler, B., D'Errico, C., Fattori, M., Jona-Lasinio, M., Müller, S., Roati, G., Inguscio, M., and Modugno, G. (2009). *Observation of an Efimov spectrum in an atomic system.* Nat Phys **5**, 586.

[Zahzam *et al.*, 2006] Zahzam, N., Vogt, T., Mudrich, M., Comparat, D., and Pillet, P. (2006). *Atom-Molecule Collisions in an Optically Trapped Gas.* Phys. Rev. Lett. **96**, 023202.

[Zenesini *et al.*, 2012] Zenesini, A., Huang, B., Berninger, M., Besler, S., Nägerl, H. C., Ferlaino, F., Grimm, R., Greene, C. H., and von Stecher, J. (2012). *Resonant Five-Body Recombination in an Ultracold Gas.* arXiv:1205.1921.

[Zürn *et al.*, 2012] Zürn, G., Lompe, T., Wenz, A. N., Jochim, S., Julienne, P. S., and Hutson, J. M. (2012). *Precise characterization of* ^{6}Li *Feshbach resonances using trap-sideband resolved RF spectroscopy of weakly bound molecules.* arXiv:1211.1512. Magnetic field behavior of the scattering length downloaded from "WWW.LITHIUM6.DE/SCATTERINGLENGTHS.TXT" (12/11/2012).

[Zwierlein *et al.*, 2005] Zwierlein, M. W., Abo-Shaeer, J. R., Schirotzek, A., Schunck, C. H., and Ketterle, W. (2005). *Vortices and superfluidity in a strongly interacting Fermi gas.* Nature **435**, 1047.

[Zwierlein *et al.*, 2006] Zwierlein, M. W., Schirotzek, A., Schunck, C. H., and Ketterle, W. (2006). *Fermionic Superfluidity with Imbalanced Spin Populations.* Science **311**, 492.

[Zwierlein *et al.*, 2003] Zwierlein, M. W., Stan, C. A., Schunck, C. H., Raupach, S. M. F., Gupta, S., Hadzibabic, Z., and Ketterle, W. (2003). *Observation of Bose-Einstein Condensation of Molecules.* Phys. Rev. Lett. **91**, 250401.

Erklärung:

Hiermit versichere ich, dass ich diese Arbeit selbständig verfasst und keine anderen als die angegebenen Quellen und Hilfsmittel benutzt habe.

Heidelberg, den 25.03.2013

.....

(Unterschrift)

Acknowledgements

Diese Arbeit wurde durch eine Vielzahl an Menschen erst ermöglicht, bei denen ich mich an dieser Stelle bedanken möchte.

Mein besonderer Dank geht an meinem Betreuer Prof. Dr. **Matthias Weidemüller**, der mir diese äußerst vielseitige Arbeit auf dem spannenden Gebiet der ultrakalten Quantengase ermöglicht hat. Die hervorragenden Arbeitsbedingungen in deiner Arbeitsgruppe und das große Vertrauen, dass du mir in der Zeit entgegen gebracht hast, waren für den Erfolg dieser Arbeit von entscheidender Bedeutung. Besonders geschätzt habe ich die Verantwortung, die du mir übertragen hast, sowie die vielen Freiheiten, die du mir gerade bei dem Neuaufbau des Experiments überlassen hast.

Prof. Dr. **Markus Oberthaler** danke ich für die Zweitbegutachtung dieser Arbeit. Die Erfahrungen, die ich während meiner Diplomarbeit in deiner Arbeitsgruppe sammeln durfte, waren sehr wertvoll für den Neuaufbau des Experiments.

Einen entscheidenden Anteil zum Gelingen dieser Arbeit haben die Menschen, mit denen ich direkt an dem Li-Cs Experiment zusammen arbeiten durfte.
Bei **Johannes Deiglmayr** bedanke ich mich für die erfolgreiche, gemeinsame Zeit an dem alten Experiment in Freiburg. Auch wenn wir den alten Aufbau, den du so wunderbar beherrscht hast, am Ende deiner Doktorarbeit abgebaut haben, so steckt in dem neuen Setup so manche Erfahrung, die du mir mitgegeben hast. **Roland Wester** hat dabei die Messungen immer mit vielen guten Ratschlägen begleitet. Furthermore, I'd like to thank **Anna Grochola** for the good collaboration in Freiburg.
Besonders danke ich **Rico Pires**, der das Experiment seit dem Umzug aus Freiburg mit begleitet und mit mir dabei alle Höhen und Tiefen durchschritten hat. Es hat mir viel Spaß bereitet, den Aufbau gemeinsam mit dir zu entwerfen, was natürlich eine akkurate Projektplanung erforderte. Eine ebenso große Freude machte

es mir, anschließend mit dir das Cäsiumsystem aufzubauen. Die von dir geplanten Spulen ermöglichten natürlich erst die Messung der Feshbachresonanzen. Einen wesentlichen Beitrag während des Wiederaufbaus lieferte **Juris Ulmanis**, der etwa ein Jahr nach dem Umzug zu uns gestoßen ist und sich dann sofort um den Lithium Part gekümmert hat. Ohne die großartige Experimentiersteuerung, die du programmiert hast, hätten wir niemals Messungen durchführen können. Nicht zu vernachlässigen sind zudem deine Elektronikkenntnisse. Des Weiteren möchte ich mich für die gute Zusammenarbeit mit **Eva Kuhnle** während des letzten Jahres bedanken, vor allem für deinen Beitrag beim Optimieren des Lithium Systems, bei der Unterstützung während der Feshbach-Resonanz Messungen, sowie für deine Leistung, zusammen mit Juris, die ersten molekularen Lithum BECs an unserem Experiment herzustellen.

Die Ergebnisse wurden nicht zuletzt erst durch die ehemaligen Diplomanden bzw. Masterstudenten, die mit sehr großem Engagement diverse Laserstrahlengänge aufgebaut und stabilisiert haben, ermöglicht. Bei **Kristina Meyer** bedanke ich mich für die Realization der 3 W Dipolfalle, bei **Stefan Schmidt** für das Aufbauen des Cäsium Lasersystem und bei **Romain Müller** für den Aufbau des Lithium Lasersystems sowie der 5 W Falle. **Robert Heck** ermöglichte uns durch das Aufbauen des Hochleistungslasers sowie des Hochfeldabbildungsystems erst die Suche der Feshbach-Resonanzen. Ebenso möchte ich mich für die gute Zusammenarbeit mit **Karin Mörtlbauer** in den ersten Monaten meiner Doktorarbeit bedanken. Ihnen allen wünsche ich ein gutes Gelingen ihrer Doktorarbeiten.

Den beiden aktuellen Masterstudenten **Arthur Schönhals** und **Stephan Häfner** wünsche ich eine ebenfalls erfolgreiche Zeit an unserem Experiment. In addition, I'd like to thank **Andy McCulloch** and **Rodrigo Figueredo Shiozaki** for their valuable contributions in setting up the degenerate Raman Side band cooling as well as **Jian Peng Ang** for his initial calculations on Li-Cs Feshbach resonances. Ebenso leisteten die ehemaligen Bachelorstudenten **Thomas Kirchner**, **Stefan Arnold** und **Gregor Urban** wertvolle Beiträge zur Laserstabilisierung, Magnetfeldstabilisierung sowie zum besseren Verständnis von Tunnelvorgängen.

Prof. Dr. **Eberhard Tiemann** danke ich für die präzisen Voraussagen der Feshbach-Resonanzen, die lediglich 20 G von den gemessenen Positionen abwichen, und die gute Zusammenarbeit während der Interpretation der Messwerte sowie beim Verfassen der Veröffentlichung.

Bei **Christoph Hofmann** vom **b**enachbarten Experiment bedanke ich mich für

den steten Austausch an guten Ideen, der beiden Experimenten zugute kam und die natürlich möglichst modularer realisiert werden sollten. Den beiden anderen langjährigen Doktoranden am Rydberg Experiment **Georg Günter** und **Hanna Schempp**, danke ich für die ebenso gute Zusammenarbeit, speziell beim Neuaufbau nach dem Umzug. In addition, I'd like to thank the two current postdocs at the Rydberg experiment **Martin Robert-de-Saint-Vincent** and especially **Shannon Whitlock** for many helpful discussions concerning our setup. Dem ehemaligen Postdoc an dem Experiment, **Thomas Amthor**, danke ich für die Beantwortung zahlreichen Fragen zur Elektronik sowie die gute Organisation des Laborumzuges. Furthermore, I wish **Vladislav Gavryusev** a good start in his project.

Zudem danke ich **Simone Götz** und **Bastian Höltkemeier** von dem MOTRIMS Experiment für die ebenfalls gute Kollaboration und manch gemeinsamen Abend außerhalb des Institutes.

Bei **Sebastian Trippel, Rico Otto, Jochen Mikosch, Terry Mullins, Christian Giese** sowie **Petr Hlavenka** bedanke ich mich für die gute Zusammenarbeit in dem schönen Jahr in Freiburg. Furthermore, I'd like to thank Prof. Dr. **Brett DePaola** for exploring together Freiburg and its surrounding during his time in our group.

Die gute Arbeitsatmosphäre innerhalb der Gruppe wurde nicht zuletzt durch die Diplomanden an den anderen Experimenten **Hannes Busche, Aline Faber, Stephan Helmrich, Henning Labuhn** und **Nele Müller** in Heidelberg und **Christian Greve, Ina Blank, Wendelin Sprenger** und **Martin Stei** in Freiburg sowie unserem Lasertechniker **Dominic Litsch** mitgeprägt. I also like to thank **Silvânia Alves de Carvalho** for her contributions to the group atmosphere. **Claudia Krämer** und **Helga Müller**, den Sekretärinen unserer Arbeitsgruppe in Heidelberg bzw. Freiburg, danke ich für die freundliche Unterstützung in Verwaltungsangelegenheiten.

Der Aufbau sowie die Instandhaltung des Experiments konnte nur durch die hervorragenden **mechanischen** und **elektronischen Werkstätten** des Physikalischen Institutes unter der Leitung von **Ralf Ziegler** sowie **Peter von Walter** bzw. Dr. **Venelin Angelov** gewährleistet werden. Besonderer Dank gilt hierbei **Thomas Fießer, Klaus Layer, Simon Rabenecker, Jessica Riedinger, Rudolf Rusnyak, Esteban Rubio** und **Maximilian von Klot**. Allerdings wurden viele kleinere Projekte durch die restlichen Mitarbeiter erst ermöglicht. Außerdem bedan-

ke ich mich für die Unterstützung durch die **Konstruktionsabteilung** unter der Leitung von Dr. **Bernd Windelbend**. Es machte mir große Freude, mit **Jürgen Gerhäuser**, **Stefan Hetzel** sowie **Kevin Stumpf** gemeinsam die Helix Spulen zu entwickeln.

Zudem war ein steter Austausch mit den Mitarbeitern der anderen beiden Heidelberger Arbeitsgruppen, die von Prof. Dr. **Markus Oberthaler** und Prof. Dr. **Selim Jochim** geleitet werden, sehr hilfreich. Besonders erwähnenswert sind die vielen Diskussionen mit **Selim Jochim** und **Thomas Lompe**.

Allen, die an meiner Arbeit Korrektur gelesen haben, danke ich für die vielen wertvollen Hinweise.

Ein besonderer Dank gilt meiner Familie und meinen Freunden für die uneingeschränkte Unterstützung während dieser Zeit.